8-2015

# Measurement of Hysteretic Shale Capillary Pressure – Saturation Relationships using a Water Activity Meter

Brendan Michael Donnelly
*University of Tennessee - Knoxville*, bdonnell@vols.utk.edu

To the Graduate Council:

I am submitting herewith a thesis written by Brendan Michael Donnelly entitled "Measurement of Hysteretic Shale Capillary Pressure – Saturation Relationships using a Water Activity Meter." I have examined the final electronic copy of this thesis for form and content and recommend that it be accepted in partial fulfillment of the requirements for the degree of Master of Science, with a major in Geology.

Edmund Perfect, Major Professor

We have read this thesis and recommend its acceptance:

Larry McKay, Peter Lemiszki

Accepted for the Council:
Carolyn R. Hodges

Vice Provost and Dean of the Graduate School

(Original signatures are on file with official student records.)

# Measurement of Hysteretic Shale Capillary Pressure – Saturation Relationships using a Water Activity Meter

A Thesis Presented for the
Master of Science
Degree
The University of Tennessee, Knoxville

Brendan Michael Donnelly
August 2015

# Acknowledgments

I would like to thank my wife Kathleen who finally convinced me that I needed to pursue this degree. Without her I definitely would not have begun this work, let alone finish it, as she helped me through my somewhat difficult transition back into academia due to several years of work that was less than mentally taxing. Also, thanks to my parents Susan and Sonny who also convinced me that I needed to go back to school and who have been nothing but supportive throughout my life.

Thanks to Dr. Edmund Perfect who accepted someone who was washing cars into his lab group and who has served as my advisor these past years. His help and guidance were invaluable throughout this process as was the customary hot tea when discussing my work, my progress, my setbacks, and whatever sporting event occurred recently. Thanks to Dr. Larry McKay and Dr. Peter Lemiszki for their advice and feedback over the past two years and for serving on my committee. Thanks to Dr. Colin Sumrall and Ryan Roney for training me and allowing me to use the 3D laser scanner and to Dr. Linda Kah and Miles Henderson for agreeing to train me in the use of the carbon coulometer before it met an untimely demise. Also many thanks to all my fellow students within the department, especially Elizabeth Gass, who helped in the data collection phase, and Blake Roberts, my office mate and constant classmate, who helped collect data, test ideas, and give invaluable feedback, and who has been my close friend these past two years. Finally, a huge thanks goes to the Department of Earth and Planetary Sciences which provided me with my GTA position and thus funded this entire endeavor.

# Abstract

Capillary pressure is the pressure difference across the interface of two immiscible fluids within a porous medium due to the interfacial tension between fluids and is related to both the properties of the fluids and the porous medium. Capillary pressure within a porous medium will change depending upon its degree of saturation. Understanding the relationship between capillary pressure and saturation for a rock allows for the modeling of multi-phase flow. Many traditional methods of measuring capillary pressure are unsuitable for the characterization of shale due to their inability to measure the high capillary pressures found within the small pores. Furthermore, the mercury injection method used to determine shale pore-size distribution may be problematic due to both compression and contamination of the sample, as well as difficulty in converting the mercury capillary pressure to reservoir fluid capillary pressure. A possible alternative to the mercury injection method is the water activity meter which has been utilized extensively in the soil sciences for measuring capillary pressure. However, its application to lithified material has been limited. This study used a water activity meter to collect capillary pressure measurements (ranging from 2-200 MPa) at several saturation levels (ranging from 10-100%) for seven types of oil and gas producing shale. Nonlinear regression was used to fit the capillary pressure-saturation data for each shale type to the Brooks and Corey model which describes the relationship between capillary pressure and saturation using four parameters. Six of the seven shale types investigated were successfully parameterized indicating that the water activity meter may be a viable method for characterizing the capillary pressure-saturation relationship of shale for inclusion in numerical reservoir models. There were no significant differences between the wetting and drying Brooks and Corey parameters for the different shales, indicating that hysteresis was not a major factor. As expected, the different shale types had significantly different Brooks and Corey parameters for a given drying/ wetting regime. Bulk density, matrix density, and porosity measurements were also made on each shale type. These properties were correlated with total organic carbon content and were also statistically different between the examined shale types.

# Table of Contents

Chapter 1 – Introduction and Literature Review ..... 1

1.1 Hydraulic Fracturing of Shale ..... 1

1.2 Capillary Pressure – Saturation and Related Parameters ..... 2

1.3 Measuring Capillary Pressure – Saturation and Related Parameters ..... 6

1.3.1 Summary and ranges of measurement methods ..... 6

1.3.2 The porous plate/pressure cell method ..... 6

1.3.3 The centrifuge method ..... 7

1.3.4 The mercury injection method ..... 8

1.3.5 Neutron scattering and gas adsorption ..... 9

1.3.6 The vapor equilibration method ..... 10

1.3.7 Water activity meters ..... 11

1.4 Goals, Objectives, and Hypotheses ..... 13

Chapter 2 – Materials and Methods ..... 15

2.1 Samples and Sample Preparation ..... 15

2.2 Porosity Determination ..... 17

2.3 Capillary Pressure – Saturation using Water Activity Method ..... 19

2.4 Data Analysis ..... 22

Chapter 3 – Results and Discussion ..... 24

3.1 Capillary Pressure – Saturation ..... 24

3.2 Shale Characterization ..... 30

Chapter 4 – Summary and Conclusions ..... 35

References ..... 38

Appendices ..... 46

Appendix 1 – Tables ..... 47

Appendix 2 – Figures ..... 53

Appendix 3 – Data ..... 71

3.1 Mancos Shale ..... 71

3.2 Eagle Ford Shale ..... 74

3.3 Barnett Shale ..... 77

3.4 Chattanooga Shale – Black ..... 80

3.5 Chattanooga Shale – Grey ..... 82

3.6 Marcellus Shale – Pennsylvania ..... 85

3.7 Marcellus Shale – West Virginia ..... 88

Vita ..... 90

# List of Tables

Table 1: Estimated Brooks and Corey (1964) parameters for wetting..... 47

Table 2: Estimated Brooks and Corey (1964) parameters for drying ..... 48

Table 3: Summary of shale properties ..... 49

Table 4: Comparison of mean values for bulk density. ..... 50

Table 5: Comparison of mean values for matrix density. ..... 51

Table 6: Comparison of mean values for porosity. ..... 52

# List of Figures

Figure 1: Capillary rise schematic ..... 53

Figure 2: Accuracy ranges of various methods of measuring capillary pressure ..... 54

Figure 3: Photos of representative subsamples of each shale type ..... 55

Figure 4: InstruQuest Inc. HumiPyc Gas Pycnometer ..... 56

Figure 5: Schematic of pycnometer ..... 57

Figure 6: NextEngine Desktop 3D Scanner ..... 58

Figure 7: Novasina LabMaster-aw water activity meter ..... 59

Figure 8: Water activity meter sensor and chambers ..... 60

Figure 9: Ultrasonic humidifier used to wet samples ..... 61

Figure 10: Paired measurements of capillary pressure and saturation for each shale type ..... 62

Figure 11: Predicted Brooks and Corey (1964) functions for all shale types ..... 63

Figure 12: Predicted wetting Brooks and Corey (1964) fits for each shale type ..... 64

Figure 13: Comparison of Brooks and Corey (1964) parameters obtained from wetting data ..... 65

Figure 14: Predicted drying Brooks and Corey (1964) fits for each shale type ..... 66

Figure 15 Comparison of Brooks and Corey (1964) parameters obtained from drying data ..... 67

Figure 16. Observed versus Brooks and Corey (1964) predicted volumetric water contents ..... 68

Figure 17: Correlation between TOC and bulk density ..... 69

Figure 18: Correlation between TOC and matrix density ..... 70

# Chapter 1 – Introduction and Literature Review

## 1.1 Hydraulic Fracturing of Shale

Hydraulic fracturing, or "fracking," has become an increasingly popular tool in the petroleum industry for the exploitation of reservoirs previously discounted due to low permeability, inadequate porosity, or high cost of development. The "fracking" process, usually used for shale formations, involves pumping a large volume of fluid containing suspended particles into a hydrocarbon reservoir at high pressure in order to fracture the rock around the well bore and thus increase the permeability of the reservoir rock (Myers, 2012). This increased permeability allows for the extraction of hydrocarbons that would otherwise not be recoverable. However, the majority of the fluid used during the fracking process is never recovered and its whereabouts have become the source of much debate and study (King, 2012). This lost fluid, often called "leak off," raises concerns from the environmental health perspective as it can potentially contaminate aquifers (Myers, 2012). Leak off can also negatively impact the profitability of a well for two reasons; the fluid cannot be recycled and its presence in the subsurface can effectively block gas flow to the well (Holditch, 1979). Numerical reservoir models are widely used by the petroleum industry in order to predict production, understand potential hazards, and improve profitability. In order to simulate the multiphase flows associated with fracking operations with numerical reservoir models, it is important to characterize the hydraulic properties of the shale formation.

Many hydraulic studies of shale have focused on determining how exposure to both water- and oil-based drilling fluids negatively impact shale strength (Chenevert, 1970a; b; Mody and Hale, 1993; Horsrud et al., 1998; Lal, 1999; Zhang et al., 2008). These studies examined the causes of shale instability (i.e., swelling, fracturing, and slaking) and various means of preventing its occurrence. More recently, spontaneous imbibition rates, or the rate at which a fluid enters a porous solid without the application of any external force, have been measured in order to provide a possible means of increased hydrocarbon production as well as determining the fate of unrecovered fracking fluids (Takahashi and Kovscek, 2010;

Wang et al., 2011; Roychaudhuri et al., 2011; Dehghanpour et al., 2012). This imbibition is mainly caused by capillary pressure which depends on both the properties of the fluids and the physical properties of the shale (Takahashi and Kovscek, 2010; Roychaudhuri et al., 2011).

## 1.2 Capillary Pressure – Saturation and Related Parameters

Capillary pressure is the pressure difference across the interface of two immiscible fluids within a porous medium due to the interfacial tension between the fluids (Fetter, 2001). This pressure difference is related to both properties of the fluids and their interaction with the solid surface (Christoffersen and Whitson, 1995). Fluids are classified as wetting when adhesive forces are greater than cohesive forces, and are non-wetting when the reverse is true (Vavra et al., 1992). As shown in Figure 1 (all figures located in Appendix 2), a wetting fluid is drawn into a capillary tube due to adhesive forces, and rises to a given height ($h_c$), until the adhesive forces drawing the liquid up the capillary tube and the interfacial tension holding the water together in the middle of the tube are offset by gravity and the pressure of the non-wetting phase (Fetter, 2001). The result of these interactions is that the interface between the fluids is curved and that the radius of curvature is related to the capillary pressure (Newsham et al., 2004). The Young-Laplace equation defines this relationship as:

$$P_c = \frac{2\sigma \cos\theta}{r} \qquad \textit{Eq. (1)}$$

where $P_c$ is the capillary pressure, $\sigma$ is the interfacial tension, $\theta$ is the contact angle between the wetting fluid and the solid surface, and r is the radius of the pore throat (Selley, 1985). It can be seen from this equation that capillary pressure will increase as pore size decreases. This relationship becomes important when working with shale and tight sand as the pore throat radii of these rocks can be orders of magnitude smaller than the pore throat radii of conventional reservoir rocks (sandstone or carbonate) (Aguilera,

2014). However, this equation is difficult to apply to natural materials due to variability of composition which impacts the contact angle, and the fact that pores may exist in a variety of sizes and shapes.

An alternative approach to measuring capillary pressure involves the Kelvin equation, which describes the relationship between the equilibrium vapor pressure of a material, the surface tension of the liquid, and the radius of curvature at the vapor/liquid interface (Thomson, 1872; Skinner and Sambles, 1972). As capillary pressure is also related to these properties, a derivation of the Kelvin formula can be used to calculate capillary pressure (Melrose, 1987). This equation is as follows:

$$P_c = \ln\left(\frac{p}{p_0}\right)\frac{RT}{V_m} \qquad \textit{Eq. (2)}$$

where p is the vapor pressure of water in a material, $p_0$ is the vapor pressure of pure water at the same temperature, R is the Universal gas constant, T is the temperature in Kelvin, and $V_m$ is the molar volume of water (Melrose, 1987; Newsham et al., 2004). This equation is better suited to describing capillary pressure in natural materials as it does not require a pore size variable like Equation (1). However, it does assume that there are no solutes present in the water. In order to utilize this equation, the ratio of vapor pressure of water in a material to the vapor pressure of pure water must first be determined.

Water activity ($a_w$) is a measure of the energy state of water within a system and is described by the following:

$$a_w = \frac{f}{f_0} \cong \frac{p}{p_0} \qquad \textit{Eq. (3)}$$

where f is the fugacity or escaping tendency of water within a system and $f_0$ is the fugacity or escaping tendency of pure water (Chenevert, 1970b). Fugacity is closely related to vapor pressure of water in a

material and the ratio $p/p_0$ can be substituted for $f/f_0$ in Equation (3) (Chenevert, 1970b). As a result of this substitution, as shown in Schmitt et al., (1994), Equation (2) can be rewritten as follows:

$$P_c = \ln(a_w)\frac{RT}{V_m} \qquad \textit{Eq. (4)}$$

The degree of saturation, or the ratio of the volume of fluid within the pore structure of a material to the total pore volume of that material, is relevant when utilizing Equation (4) to characterize capillary pressure in porous media. This is important as it relates to characterizing shale and tight sands reservoirs as these rock types will typically have low (<30%) initial saturation, although initial saturations of 60% have been found in the Barnett Shale (Newsham et al., 2004; Penny et al., 2005; Wang and Reed, 2009). As a sample dries from complete saturation, the wetting fluid (brine in a water-wet reservoir) is displaced by the non-wetting fluid (hydrocarbons) and is contained in pore spaces of decreasing size which results in higher capillary pressures (Brooks and Corey, 1964; Vavra et al., 1992). During imbibition, the wetting fluid occupies the smallest pores first before entering larger pores and displaces the non-wetting fluid; this results in a decrease in capillary pressure as the material becomes more saturated (Vavra et al., 1992; Schmitt et al., 1994). This interaction between the wetting and non-wetting fluid systems allows for several reservoir properties to be determined. Accurate measurements of capillary pressure can be used to determine reservoir quality, recovery efficiency, and seal potential (Vavra et al., 1992; Christoffersen and Whitson, 1995; Sigal, 2013). Furthermore, an understanding of the relationship between the wetting and non-wetting fluids at different saturation levels can be used to model fluid flow, estimate recovery of oil and gas, and enhance recovery of oil and gas from a well (Li and Horne, 2007; Takahashi and Kovscek, 2010; Dehghanpour et al., 2012; Sakhaee-Pour and Bryant, 2014). Finally, this hysteretic relationship impacts the permeability of a material and can reflect the heterogeneity of the pore

structure or indicate chemical interactions between the fluid and the material (Purcell, 1949; Shang et al., 1995).

Many models exist for characterizing the capillary pressure-saturation relationship, however one of the earliest and most widely utilized is the Brooks and Corey (1964) model (Fredlund and Xing, 1994; Hunt, 2004; Ghezzehei et al., 2007; Zhuang et al., 2008; Li, 2010). The Brooks and Corey (1964) model is given as follows:

$$\theta_v = \phi \qquad \{0 \leq \Psi \leq \Psi_a\} \qquad \textit{Eq. (5a)}$$

$$\theta_v = \theta_r + (\phi - \theta_r)\left(\frac{\Psi_a}{\Psi}\right)^{\lambda} \qquad \{\Psi > \Psi_a\} \qquad \textit{Eq. (5b)}$$

where $\theta_v$ is the volumetric water content, or the ratio of the volume of water contained in the pores of a material to the bulk volume of the material, $\theta_r$ is the residual water content, or the ratio of the volume of water that is non-drainable in a material to the bulk volume of the material, $\phi$ is porosity, $\Psi_a$ is the air/water-entry value, or the capillary pressure at which the largest pores in a material drain or fill with water, and $\lambda$ is the pore size distribution index, which describes the range of pore sizes within a material. Equation (5a) holds true for all capillary pressures less than or equal to $\Psi_a$; within this pressure range, all of the pore space within the material is fully saturated. Equation (5b) holds true for all pressures greater than $\Psi_a$; beyond this point, the sample drains or rewets with changing pressures until the pressure increases to the point that an irreducible volume of water remains in the pore structure of the material. Combined, these equations are able to characterize the capillary pressure-saturation relationship. However, in order to apply this model, accurate measurements of both capillary pressure and saturation need to be carried out.

## 1.3 Measuring Capillary Pressure – Saturation and Related Parameters

### *1.3.1 Summary and ranges of measurement methods*

The necessity of accurate capillary pressure-saturation data for modeling petroleum reservoir flow characteristics has been noted in many studies (Slobod et al., 1951; Melrose, 1990; Donaldson et al., 1991; Morrow and Mason, 2001). These measurements have become more important as the petroleum industry moves to the production of tight sand and shale petroleum reservoirs (Clarkson et al., 2011; Josh et al., 2012). Several techniques, including water vapor equilibration, high speed centrifugation, porous plate/pressure cell, and mercury injection, exist for quantifying the capillary pressure-saturation relationship. All of these methods require the paired measurement of the volume of water within the sample and the energy state or capillary pressure of that water (Melrose et al., 1994). These methods, their advantages and disadvantages, as well as their accuracy ranges (Figure 2) will be discussed in the following sections.

### *1.3.2 The porous plate/pressure cell method*

The porous plate/pressure cell method is ostensibly the simplest method of measuring capillary pressure. In this technique, described by McCullough et al. (1944), a fully saturated sample, where the volume of fluid within the sample is known, is placed on a semi-permeable pressure plate in a sealed container. Gas pressure is applied to the sample, thus displacing fluid from within the sample. The volume increments of expelled fluid are monitored until no changes in saturation are noted. At this point, the fluid remaining in the pores of the sample is held at a pressure equivalent to the applied gas pressure. By increasing the input gas pressure and measuring the change in saturation, a series of paired measurements of both water content and capillary pressure can be recorded (McCullough et al., 1944). This method, while simple, has several inherent disadvantages, most notably the maximum capillary pressure and the long time needed for equilibration between successive pressure increases (Purcell, 1949;

Newsham et al., 2004). These limitations make this method a poor choice for work involving low porosity, tight sands and shale.

### *1.3.3 The centrifuge method*

The high speed centrifugation technique was developed in part to overcome the disadvantages in both equilibration time and maximum achievable pressures associated with the porous plate/pressure cell method (McCullough et al., 1944). This method is similar to the porous plate/pressure cell method, however in this case, the saturated sample is placed in a holder within a centrifuge and the pressure is applied to the sample by rotating the sample at high speeds (McCullough et al., 1944; Slobod et al., 1951). As described by Slobod et al. (1951), the applied pressure is related to both the number of rotations per minute and the distance between the sample and the axis of rotation. Water is displaced from the core as it is rotated in the centrifuge and the volume of displaced water is measured in an outflow chamber. Once there is no change noted in the volume of water in the outflow chamber, the water content of the sample is calculated by taking the difference between the water content of the saturated sample and the volume of displaced fluid. At this point, the remaining fluid is held at a pressure equivalent to the applied pressure. Further measurements of both capillary pressure and water content are made by increasing the rotational speed and noting the resulting change in the volume of water in the outflow chamber (Slobod et al., 1951). This method while allowing quicker measurements of capillary pressure and saturation than the porous plate/pressure cell method can still have long equilibration times, and poor speed control can lead to large errors in measurements of both capillary pressure and its associated saturation (Ward and Morrow, 1987; Newsham et al., 2004). Furthermore, the maximum capillary pressure is limited due to the maximum rotational speed of the centrifuge which may limit its applicability to tight sands and shale.

*1.3.4 The mercury injection method*

The mercury injection method of measuring the capillary pressure-saturation relationship is markedly different from other techniques in that it involves the use of an immiscible fluid (mercury) that does not spontaneously imbibe (Purcell, 1949). This method addresses many of the disadvantages of the previously described centrifuge and porous plate methods. Namely, the method is much quicker (measurements can be made in a single day) and can achieve the high pressures needed in order to assess tight sands and shale (Newsham et al., 2004; Shikhov and Arns, 2015). In order to achieve those high pressures, as described by Purcell, an external force, typically gas pressure, must be applied to the mercury in order for it to enter the pore structure of the material in question. The volume of mercury entering the sample is noted at a given pressure and the pressure is increased stepwise in order to make several sets of paired measurements of mercury saturation and pressure. These pressures for mercury capillary pressure must then be converted to the equivalent water capillary pressure in order to mimic reservoir conditions (Purcell, 1949). The equation for converting capillary pressure between different fluid systems is given as follows:

$$P_{Cw} = P_{Cm} \times \frac{\sigma_w \cos\theta_w}{\sigma_m \cos\theta_m} \qquad \textit{Eq. (6)}$$

where $P_{Cw}$ is the capillary pressure of the water/air system, $P_{Cm}$ is the capillary pressure of the air/mercury system, $\sigma_w$ and $\sigma_m$ are the interfacial tensions of the water/air and air/mercury systems, respectively, and $\theta_w$ and $\theta_m$ are the contact angles of the water/air/solid and air/mercury/solid systems, respectively (Vavra et al., 1992). This method, while able to measure the entire range of capillary pressure needed to describe low porosity reservoir rocks, does have several drawbacks. These include the compression and possible alteration of the pore structure due to the high pressures needed for mercury to enter the material, the permanent contamination of the sample due to mercury remaining within the pore structure after

measurements, and difficulty in accurately converting the mercury capillary pressure measurements to water capillary pressure at high pressures (Newsham et al., 2004; Sigal, 2013; Shikhov and Arns, 2015).

The most comprehensive use of the mercury intrusion method to characterize the capillary pressure-saturation relationship of shale comes from Sigal (2013). The study identified three classes of capillary pressure-curves in the Barnett Shale based on their ability to produce hydrocarbons. The first class of capillary pressure-curves, called the Type 1 curve, shows mercury intrusion increasing with increasing pressure until sharply falling off as the instrument reaches it maximum pressure, which resembles the capillary pressure curve of a conventional reservoir rock. Mercury was allowed to then drain and a significant amount of mercury remained in the sample, confirming mercury intrusion. Type 2 curves show saturation increasing with increasing pressure and leveling off at the instruments maximum pressure. It was assumed that intrusion would continue if the instrument could reach higher pressures. Finally, the Type 3 curve did not show any significant mercury intrusion until the instrument reached its maximum pressure. Mercury intrusion at this pressure was concluded to be due to conformance, which is simply the filling of surface depressions (Dewhurst et al., 2002). This type curve correlated with a seal rock rather than a reservoir rock.

### *1.3.5 Neutron Scattering and Gas Adsorption*

Small-angle neuron scattering (SANS) and ultra-small-angle neutron scattering (USANS) are two non-destructive methods of characterizing the pore size distribution of shale (Mastalerz et al., 2012; Clarkson et al., 2013). As described in Radlinski et al., (2013), these methods direct a beam of neutrons on to a sample. The neutrons are attenuated by the sample and scattered. Finally, the intensity and scattering angle of these neutrons are measured (Radlinski et al., 2013). The pore size distribution of the shale is related to the relationship between the intensity and angle of the scattered neutrons (Mastalerz et al., 2012).

Gas adsorption is also used to characterize the pore size distribution of shale (Clarkson et al., 2013). In this method, as described by Lu et al., (1995) and Chareonsuppanimit et al., (2012) a known volume of gas (i.e. $N_2$, $CO_2$, He, or $CH_4$) is released under pressure into a measurement chamber containing a sample. The gas is then released into another chamber where pressure is measured. This pressure is then used to determine the volume of gas that was released from the measurement chamber, and by difference, the volume of gas adsorbed adsorbed by the sample. This process is repeated using increasingly higher injection pressures (Lu et al., 1995; Chareonsuppanimit et al., 2012). The resulting adsorption isotherm can then be used to characterize the pore size distribution and more importantly be used to determine the gas storage capacity of a reservoir (Ross and Bustin, 2009).

While it is possible to relate pore sizes determined by both neutron scattering and gas adsorption to capillary pressure through the use of Equation (1), in practice this is rarely done; the reason being that these measurements do not take into account interactions between a liquid phase and the solid matrix (Clarkson et al., 2013).

### *1.3.6 The vapor equilibration method*

The vapor equilibration method of measuring capillary pressure is based on the relationship between the radius of curvature of water held by capillary forces and the relative vapor pressure of the water in that system which has been previously illustrated in Equation (2) (Melrose, 1988; Newsham et al., 2004). Thus, capillary pressure will change in accordance to changes in vapor pressure or relative humidity, assuming there are no solutes in the pore water. The major advantages of this method are that capillary pressure can be measured across the entire range of saturation with measurement precision only decreasing at high saturations, it can be used to measure materials with small pore sizes and associated high capillary pressures, and it does not use a non-representative fluid like the mercury intrusion method (Newsham et al., 2004). Furthermore, the capillary pressure values are essentially direct measurements,

unlike the centrifuge and mercury intrusion methods, as this technique is based on the relationship between the vapor pressure of water and capillary pressure (Melrose, 1987).

In this method, measurements are taken by placing samples in a desiccator with a controlled humidity and weighing the sample periodically until no changes in mass are noted (Chenevert, 1970b). At this point, the water in the sample is in equilibrium with the desiccator and capillary pressure can be calculated based on the relative humidity within the desiccator using Equation (2). Water content is calculated based on the mass change between the dry sample and the equilibrium mass of the sample. Humidity within the desiccator is then changed in order to perform more paired measurements of water content and capillary pressure (Melrose, 1987). This is typically accomplished through the use of various salt solutions which impact the vapor pressure of water and thus the relative humidity within the desiccator (Chenevert, 1970b; Melrose, 1987; Newsham et al., 2004). While this method presents many advantages over the previously described techniques, it does have several inherent disadvantages, namely long equilibration times, inaccuracies at high saturations, and the need to correct for the presence of dissolved salts in the pore fluids (Melrose, 1988; Newsham et al., 2004).

The water vapor equilibration method has been applied to shale mainly in the development of drilling mud (Chenevert, 1970b; Mody and Hale, 1993; Oleas et al., 2010). Chenevert (1970) used the vapor equilibration technique in order to characterize the water activity-saturation relationship. The theory is that once the water activity of shale at its in-situ saturation is known, the water activity of the drilling fluid can be matched to it in order to combat fluid loss and the subsequent swelling of shale (Chenevert, 1970b; Mody and Hale, 1993; Zhang et al., 2008). However, none of these studies noted that water activity can be converted to $P_c$ for characterizing the capillary pressure – saturation relationship.

### *1.3.7 Water activity meters*

Water activity meters indirectly measure the activity of water due to the fact that under equilibrium conditions in a sealed chamber, the relative humidity of the air in the chamber is equivalent to

the vapor pressure ratio (Jarrett et al., 2004). Once the water activity of the sample is known, Equation (4) can be used to calculate capillary pressure, assuming no solutes are present in the pore water. This method is similar to the water vapor equilibration method in that the determination of capillary pressure relies on the relationship between the curved surface of a liquid held by capillary forces and the vapor pressure ratio under equilibrium conditions. However, in using the water activity meter, equilibrium conditions are determined when the vapor pressure ratio reaches equilibrium. In the water vapor equilibration method, equilibrium conditions are determined when the sample's mass no longer changes with time. Like the water vapor equilibration method, water activity meters are capable of measuring water held at very high capillary pressures (up to ~450 MPa). As noted earlier, this is of great importance when characterizing materials with small pore sizes, especially at low saturation values. However, unlike the water vapor equilibration method, individual measurements of water activity and thus capillary pressure, can be completed in a matter of hours (Jarrett et al., 2004).

Water activity meters have been used in the soil sciences to measure the capillary pressure-saturation relationships of various soils (Gee et al., 1992; Perfect et al., 2004; Cancela et al., 2006; Ojeda et al., 2006; Zhuang et al., 2008). However, their use has been fairly limited in the study of lithified materials. One study advocated for their use over the traditional water vapor equilibration method in determining the water activity of shale at its in-situ saturation and the water activity of drilling fluids (Jarrett et al., 2004). This information can be used to prevent the loss of drilling fluids to the shale formation and the subsequent borehole problems that occur when drilling petroleum wells (Chenevert, 1970b; Zhang et al., 2008; Oleas et al., 2010). However, this undervalues the utility of the water activity meter by limiting its use to one measurement of capillary pressure at one in-situ saturation for the sole purpose of maintaining wellbore stability. As noted earlier, capillary pressure is a major control on many aspects of flow within a petroleum reservoir, and as such should be characterized at multiple levels of saturation. To the best of the author's knowledge, only two studies have previously utilized water activity meters to fully characterize the capillary pressure-saturation relationship of lithified material (Green et al.,

1995; Flint, 2003). In both cases, the meters were used on igneous rocks and neither study noted the novelty of the technique or its inherent advantages in the low saturation range typically applicable to shale.

## 1.4 Goals, Objectives, and Hypotheses

The overall goal of this study was to test the efficacy of the water activity meter method for characterization of capillary pressure-saturation relationships of samples from a range of shale formations. The shale types used in this study are from major oil and gas producing shale units in the United States. However it is not currently possible to characterize the low saturation region of these shale types with either the centrifuge or porous plate/pressure cell methods. As noted earlier, the capillary pressure-saturation relationship is important in the modeling of fluid flow in porous media, evaluating reservoir quality, and estimating ultimate recovery of oil or gas from a reservoir. As a result, accurate characterization of this relationship is of great economic importance to the petroleum industry. It is expected that this study will demonstrate the water activity meter to be both quicker and simpler than the water vapor equilibration method and less problematic than the mercury intrusion method.

In order to pursue this goal, several objectives must be met. First, in order for the water activity meter method to be relevant to oil and gas shale industry, a water activity meter must be able to collect capillary pressure-saturation data over a wide range of saturations while wetting and drying. As noted in Chapter 1.2, initial water saturations of shale can range from less than 30% to 60%; as a result, the water activity meter should be able to measure capillary pressure within, and hopefully beyond, that range. Second, in order for these data to be used by the oil and gas industry, raw data from the water activity meter method should be capable of being parameterized using the Brooks and Corey (1964) equations. Since the rocks studied were from a range of petroleum producing shale units in the United States with different compositions, different ages, and different estimates of ultimate recovery of oil and gas, it was hypothesized that the shale types would have different Brooks and Corey (1964) parameters [i.e. the null

hypothesis that must be rejected was that the shale types will have similar Brooks and Corey (1964) parameters]. Also, the Brooks and Corey (1964) parameters would be different between the wetting and drying capillary pressure-saturation curves for a given shale type due to hysteresis [i.e. the null hypothesis that must be rejected was that the Brooks and Corey (1964) parameters obtained from the wetting and drying measurements for a given shale will be similar].

An accurate characterization of the bulk physical properties of each shale type must be carried out in order to determine if any physical differences exist between the shale types. This was necessary as demonstrable differences between the shale types were needed to support any claims to the efficacy of the water activity meter in characterizing the capillary pressure saturation relationships of shale. It was hypothesized that the shale types would have different values of bulk density, matrix density, and porosity [i.e. the null hypothesis that must be rejected was that the different shale types will have similar values of bulk density, matrix density, and porosity]. The determination of any differences in these physical properties was important as it may help explain differences in the capillary pressure-saturation relationships and thus the Brooks and Corey (1964) parameters.

# Chapter 2 - Materials and Methods

## 2.1 Samples and Sample Preparation

Several types of shale were examined in the course of this study, all of which are from oil or gas producing formations within the United States. Photos of the shale cores were not taken prior to subsampling with a rock saw, however representative photos of subsamples of all shale types examined can be found in Figure 3. An industry partner, Consol Energy Inc. (Pittsburgh, PA), provided core samples of two types of Chattanooga Shale-an organic rich core and an inorganic core, as well as two samples of Marcellus Shale. The Chattanooga Shale is a gas producing, bituminous, siliceous, and sulfide shale from the Late Devonian (Glover, 1954; Roen and Kepferle, 1993). The Marcellus Shale is a carbonaceous shale found in Ohio, New York, Pennsylvania, Virginia, and West Virginia (Bruner and Smosna, 2011). The Marcellus Shale is one of the most prolific gas producing formations in the United States with estimates of recoverable natural gas ranging from 53.2 to 14,000 billion cubic meters (1.9 to 500 trillion cubic feet) (Stevens and Ruuskraa, 2009). The Chattanooga Shale samples were from Scott County, Tennessee with the inorganic sample coming from a depth of ~990 m (3250 ft.) and the organic sample from a depth of ~975 m (3200 ft.). The inorganic sample was light grey in color and contained visible pyrite grains while the organic core was black in color with dark grey inter-bedding. One Marcellus sample came from Armstrong County, Pennsylvania at a depth of ~2315 m (7600 ft.); the other was from Lewis County, West Virginia from a depth of ~2070 m (6800 ft.). Both cores of Marcellus Shale were dark grey to black in color with lighter grey lenses interspersed throughout.

Cores of Mancos Shale, Barnett Shale, and Eagle Ford Shale were obtained from outcrops with unknown locations by Kocurek Industries Inc. (Caldwell, TX), a commercial vendor. The Mancos Shale is an interbedded siltstone and shale located in New Mexico, Wyoming, and Utah, from the Late Cretaceous with an estimated 588 billion cubic meters (21 trillion cubic feet) of recoverable gas (McLennan et al., 1983; U.S. Energy Information Administration, 2011). The Mancos samples were grey in color with light grey inter-bedding. The Barnett Shale is a petroliferous and fossiliferous shale located

in north Texas and is Mississippian in age (Bruner and Smosna, 2011). As of 2011, the Barnett Shale has estimated recoverable reserves of 1,203 billion cubic meters (43 trillion cubic feet) which represented 6% of the total shale gas in the United States (U.S. Energy Information Administration, 2011). The Barnett Shale samples were black in color with rare dark grey lenses. Finally, the Eagle Ford Shale is a late Cretaceous, bituminous shale found in south Texas (Mullen, 2010). The Eagle Ford samples obtained for this study were black in color with light grey inter-beds found throughout. The United States Energy Information Administration (2011) estimates there to be 588 billion cubic meters (21 trillion cubic feet) of recoverable natural gas and 3 billion barrels of recoverable oil, making it one of the most prolific shale reservoirs in the country.

The Chattanooga Shale and Marcellus Shale cores were 7.62 cm (3 in.) and 8.89 cm (3.5 in.) in diameter respectively. These cores were subsampled using a rock saw in order to obtain 6 samples of each that they had max side lengths of ~2 cm (0.75 in.) and were ~0.5 cm (0.2 in.) thick. This was done due to sample size restrictions associated with the water activity meter. The commercially acquired shale cores were 1.9 cm (0.75 in.) in diameter and 15.24 cm (6 in.) in length. The cores were cut using a rock saw in order to obtain 6 samples with unchanged diameters and were ~0.5 cm (0.2 in.) thick. No cutting fluid was used in the operation of the rock saw, however the subsamples were wiped with a dry tissue (Chem-Wipe) in order to remove dust leftover from the cutting process. Leftover material from all cores was retained for porosity measurements. All of the samples were then placed in an oven and dried for 24 hours at 105°C in order to remove any in situ water within the samples following the protocol established by Ojeda et al. (2006). Samples were not weighed before drying so the initial water saturation of these cores is unknown. Also, drying times were not lengthened to determine if the mass remained constant after that initial 24 hour drying period. Samples were then weighed in order to determine the oven dry, or zero water content, mass of the sample.

Approximately 1 gram of each shale type was ground using a mortar and pestle for total organic carbon analysis. This ground material was sent to Ellington and Associates, Inc.

(http://www.ellingtongeologic.com, Houston, TX) where total organic carbon content (TOC, weight %) was measured using standard methods (Mull, 1995; Schumacher, 2002). The ground material was first weighed, and then leached using hydrochloric acid. Leached material was then combusted with pure oxygen at 2100°C and the mass of the resulting carbon dioxide is measured in an infrared detection cell using a LECO C-230 Carbon Analyzer. This mass is then converted to percent carbon based on the pre-combustion mass of the sample.

## 2.2 Porosity Determination

Total porosity is an important parameter needed for the petrophysical characterization the shale samples. It determines the maximum capacity for fluid storage. An accurate determination of porosity is also needed to calculate both the volumetric water content and degree of saturation of the samples. Immediately after oven drying the samples were placed in an InstruQuest Inc. HumiPyc gas pycnometer (InstruQuest Inc., Coconut Creek, FL, USA) (see Figure 4). This instrument operates based on the ideal gas law in order to calculate the solid phase volume of a material (Oppenheimer et al., 1997). Two chambers, a reference chamber of known volume, and a sample chamber of unknown volume connected to a pressure transducer are linked via a valve (Figure 5). During operation, helium is allowed to enter the sample chamber and a pressure reading is taken. The valve between the sample chamber and the reference chamber is then opened allowing the pressure to equilibrate between the two chambers. At this point another pressure reading is taken and the volume of the sample chamber is calculated using the ideal gas law. This second reading is necessary because the sample chamber can be configured in a variety of ways in order to minimize the amount of air space around the sample, which allows for fewer errors in measurement. In order to determine the solid phase volume of an unknown sample, two measurements are carried out. The first is with the sample chamber empty and is used to determine the volume of the sample chamber. The second measurement is carried out with the sample. The difference between the measured sample chamber volume without the sample and the measured sample chamber volume with the

sample is equivalent to the solid phase volume of the unknown sample. Water immersion was not utilized for determination of volume due to shale slaking when submerged in water (Schmitt et al., 1994).

The bulk volume of Eagle Ford Shale samples were measured using calipers as these samples were cylindrical. However, due to their non-uniform shape, the bulk volume of the Mancos Shale, Barnett Shale, Chattanooga Shale and Marcellus Shale samples were measured with a NextEngine Desktop 3D scanner (NextEngine Inc., Santa Monica, CA, USA) using a modified version of the method described by Rossi et al., (2008). In this scanner, samples are held by an auto-rotating holder which is controlled via included computer software (Figure 6). The software allows a user defined number of scans, which corresponds to the degree of rotation between scans. Each sample was scanned 8 times, which corresponds to a 45° rotation between scans. The sample was then realigned so that the sample holder was in contact with a different portion of the material and rescanned an additional 8 times. Completed scans were "trimmed" in order to remove the sample holder using the manufacturer's software. The two sets of scans were then "aligned" and "fused" together in order to create one single, seamless, three dimensional model of the sample. Completed scans were then exported to Rhino 5 (Robert McNeel & Associates, Seattle, WA, USA), a three dimensional modeling program, which includes a tool to calculate the enclosed volume of a scan, thus giving the bulk volume of the sample.

The mass of each sample was obtained by weighing and used, along with the solid phase volume from the gas pycnometer and the bulk volume from the laser scanner or caliper measurements, to determine the matrix density ($p_s$) and bulk density ($p_b$), respectively. These measurements were then used to calculate the total porosity ($\phi$) based on the following equation:

$$\phi = 1 - \frac{p_b}{p_s} \qquad \textit{Eq. (7)}$$

## 2.3 Capillary Pressure – Saturation using Water Activity Method

Water activity ($a_w$), for both the main wetting and main drying branches of the capillary pressure-saturation curve, was measured using a Novasina LabMaster-aw (Novasina AG, Lachen, Switzerland) (Figure 7). This instrument measures the equilibrium relative humidity, or the water activity, of a sample in a sealed chamber using a resistive-electrolytic sensor at a controlled temperature. The water activity meter contains a primary measurement chamber and a secondary chamber that allows for temperature equilibration (Figure 8). Each subsample of a given shale type was placed in an individual, sealable container ~4 cm in diameter and 1 cm in height. All subsamples of a given shale type were oven dried for 24 hours at 105°C and allowed to cool to room temperature before being vapor wetted with distilled water using an ultrasonic humidifier (Model 693-12/ 809996, Sunbeam Products Inc., Hattiesburg, MS) (Figure 9). Using a modified version of the method described by Ojeda et al., (2006), each subsample of a given shale type was vapor wetted for an interval of 10 seconds. After wetting, each subsample was allowed to equilibrate for 24 hours in a dry, sealed sample container. This was done to allow water to move into the pore structure of the rock rather than remain on the surface. While the samples equilibrated, the water activity meter was calibrated using six controlled activity salt solutions, with $a_w$ values ranging from 0.113 to 0.973 (~3000 to 38 MPa). A manufacturer recommended universal, chemical pre-filter was also placed between the instrument sensor and the sample chamber in order to prevent the influence of chemicals on the measured values of $a_w$. This filter protected against nitrogen oxides, amines, aldehydes, aromatic hydrocarbons, oil vapors, and dust. After equilibration, one subsample was placed in the water activity meter and analyzed, while another subsample was placed into the secondary chamber. The temperature of the meter was set to 25°C and the equilibration time was set to the instrument maximum of 30 minutes. This means that the instrument will report a water activity value only after the reading stays constant for 30 minutes. Once water activity is measured, the subsample in the secondary chamber is placed in the primary chamber and analyzed and another subsample is placed in the secondary chamber.

The mass of the subsample was recorded using a Mettler-Toledo AG104 analytical balance (Mettler Toledo, LLC, Toledo, OH) after a water activity value was reported by the meter. The process of removing the sample from the water activity meter, placing it on the balance, obtaining a mass value, and resealing the sample took less than 30 seconds. Any evaporation in this process was assumed to be negligible as the scale being used was accurate to ±0.0001g and the mass reading was not taken until the scale indicated that the mass was stable. The difference between the oven dry mass and the partially saturated mass allows for the calculation of the gravimetric water content ($\theta_g$). Volumetric water content was then calculated using the following equation:

$$\theta_v = \frac{\theta_g \, p_b}{p_w} \qquad \textit{Eq. (8)}$$

where $\theta_v$ is the volumetric water content and $p_w$ is the density of water. Errors in the calculation of volumetric water content were propagated in a several step process using standard equations for the calculation of total error. Errors in the determination of the volume of water contained in the sample were based on the uncertainty of the scale being used to weigh the samples (i.e., ±0.0001g). Errors in the determination of the bulk volume of a given subsample were accounted for by using the standard deviation of all bulk volume determinations of a given shale type.

Using the reported water activity values, capillary pressure was then calculated using Equation (4). The uncertainty in these measurements was calculated based on the manufacturer's specifications for the water activity meter; this uncertainty is greater at high water activity values than at low water activity values. At water activity values greater than or equal to 0.970 or approximately 4.2 MPa, the error is equal to a water activity of plus or minus 0.01 or approximately 1.4 MPa. At water activity values less than 0.970, the error is equal to a water activity of plus or minus 0.003, which when using Equation (4) to convert to capillary pressure, is approximately 0.4-1.0 MPa.

After all subsamples of a given shale type were vapor wetted for 10 seconds, analyzed by the water activity meter and weighed, the partially saturated samples were vapor wetted for 20 seconds. The subsamples were again allowed to equilibrate in a sealed container for 24 hours, analyzed using the water activity meter and then weighed. This process continued to repeat with paired measurements of capillary pressure and water content being taken after doubling the wetting time between measurements. Wetting intervals of 40, 80, 120, 240, and 480 seconds were used, after which the subsamples were submerged in distilled, deionized water for a period of ~2 weeks in order to achieve near complete saturation after which they were analyzed in the water activity meter and weighed for the last time. After this process was completed for a given shale type, the instrument's calibration was checked using controlled activity salt solutions. At no point did the instrument drift out of calibration. The paired measurements of capillary pressure and water content allowed for the main wetting branch of the capillary pressure-saturation relationship to be plotted on a semi-logarithmic plot with capillary pressure (in MPa) on the x-axis in a logarithmic scale, and volumetric water content on the y-axis.

The main drying branch of the capillary pressure-saturation relationship was measured in much the same way as the wetting branch. However, instead of wetting the subsamples, an initially saturated subsample was exposed to the air for 10 seconds and then allowed to equilibrate for 24 hours in a sealed sample container. After equilibration, capillary pressure and volumetric water content were determined using the same method as for the wetting branch. After all subsamples of a given shale type that were dried for 10 seconds were analyzed by the water activity meter and weighed, the partially dried subsamples were dried for 20 seconds. The subsamples were then allowed to equilibrate for 24 hours in a sealed container before being analyzed in the water activity meter and then weighed. This process was repeated with paired measurements of capillary pressure and water content being taken after doubling the drying time between measurements. Drying intervals continued to double until the mass of the sample stabilized.

## 2.4 Data Analysis

The Brooks and Corey (1964) parameters (Equation 5), $\theta_r$, $\Psi_a$, and $\lambda$, were estimated from the capillary pressure-saturation data for each shale type using segmented non-linear regression analysis (SAS, 2012). Equation 5 was fitted to the data using three values of porosity for a given shale type. The $\phi$ parameters used corresponded to the mean porosity value for a given shale type, the maximum porosity value measured for a given shale type, and the minimum porosity value measured for a given shale type. Furthermore, a bounds statement was set to 0.0 for the $\theta_r$ parameter which prohibited the regression from estimating negative residual water contents. As noted in Chapter 2.3, the uncertainty in the measurement of capillary pressure is high at values of low capillary pressure, as measured with the water activity meter used in this study. As a result of this uncertainty, there is no statistical difference between a measured capillary pressure of 1.3 MPa and 0 MPa. To reflect this uncertainty, all capillary pressure measurements whose calculated uncertainty was less than or equal to 1.3 MPa were not included in the regression analyses.

There were 6 subsamples of each shale type for the drying measurements, and for the wetting measurements there were 6 subsamples of the Mancos Shale, Eagle Ford Shale, and Barnett Shale and 3 subsamples of the Marcellus Shale and Chattanooga Shale. The regression analyses were performed on the pooled data from each of these subsamples. This means that while capillary pressure measurements were taken for each of the subsamples, the fitting was done using all of the subsamples for a given shale type. Goodness of fit was assessed using the coefficient of determination ($R^2$) between the observed and predicted values. The fit of each regression was also checked by examining the residuals for normality using the Shapiro-Wilk test, autocorrelation using the Durbin-Watson test, and homoscedasticity using the Chi-squared test. Similarities between estimated Brooks and Corey (1964) parameters were assessed by comparing the 95% confidence levels of the estimated parameters. If these confidence intervals overlapped between multiple shale types there was no difference between the parameters for those shale types. These comparisons were only made however when the best Brooks and Corey (1964) fit to the

measured data (determined by the highest $R^2$ value) was obtained when using the mean value of porosity in the fitting process.

Bulk density, matrix density, and porosity measurements were obtained for each rock type using material from the same cores as the subsamples used for capillary pressure-saturation measurements. However, this material was never subjected to saturation. The Tukey's Studentized Range Test, which compares multiple mean values in conjunction with an Analysis of Variance (ANOVA), was used to test the hypothesis that different shale types have different bulk densities, matrix densities, and porosities (SAS, 2012).

# Chapter 3 - Results and Discussion

## 3.1 Capillary Pressure - Saturation

Capillary pressure measurements were taken at varying levels of saturation in both the wetting and drying directions for each shale type. All of the paired measurements of capillary pressure and volumetric water content, as well as the mass of each subsample, can be found in Appendix 3. Figure 10 contains a graphical representation of all these data points, plotted on the same scale. Error bars in the X-direction are based on the uncertainty of the water activity measurement. This instrument is accurate to ±0.003 $a_w$ (~0.4 MPa) between 0.04-0.97 $a_w$ (~ 440-4 MPa) and accurate to ±0.010 $a_w$ (~1.5 MPa) outside that range. Error bars in the Y-direction are based on the uncertainty of the volumetric water content. This uncertainty was primarily driven by the error associated with the bulk density determination. As a result, volumetric water content uncertainty is the greatest at ±0.009 $m^3m^{-3}$ for the Barnett Shale (Figure 10A), and the least at ±0.0009 $m^3m^{-3}$ for the Eagle Ford Shale (Figure 10D).

It should be noted that capillary pressure measurements whose calculated uncertainty was less than or equal to 1.3 MPa were not included in Figure 10 or in the regression analyses. This was due to the fact that there was no significant difference between a measurement that fell within this range and a measurement of 0.0 MPa. It can be seen in Figure 10 that, at least visually, the different shale types appear to have different capillary pressure-saturation relationships. The slopes of the data points appear to be different in many cases and also the maximum water content values appear to be different. Also, a visual inspection of Figure 10 shows that there is little if any difference between the wetting and drying data points, indicating a lack of hysteresis. However, all of these visual trends must be confirmed with statistical analyses.

Overall, fewer measurements of capillary pressure were obtained while bringing a sample from oven dryness up to saturation than were taken when drying an initially saturated sample, most likely due to differences in methodology. In all cases, more data points exist in the low saturation/high capillary pressure range. This trend is more noticeable for the drying measurements and is important because as

noted in the introduction, shale formations typically have low initial water saturations (60% to less than 30%) prior to the production of oil or gas. Combined with the larger uncertainty associated with measuring capillary pressure at high saturations, this means that the water activity meter functions better at the saturations applicable to oil and gas producing shales.

From the paired measurements of capillary pressure and volumetric water content, three sets of Brooks and Corey (1964) parameters were obtained for all shale types for both wetting and drying, except for the grey Chattanooga and the black Chattanooga Shale which had two sets of parameters for drying. Parameters for the grey Chattanooga Shale were not obtained because the regressions did not successfully converge. These parameters were obtained using fixed values of porosity for a given rock type, corresponding to the mean value of porosity, the greatest value of porosity, and the minimum value of porosity. All estimated parameters for each of these three fits, along with their corresponding $R^2$ value (indicating goodness of fit) can be found in Table 1, for the parameters estimated from wetting data, and Table 2 for parameters obtained from the drying data (all tables found in Appendix 1).

A possible explanation for the model not converging for the grey Chattanooga could be related to the concave down shape seen in its data points (Figure 10C), while all other shale types were concave up. This shape has been associated with so called pore-bridging clay minerals (Neasham, 1977). These are illite and smectite clays that swell, span pores, and reduce permeability (Neasham, 1977; Spencer, 1985). X-ray diffraction and scanning electron microscopy could be used in the future to ascertain the presence of these clays and determine if they are indeed pore-bridging. The presence of these clays reduces the permeability of the sample and would thus make this rock type unsuitable for development of oil or gas (Wu and Berg, 2003). Alternative explanations to this lack of fit could be due to improper handling of the subsamples, measurement error, or some other innate property of the rock. The grey Chattanooga Shale was the first material examined in this study and it could be possible that these samples were exposed to air in non-controlled circumstances (i.e. weighing) longer than later samples as experience was gained. Alternatively, as seen in Table 1, the grey Chattanooga Shale had the lowest porosity and TOC of all rock

types examined in this study, but it is not possible to correlate these properties to the inability of the regression to fit the model to the data.

To the best of the author's knowledge there are no published Brooks and Corey parameters for any of the shale types examined in this study. As such, no comparisons could be made between the values presented here and reported values from the literature. The mercury intrusion method does characterize the pore size distribution, but comparisons between pore size distributions are difficult to make when measured using different fluid systems (mercury/air and water/air) due to uncertainties in both the interfacial tensions and the contact angles of these fluid systems (Melrose et al., 1994). As noted in Chapter 1.3.5, SANS and USANS can be used to characterize the pore size distribution of shale, however these methods do not account for the interaction of water with the shale matrix and cannot be compared to the estimated pore size distributions from this study (Radlinski et al., 2004; Clarkson et al., 2013).

Figure 11 contains the predicted Brook and Corey (1964) relationships associated with the greatest $R^2$ value for all of the shale types examined in this study, in both the wetting and drying directions. The differences in the shapes of these fit lines illustrate how changes to the model parameters impact the overall capillary pressure-saturation relationship. For example, the steepness of the curve is related to the pore size distribution, with steeper curves having a narrower range of pore sizes and is most easily seen by comparing the Barnett or Eagle Ford Shale to all other shale types. The ability to extract estimates of the pore size distribution from capillary pressure measurements is important as it can be related to permeability (Minagawa et al., 2009). Furthermore, recovery efficiency decreases with greater variation in pore sizes (Vavra et al., 1992; Jang and Santamarina, 2011). Assessing differences in the pore size distribution index values for the different shale types could be used to explain differences in production rates from each of these reservoirs. Also, differences can be seen in the air/water entry pressure (the junction between the linear and curved portions of the predicted fits). These pressure values are important in the estimation of oil recovery which in turn can help determine the economic feasibility of a well in a given rock type (Vavra et al., 1992; Morsy et al., 2014). When examining the parameters

associated with the best fit for each shale type, the Eagle Ford Shale was the only shale type that had an estimated value for residual water content greater than zero. For all of the other shale types Equation (5) best fitted the data with a value of zero for the residual water content. A residual value of zero was to be expected, especially when estimated from measurements made in the high capillary pressure, low saturation region, as evidence suggests that non-zero values of residual water content may be artifacts of the measurement process (Ward and Morrow, 1987; Melrose et al., 1994).

Figure 12 contains all paired measurements of capillary pressure and water content for each rock type and the three Brooks and Corey (1964) fits obtained from those measurements plotted on the same scale, along with the associated $R^2$ value for each fit. The best fit for both the Mancos Shale (Figure 12 D) and the black Chattanooga Shale (Figure 12 B) came from using the maximum value of porosity measured for that rock type in the regression analysis. When the mean value of porosity was used for the regression analysis for these rock types, several of the water content measurements fall well above Brooks and Corey (1964) fit line. If the mean value of porosity is assumed to be the true value of porosity then these points represent saturations of greater than 100%, which is not possible. These data points were measured immediately after immersion in water for 2 weeks and could be related to free water on the surface of the samples. However, the samples were wiped with a damp tissue (Chem-Wipe) in order to remove as much of this water as possible.

An alternative explanation for these points is related to the data processing. One shortcoming of the method used for this study was pooling all subsamples of a given rock type together for the regression analysis. The primary advantage of this was obtaining sufficient data for the regression to successfully converge. The major disadvantage was that this necessitated applying a single value of porosity to all subsamples during the regression. As a result, much of the heterogeneity in the material is lost.

The Brooks and Corey (1964) fits using the minimum value of porosity for both the Eagle Ford Shale (Figure 12 C) and the Marcellus Shale from Pennsylvania (Figure 12 E), while not the best fit for these rock types, are conforming to localized peaks of higher water contents which could be indicative of

a more bi-modal distribution of pore sizes in these rock types instead of the continuous distribution that the model requires. Finally, as Figure 12 F shows, the three Brooks and Corey (1964) fits for the Marcellus Shale from West Virginia were identical except for the water entry pressure. This is related to the inaccuracies of the water activity meter at high saturations and the fitting process. This inability to accurately estimate the water entry pressure is disappointing as imbibition, or a wetting fluid (water) displacing a non-wetting fluid (air here, gas/oil in a reservoir), is an important oil recovery mechanism (Takahashi and Kovscek, 2010; Morsy and Sheng, 2014).

Comparisons between the estimated Brooks and Corey (1964) parameters obtained from wetting data can be found in Figure 13. Only shale types with a best Brooks and Corey (1964) fit obtained using the mean value of porosity were compared. Comparisons were performed by evaluating the 95% confidence limits for the estimated parameters. The Eagle Ford Shale and Barnett Shale had statistically different values for both the water entry pressure and pore size distribution index, while the Marcellus Shale samples from both locations had non-different values for those parameters. This was expected as the Marcellus Shale samples should have similar properties, and the other shale types should have different parameters as they are from different formations. These differences support accepting the hypothesis that the different shale types would have different Brooks and Corey (1964) parameters [i.e. rejecting the null hypothesis that the different shale types would have similar Brooks and Corey (1964) parameters] as would be expected from shales which were deposited at different times, have different compositions, and have differing estimates of ultimate recovery of oil and gas (U.S. Energy Information Administration., 2011).

Figure 14 contains all paired measurements of capillary pressure and water content for each rock type, as well as the three Brooks and Corey (1964) fits obtained from those measurements plotted on the same scale, along with the associated $R^2$ value for each fit. In all cases, the model fit the drying data better than the wetting data for a given rock type as evidenced by the higher $R^2$ values. This may be due to having more measurements of capillary pressure in the drying direction than in the wetting direction.

The best fit for both the Barnett Shale (Figure 14 A) and the Mancos Shale (Figure 14 D) came from using the maximum value of porosity for the regression analysis. Similar to the wetting fits, the air entry value in many cases (Figures 14 C, E, and F) had to be estimated from data points well below saturated water content. This is again related to inaccuracies in the water activity meter at high saturations. Inaccurate determinations of the air entry value could lead to poor estimates of sealing potential of a rock unit (Vavra et al., 1992). Also, notable is the fit for the Marcellus Shale from Pennsylvania (Figure 14 E). There are two distinct groupings of data points on either side of the Brooks and Corey (1964) fit lines which are most likely due to heterogeneities in the subsamples or from the utilization of three additional subsamples for the drying measurements that were larger than the three used in both the wetting and drying measurements. However, fitting the Brooks and Corey (1964) model to the three larger subsamples and three smaller subsamples alone produced non-different parameter estimates.

Comparisons between the estimated Brooks and Corey (1964) parameters obtained from drying data can be found in Figure 15. Only shale types with a best Brooks and Corey (1964) fit obtained using the mean value of porosity were compared. Eagle Ford Shale and the black Chattanooga Shale had different pore size distributions from each other and both Marcellus types, while the Marcellus Shale samples has non different pore size distributions. This was expected as the Marcellus Shale samples should have similar properties, and the other shale types should have different parameters as they are from different formations. However, the Marcellus Shale samples did have different estimated air entry values which was not expected. This may be related to having more measurements near complete saturation for the Marcellus sample from Pennsylvania which would allow for a more accurate estimation of the air entry value. Overall though, the differences that existed between the estimated parameters for these rock types support the hypothesis that the different shale types would have different Brooks and Corey (1964) parameters [i.e. support rejecting the null hypothesis that they would have similar parameters].

When examining the 95% confidence limits of the estimated Brooks and Corey (1964) parameters associated with the best fit (highest $R^2$ value), no differences existed between the estimated parameters obtained from the wetting and drying data for a given shale type. This means that there is little evidence of hysteresis in these samples, and disproves the hypothesis that there would be a difference between the wetting and drying parameters [i.e. accept the null hypothesis that the parameters would be similar]. In a study on sewage sludge amended soils by Ojeda et al. (2006), using essentially the same method, hysteresis was also not pronounced, suggesting that vapor wetting and drying may not produce hysteresis to the same extent that liquid wetting and drying does. In mercury capillary pressure measurements, the only other method which measures similarly high values of capillary pressure, lack of hysteresis has been suggested as being indicative of measurement error (Kale et al., 2010). However, there is no indication that measurement error was a factor in the present study or the one by Ojeda et al. (2006).

Figure 16 shows the measured versus predicted water contents for all shale types. While not a perfect 1:1 relationship, there appears to be less dispersion in the lower water content region, the area in which the water activity meter is more accurate, than at higher water contents. As such, it is most likely the inability to accurately estimate the air/water entry value that is driving this deviation from a 1:1 fit. If this is the case, then the water activity meter is accurately characterizing the pore size distribution index and the residual water content. This is important as these properties are important for estimating both permeability and both expected rates of recovery and ultimate recovery of oil/gas from a reservoir (Vavra et al., 1992; Minagawa et al., 2009; Jang and Santamarina, 2011). Overall, the high $R^2$ value associated with this fit indicated that the water activity meter can be used to collect capillary pressure-saturation data that can be accurately characterized by the Brooks and Corey (1964) model.

### 3.2 Shale Characterization

Average values of bulk density, matrix density, and porosity, along with their standard deviations for all of the shale types analyzed in this study, as well as representative published values for porosity, are

given in Table 3. Total organic carbon (TOC) measurements for all shale types, along with representative published values, can also be found in Table 3.

The Barnett Shale had the greatest porosity at 13.6% and the grey, inorganic Chattanooga Shale had the least porosity at 2.5%. Accounting for uncertainty of the measured values, all measured porosity values for all rock types, except Barnett Shale and the black, Chattanooga Shale, were within the range of published values of porosity for all rock types. Also, there is good agreement between the measured values and the published values for TOC. Large uncertainties were associated with the porosity values for both Chattanooga Shale types, both Marcellus Shale types, Barnett Shale, and Mancos Shale. It was thought that this could be caused by measuring bulk densities for these shale formations with the laser scanner as opposed to calipers, however the bulk density of the Barnett and Mancos Shale samples were measured with both the laser scanner and calipers and there was no significant difference between the two methods. An alternative explanation for the large uncertainties associated with these rock types could be greater heterogeneity in these samples; future work could focus on better characterizing the composition of these shale types. Also, water remaining in some subsamples of a given rock type and not others after the 24 hour drying period could also contribute to the uncertainties in these density measurements. However, the pre-drying water content was not measured and the impact of longer drying times was not assessed.

Oven dry masses were recorded both before wetting and again after complete saturation and subsequent air drying. All shale samples experienced a loss of mass after this process. This mass loss most likely occurred during the wetting portion of the measurements. Furthermore, four of the six subsamples of Mancos Shale visibly broke apart during wetting. This breakage most likely occurred along bedding planes, as these samples were cut perpendicular to bedding. An earlier study noted the failure of shale along bedding planes due to air entrapment and pressurization when shale was immersed in water (Schmitt et al., 1994). Vapor wetting was expected to prevent shale breakage (slaking), and in all but the four Mancos Shale subsamples, this proved true. The average percentage of mass lost by a given

shale type after wetting and drying is given in Table 3. The exact cause of this lost mass is unknown, but could be due to slaking, which has been shown to occur in shale with density values less than 2.34 g/cm$^3$ (Seedsman, 1986), dissolution, from the wetting process removing dust remaining from the cutting process, or from incomplete initial oven drying. If incomplete drying occurred, longer drying times for zero water content mass measurements would be necessary, while better cleaning of the core could be accomplished via compressed air cleaning, which would prevent any interactions between a cleaning fluid and the shale.

The results of the comparisons of bulk density, matrix density, and porosity for the shale types will now be discussed. These comparisons were made in order to both demonstrate that these different shale formations do indeed have different bulk properties and thus help prove the efficacy of the water activity meter in measuring the capillary pressure-saturation relationship of a wide range of shale types. This basic physical characterization also served as the starting point for the search for possible correlations between the physical properties of the shale and their estimated Brooks and Corey (1964) parameters. If correlations between these properties existed then it may be possible to predict Brooks and Corey (1964) parameters from wire-log data from wells. This would negate the need for laboratory measurements of capillary pressure and saturation along with the associated costs of those measurements.

The results of the Tukey's Studentized Range Test for bulk density can be found in Table 4. The mean value of bulk density for the Marcellus Shale samples from both Pennsylvania and West Virginia were not significantly different from each other or from the organic rich, black Chattanooga Shale. This is not surprising as the Marcellus Shale samples are from the same formation. However, the grey Chattanooga Shale, Eagle Ford Shale, and the Barnett Shale all have mean values of bulk density that are significantly different from all other shale types ($p<0.05$). As a result, the ANOVA and Tukey's Studentized Range Test results support accepting the hypothesis that the different shale types would have different values for bulk density [i.e. rejecting the null hypothesis that the different shale types would have similar values for bulk density].

The results of the Tukey's Studentized Range Test for matrix density can be found in Table 5. As with bulk density, the matrix density for the Marcellus Shale samples from both locations and the black, organic Chattanooga Shale were not significantly different from each other. This was the expected result because the Marcellus Shale samples are from the same formation, and the black Chattanooga Shale had similar TOC values. Also, the mean matrix density of the inorganic, grey Chattanooga Shale and the Mancos Shale were not significantly different from each other, but differed from all of the other samples. Again, these results might be explained by differences in TOC. The grey Chattanooga Shale and the Mancos Shale samples had the least organic carbon in this study and were not significantly different from one another in terms of matrix density, while the Barnett Shale, the only shale type that was significantly different from all the other shale types ($p<0.05$), had the greatest organic carbon content. The results of the ANOVA and this test support accepting the hypothesis that different shale types will have different matrix densities [i.e. rejecting the null hypothesis that the different shale types would have similar matrix densities].

Finally, the results of the Tukey's Studentized Range Test for porosity can be found in Table 6. In terms of the mean value of porosity, each shale type was not significantly different from at least two other shale types. This similarity in porosity may be the result of errors associated with the determination of both bulk density and matrix density, as the porosity values are calculated rather than measured. However, significant differences ($p<0.05$) did exist between the porosity value of each shale type and at least two other shale types. The ANOVA for this test was significant ($p<0.05$) and these results support accepting the hypothesis that the different shale types would have different porosities [i.e. rejecting the null hypothesis that the different shale types would have similar porosities].

Overall, it has been shown that these different shale types have different bulk properties. The major exceptions are the two Marcellus Shale types, which have non-different bulk properties because they are from the same formation. However, the two Chattanooga samples do have differing densities; they also have different values of TOC and are visually different (one is black, the other grey). As such,

no similarities were expected to exist for the two Chattanooga samples. These differences help support the claim that the water activity meter method can be used to characterize the capillary pressure-saturation relationship of shale since it has been statistically demonstrated that these shale types are different. Possible relationships between the shale densities, porosity, TOC, sample depths and estimated Brooks and Corey (1964) parameters were evaluated using linear regression. The only statistically significant ($p<0.05$) relationships were between TOC and bulk density and TOC and matrix density. This is not surprising as these properties have been correlated in the past, and density measurements from well logs have been used to predict TOC; these results support those claims (Kamali and Mirshady, 2004; Vernik and Milovac, 2011; Quirein et al., 2012). Figures 20 and 21 are plots of bulk density versus TOC and matrix density versus TOC, respectively. In both cases, TOC values increase with decreasing density, as expected. Unfortunately no statistically significant correlation could be found between any of the estimated Brooks and Corey (1964) parameters and the measured bulk properties. As a result, further characterization of the physical properties of these shale types should be carried out in order to determine if Brooks and Corey (1964) parameters can be predicted from physical properties.

# Chapter 4 – Summary and Conclusions

The overall goal of this study was to test the efficacy of the water activity meter method for characterization of capillary pressure-saturation relationships of samples from a range of shale formations. In order to test the efficacy of this method, seven different shale types were examined: Eagle Ford, Barnett, Mancos, Marcellus, from Pennsylvania and West Virginia, an organic rich, black colored Chattanooga Shale, and a grey colored, inorganic Chattanooga Shale. These shale types represent a range of oil and gas producing shale formations within the United States. As such, an accurate characterization of the capillary pressure-saturation relationship, which is used for determining reservoir quality and modeling fluid flow, for these rock types is economically important.

Several petrophysical properties were also examined as part of this study. Determinations of bulk density, matrix density, porosity, and total organic carbon were carried out on each of the shale types. These measurements were both necessary for the characterization of the capillary pressure-saturation relationship and were made to assess any differences between the shale types. This was important because a range of materials needed to be examined in order to demonstrate the efficacy of the water activity meter method. These measurements also provided statistical evidence of differences existing between several of the shale types. The two Marcellus Shale samples had non-significantly different values of matrix density, bulk density, and porosity as would be expected.

The TOC correlated negatively with both bulk density and matrix density as expected because solid organic matter has a much lower density than clay minerals. Measured porosity values for the different shale types ranged from 2% to nearly 17%. For all shale types, except the black Chattanooga and Barnett Shale, the mean value of porosity fell within the reported range of porosities for that shale type. Overall, significant differences existed in the values of bulk density, matrix density, and porosity for all shale types. With these differences, it was expected that the different shale types would have different capillary pressure – saturation relationships, and this is the case, as can be clearly seen in Figure 10.

It was expected that the Brooks and Corey (1964) equations would be able to fit the capillary pressure-saturation data in order to parameterize the capillary pressure-saturation relationship. These parameters are important as they can be used to model flow within a reservoir (Olafuyi et al., 2008; Altundas et al., 2011). The Brooks and Corey (1964) equations were fitted to both the wetting and drying measurements of capillary pressure using segmented, non-linear regression in SAS (2012) in order to estimate the pore size distribution index, the air/water entry pressure, and the residual water content of each of the shale types. The regression analysis was able to estimate the Brooks and Corey (1964) parameters for all shale types examined in this study except for the grey, inorganic Chattanooga Shale. Goodness of fit was assessed using the coefficient of determination ($R^2$) and for several of the fits, was greater than 0.90. No evidence for hysteresis was found, thus rejecting the hypothesis that the Brooks and Corey (1964) parameters would be different between wetting and drying for a given shale type. It was thought that the lack of hysteresis was due to vapor wetting and drying rather than experimental or measurement error. In all cases, except for the Eagle Ford Shale, the regression estimated a residual water content of zero. This was expected as evidence suggests that there is no residual water content at high capillary pressure values (Melrose et al., 1994). The estimated Brooks and Corey (1964) parameters were not significantly different between the two Marcellus Shale types except for the air entry value. This was also expected as these two rock types, although from different locations, were from the same rock formation and should have similar properties. Differences did exist in the estimated Brooks and Corey (1964) parameters between several of the shale types as was hypothesized and could be used to explain differences in oil recovery efficiency or be used for reservoir characterization. However, there were no correlations between the bulk physical properties examined and any of the estimated Brooks and Corey (1964) parameters.

Overall, this work accomplished the goal of characterizing the capillary pressure-saturation relationship of various shale types using a water activity meter. This has been shown through the successful parameterization of demonstrably different shale types with high goodness of fit values. Also,

these different shale types had significantly different Brooks and Corey (1964) parameters, except for the two Marcellus Shale samples. In all cases, except for the Eagle Ford Shale there was an estimation of zero residual water content. In proving the efficacy of the water activity meter, this study also served as a test bed for a method of measuring capillary pressure that has been essentially unused until now for lithified material. One shortcoming of the method outlined herein was the lack of characterization at the subsample scale. This led to difficulties in both the ability to compare different shale types to one another and obfuscated any heterogeneities within a given shale type.

In the future, Brooks and Corey (1964) fits should be made at the subsample scale which would allow for more accurate parameterization, allow for more robust statistical comparisons to be made both within and between shale types, and would minimize the impact of experimental error. Future work should also focus on finding a material whose capillary pressure – saturation relationship can be measured by both the water activity meter and a more established method, such as the centrifuge method, so that the measurements from both methods can be compared. Also, a more controlled method of wetting and drying shale samples needs to be developed in order to both prevent fractures forming within samples, and to have more measurements of capillary pressure at intermediate saturations. Capillary pressure measurements could also be made at higher temperatures in order to better mimic reservoir conditions as the capillary pressure-saturation relationship will change with temperature (Bachmann and van der Ploeg, 2002). Finally, capillary pressure measurements for more rock types should be taken, along with a more complete characterization of their physical properties, in order to establish criteria for when the water activity meter is a more appropriate method than the traditional methods for measuring capillary pressure.

# References

Aguilera, R. 2014. Flow units: From conventional to tight-gas to shale-gas to tight-oil to shale-oil reservoirs. SPE Reserv. Eval. Eng. 17(02): 190–208

Altundas, Y.B., T.S. Ramakrishnan, N. Chugunov, and R. de Loubens. 2011. Retardation of $CO_2$ caused by capillary pressure hysteresis : A new $CO_2$ trapping mechanism. SPE J. 16(4): 784–794.

Bachmann, J., and R.R. van der Ploeg. 2002. A review on recent developments in soil water retention theory: Interfacial tension and temperature effects. J. Plant Nutr. Soil Sci. 165(4): 468–478.

Brooks, R.H., and A. Corey. 1964. Hydraulic properties of porous media. Hydro Paper No. 3. Colorado State University: 37 pp.

Bruner, K.R., and R. Smosna. 2011. A comparative study of the Mississippian Barnett Shale, Fort Worth Basin, and Devonian Marcellus Shale, Appalachian Basin. U.S. Dept. of Energy: 118 pp.

Cancela, J.J., J. Dafonte, E.M. Martínez, T.S. Cuesta, and X.X. Neira. 2006. Assessment of a water activity meter for rapid measurements of soil water potential. Biosyst. Eng. 94(2): 285–295.

Chareonsuppanimit, P., Mohammad, S. A., Robinson, R. L., & Gasem, K. A.M. 2012. High-pressure adsorption of gases on shales: Measurements and modeling. International Journal of Coal Geology, 95: 34–46.

Chenevert, M. 1970a. Shale alteration by water adsorption. J. Pet. Technol. 22(9): 1141–1148.

Chenevert, M.E. 1970b. Shale control with balanced-activity oil-continuous muds. J. Pet. Technol. 22(10): 1309–1316.

Christoffersen, K.R., and C.H. Whitson. 1995. Gas/oil capillary pressure of chalk at elevated pressures. SPE Form. Eval. 10(3): 153–159.

Churcher, P. L. 1991. Rock properties of Berea Sandstone, Baker Dolomite, and Indiana Limestone. p. 431-466. *In* SPE International Symposium on Oilfield Chemistry. Society of Petroleum Engineers. Anaheim, California, USA

Clarkson, C., J. Jensen, and T. Blasingame. 2011. Reservoir Engineering for unconventional gas reservoirs: What do we have to consider? Paper SPE 145080. 45 pp. *In* SPE North American Unconventional Gas Conference and Exhibition. The Woodlands, Texas, USA.

Clarkson, C.R., N. Solano, R.M. Bustin, A.M.M. Bustin, G.R.L. Chalmers, L. He, Y.B. Melnichenko, A.P. Radliński, and T.P. Blach. 2013. Pore structure characterization of North American shale gas reservoirs using USANS/SANS, gas adsorption, and mercury intrusion. Fuel 103: 606–616.

Dehghanpour, H., H. a. Zubair, A. Chhabra, and A. Ullah. 2012. Liquid intake of organic shales. Energy & Fuels 26(9): 5750–5758.

Dewhurst, D.N., R.M. Jones, and M.D. Raven. 2002. Microstructural and petrophysical characterization of Muderong Shale: application to top seal risking. Pet. Geosci. 8(4): 371–383.

Donaldson, E.C., N. Ewall, and B. Singh. 1991. Characteristics of capillary pressure curves. J. Pet. Sci. Eng. 6(3): 249–261.

Dong, Z., Holditch, S.A., and D.A. Mcvay. 2013. Resource evaluation for shale gas reservoirs. SPE Economics & Management, 5(1), 5–16.

Fetter, C.W. 2001. Applied Hydrogeology. Fourth Ed. Prentice-Hall, Inc., Upper Saddle River, New Jersey.

Flint, L.E. 2003. Physical and hydraulic properties of volcanic rocks from Yucca Mountain, Nevada. Water Resour. Res. 39(5): 1–13.

Forsans, T., and L. Schmitt. 1994. Capillary forces: The neglected factor in shale instability studies? Paper SPE 28029. p. 71–84. *In* Proceedings of Rock Mechanics in Petroleum Engineering. Society of Petroleum Engineers, Delft, Netherlands.

Fredlund, D.G., and A. Xing. 1994. Equations for the soil-water characteristic curve. Can. Geotech. J. 31(3): 521–532.

Gee, G.W., M.D. Campbell, G.S. Campbell, and J.H. Campbell. 1992. Rapid measurement of low soil-water potentials using a water activity meter. Soil Sci. Soc. Am. J. 56(4): 1068–1070.

Ghezzehei, T.A., T.J. Kneafsey, and G.W. Su. 2007. Correspondence of the Gardner and van Genuchten-Mualem relative permeability function parameters. Water Resour. Res. 43(10): 7 pp.

Glover, L. 1954. Chattanooga Shale investigations along the Sequatchie Anticline of Tennessee and Alabama. U.S. Dept. of the Interior Geological Survery: 38 pp.

Green, R.T., G. Rice, and K.A. Meyer-James. 1995. Hydraulic characterization of hydrothermally altered Nopal Tuff. U.S. Nuclear Regulatory Commission: 68 pp.

Holditch, S. 1979. Factors affecting water Blocking and gas flow from hydraulically fractured gas wells. J. Pet. Technol. 31(12): 1515–1524.

Horsrud, P., B. Bostrom, E.F. Sonstebo, and R.M. Holt. 1998. Interaction between shale and water-based drilling fluids: Laboratory exposure tests give new insight into mechanisms and field consequences of KCl contents. Paper SPE 48986. p. 215–225. *In* Proceedings of SPE Annual Technical Conference and Exhibition. Society of Petroleum Engineers, New Orleans, Louisiana, USA.

Hunt, A.G. 2004. Percolative transport in fractal porous media. Chaos, Solitons & Fractals 19(2): 309–325.

Jang, J., and J.C. Santamarina. 2011. Recoverable gas from hydrate-bearing sediments: Pore network model simulation and macroscale analyses. J. Geophys. Res. Solid Earth 116(8): 1–12.

Jarrett, M.A., B. Gusler, T. Xiang, and D. Clapper. 2004. Improved competence in water activity measurement. Paper AADE-04-DF-HO-31. 8 pp. *In* AADE Technical Conference. Houston, Texas, USA.

Josh, M., L. Esteban, C. Delle Piane, J. Sarout, D.N. Dewhurst, and M.B. Clennell. 2012. Laboratory characterisation of shale properties. J. Pet. Sci. Eng. 88-89: 107–124.

Kale, S.V., C.S. Rai, and C.H. Sondergeld. 2010. Petrophysical characterization of Barnett Shale. p. 1–17. *In* SPE Unconventional Gas Conference. Society of Petroleum Engineers.

Kamali, M.R., and A.A. Mirshady. 2004. Total organic carbon content determined from well logs using ΔLogR and Neuro Fuzzy techniques. J. Pet. Sci. Eng. 45(3-4): 141–148.

King, G.E. 2012. Hydraulic fracturing 101: What every representative, environmentalist, regulator, reporter, investor, university researcher, neighbor and engineer should know about estimating frac risk and improving frac performance in unconventional gas and oil wells. 80 pp. *In* Proceedings of the SPE Hydraulic Fracturing Technology Conference. The Woodlands, Texas, USA.

Lal, M. 1999. Shale stability: Drilling fluid interaction and shale strength. Paper SPE 54356. 10 pp. *In* Proceedings of SPE Latin America and Caribbean Petroleum Engineering Conference. Society of Petroleum Engineers, Caracas, Venezuela.

Li, K. 2010. Analytical derivation of Brooks-Corey type capillary pressure models using fractal geometry and evaluation of rock heterogeneity. J. Pet. Sci. Eng. 73(1-2): 20–26

Li, K., and R.N. Horne. 2007. Systematic study of steam-water capillary pressure. Geothermics 36: 558–574.

Lu, X.C., Li, F.C., & Watson, A. T. 1995. Adsorption measurements in Devonian shales. Fuel, 74(4): 599–603.

Mastalerz, M., He, L., Melnichenko, Y. B., & Rupp, J. A. 2012. Porosity of coal and shale: Insights from gas adsorption and SANS/USANS techniques. Energy and Fuels, 26(8): 5109–5120.

McCullough, J.J., F.W. Albaugh, and P.H. Jones. 1944. Determination of the interstitial-water content of oil and gas sand by laboratory tests of core samples. p. 180–188. *In* Drilling and Production Practice. American Petroleum Institute, New York, NY, USA.

McLennan, J.D., J.C. Roegiers, and W.P. Marx. 1983. The Mancos Formation: An evaluation of the interaction of geological conditions. 10 pp. *In* SPE/DOE Low Permeability Gas Reservoirs Symposium. Society of Petroleum Engineers, Denver, Colorado, USA.

Melrose, J.C. 1987. Use of water vapor desorption data in the determination of capillary pressures. Paper SPE 16286. p. 465–475. *In* SPE International Symposium on Oilfield Chemistry. San Antonio, Texas, USA.

Melrose, J.C. 1988. Use of water-vapor desorption data in the determination of capillary pressures at low water saturations. SPE Reserv. Eng. 3(3): 913–918.

Melrose, J.C. 1990. Valid capillary pressure data at low wetting-phase saturations. SPE Reserv. Eng. 5(1): 95–99.

Melrose, J.C., J.R. Dixon, and J.E. Mallinson. 1994. Comparison of different techniques for obtaining capillary pressure data in the low-saturation region. SPE Form. Eval. 9(3): 185–192.

Minagawa, H., Y. Sakamoto, T. Komai, H. Narita, K. Mizutani, K. Ohga, N. Takahara, and T. Yamaguchi. 2009. Relation between pore-size distribution and permeability of sediment. p. 25–32. *In* Proceedings of the Nineteenth International Offshore and Polar Engineering Conference. Osaka, Japan.

Mody, F.K., and A.H. Hale. 1993. Borehole-stability model To couple the mechanics and chemistry of drilling-fluid/shale interactions. J. Pet. Technol. 45(11): 1093–1101.

Morrow, N.R., and G. Mason. 2001. Recovery of oil by spontaneous imbibition. Curr. Opin. Colloid Interface Sci. 6(4): 321–337.

Morsy, S., A. Gomma, and J.J. Sheng. 2014. Imbibition characteristics of Marcellus Shale Formation. 9 pp. *In* SPE Improved Oil Recovery Symposium. Society of Petroleum Engineers, Tulsa, Oklahoma, USA.

Morsy, S., A. Gomma, and J. J. Sheng. 2014. Improvement of Mancos Shale oil recovery by wettability alteration and mineral dissolution. 10 pp. *In* SPE Improved Oil Recovery Symposium. Society of Petroleum Engineers, Tulsa, Oklahoma, USA.

Morsy, S., and J.J. Sheng. 2014. Imbibition characteristics of the Barnett Shale Formation. 8 pp. *In* SPE Unconventional Resources Conference. The Woodlands, Texas, USA.

Mountain States Research and Development, & PRC Toups Corporation. 1978. Engineering assessment and feasibility study of chattanooga shale as a future source of uranium. U.S. Dept. of Energy: 218 pp.

Mull, C.G. 1995. Preliminary evaluation of the hydrocarbon source rock potential of the Tingmerkpuk Sandstone (Neocomian) and related rocks, northwestern De Long Mountains, Brooks Range, Alaska. State Alaska, Dep. Nat. Resour. Div. Geol. Geophys. Surv.: 22 pp.

Mullen, J. 2010. Petrophysical characterization of the Eagle Ford Shale in South Texas. 19 pp. *In* Canadian Unconventional Resources & International Petroleum Conference. Society of Petroleum Engineers, Calgary, Alberta, Canada.

Myers, T. 2012. Potential contaminant pathways from hydraulically fractured shale to aquifers. Groundwater 50(6): 872–882.

Neasham, J.J.W. 1977. The morphology of dispersed clay in sandstone reservoirs and its effect on sandstone shaliness pore space and fluid flow properties. 8 pp. *In* SPE Annual Fall Technical Conference and Exhibition of the Society of Peteroleum Engineers of AIME. Denver, Colorado, USA.

Newsham, K.E., J.A. Rushing, P.M. Lasswell, J.C. Cox, and T.A. Blasingame. 2004. A comparative study of laboratory techniques for measuring capillary pressures in tight gas sands. Paper SPE 89866. 11 pp. *In* Proceedings of SPE Annual Technical Conference and Exhibition. Society of Petroleum Engineers, Houston, Texas, USA.

Ojeda, G., E. Perfect, J.M. Alcañiz, and O. Ortiz. 2006. Fractal analysis of soil water hysteresis as influenced by sewage sludge application. Geoderma 134(3-4): 386–401.

Olafuyi, O., Y. Cinar, M. Knackstedt, and W. Pinczewski. 2008. Capillary pressure and relative permeability of small cores. 10 pp. *In* SPE/DOE Improved Oil Recovery Symposium. Tulsa, Oklahoma, USA.

Oleas, A.M., C.E. Osuji, M.E. Chenevert, and M.M. Sharma. 2010. Entrance pressure of oil-based mud into shale: Effect of shale , water activity , and mud properties. SPE Drill. Complet. 25(1): 39–44.

Oppenheimer, J.R., A.G. Martin, and L.P. Walker. 1997. Measurements of air-filled porosity in unsaturated organic matrices using a pycnometer. Bioresour. Technol. 59(2-3): 241–247.

Penny, G., J. Pursley, and D. Holcomb. 2005. The application of microemulsion additives in drilling and stimulation results in enhanced gas production. 9 pp. *In* Proceedings of SPE Production Operations Symposium. Society of Petroleum Engineers.

Perfect, E., A.B. Kenst, M. Díaz-Zorita, and J.H. Grove. 2004. Fractal analysis of soil water desorption data collected on disturbed samples with water activity meters. Soil Sci. Soc. Am. J. 68(4): 1177–1184.

Purcell, W.R. 1949. Capillary pressures - their measurement using mercury and the calculation of permeability therefrom. J. Pet. Technol. 1(2): 39–48.

Quirein, J., E. Murphy, G. Praznik, J. Witkowsky, S. Shannon, and D. Buller. 2012. A comparison of core and well log data to evaluate porosity, toc, and hydrocarbon volume in the Eagle Ford Shale. 13 pp. *In* SPE Annual Technical Conference and Exhibition. Society of Petroleum Engineers, San Antonio, Texas, USA.

Radlinski, a. P., M. Mastalerz, a. L. Hinde, M. Hainbuchner, H. Rauch, M. Baron, J.S. Lin, L. Fan, and P. Thiyagarajan. 2004. Application of SAXS and SANS in evaluation of porosity, pore size distribution and surface area of coal. Int. J. Coal Geol. 59(3-4): 245–271.

Roen, J. B. 1984. Geology of the Devonian black shales of the Appalachian Basin. Organic Geochemistry, 5(4), 241–254.

Roen, J.B., and R.C. Kepferle. 1993. Petroleum geology of the Devonian and Mississippian black shale of Eastern North America. U.S. Geological Survey Bulletin 1909: 417 pp.

Roychaudhuri, B., T. Tsotsis, and K. Jessen. 2011. An experimental and numerical investigation of spontaneous imbibition in gas shales. Paper SPE 147652. 11 pp. *In* Proceedings of SPE Annual Technical Conference and Exhibition. Society of Petroleum Engineers, Denver, Colorado, USA.

Ross, D. J. K., & R. Marc Bustin. 2009. The importance of shale composition and pore structure upon gas storage potential of shale gas reservoirs. Marine and Petroleum Geology, 26(6): 916–927.

Sakhaee-Pour, A., and S.L. Bryant. 2014. Effect of pore structure on the producibility of tight-gas sandstones. Am. Assoc. Pet. Geol. Bull. 98(4): 663–694.

SAS Institute Inc. 2012. SAS/STAT Version 9.4 Cary, NC, USA. Computer Software.

Schmitt, L., T. Forsans, and F.J. Santarelli. 1994. Shale testing and capillary phenomena. Int. J. Rock Mech. Min. Sci. Geomech. 31(5): 411–427.

Schumacher, B.A. 2002. Methods for the determination of total organic carbon (TOC) in soils and sediments. U.S. Environ. Prot. Agency: 25 pp.

Seedsman, R. 1986. The behaviour of clay shales in water. Can. Geotech. J. 23(1): 18–22.

Selley, R.C. 1985. Elements of Petroleum Geology. First Ed. W. H. Freeman and Company.

Shang, S., R.N. Horne, and H.J. Ramey. 1995. Water vapor adsorption on geothermal reservoir rocks. Geothermics 24(4): 523–540.

Shikhov, I., and C.H. Arns. 2015. Evaluation of capillary pressure methods via digital rock simulations. Transp. Porous Media: 18 pp.

Sigal, R.F. 2013. Mercury capillary pressure measurements on Barnett core. SPE Reserv. Eval. Eng. 16(4): 432–442.

Skinner, L.M., and J.R. Sambles. 1972. The Kelvin equation- A review. J. Aerosol Sci. 3(3): 199–210.

Slobod, R.L., A. Chambers, and W.L. Prehn Jr. 1951. Use of centrifuge for determining connate water, residual oil, and capillary pressure curves of small core samples. J. Pet. Technol. 3(4): 127–134.

Spencer, C.W. 1985. Geologic aspects of tight gas reservoirs in the Rocky Mountain region. J. Pet. Technol. 37(7): 1308–1314.

Stevens, S., and V. Ruuskraa. 2009. Special report: Gas shale-1: Seven plays dominate North America activity. Oil Gas J.: 36–41.

Takahashi, S., and A.R. Kovscek. 2010. Spontaneous countercurrent imbibition and forced displacement characteristics of low-permeability, siliceous shale rocks. J. Pet. Sci. Eng. 71(1-2): 47–55.

Thomson, W. (Lord Kelvin) 1872. On the Equilibrium of Vapour at a Curved Surface of Liquid. Proc. R. Soc. Edinburgh 7: 63–68.

U.S. Energy Information Administration. 2011. Review of emerging resources: U.S. shale gas and shale oil plays. Washington D.C. 105 pp.

Vavra, C.L., J.G. Kaldi, and R.M. Sneider. 1992. Geological applications of capillary pressure: a review. Am. Assoc. Pet. Geol. Bull. 76(6): 840–850.

Vernik, L., and J. Milovac. 2011. Rock physics of organic shales. Lead. Edge 30(3): 318–323.

Wang, D., R. Butler, H. Liu, and S. Ahmed. 2011. Flow-rate behavior and imbibition in shale. Paper SPE 138521. SPE Reserv. Eval. Eng. 14(4): 505–512.

Wang, F.P., and R.M. Reed. 2009. Pore networks and fluid flow in gas shales. 8 pp. *In* SPE Annual Technical Conference and Exhibition. Society of Petroleum Engineers.

Ward, J., and N. Morrow. 1987. Capillary pressures and gas relative permeabilities of low-permeability sandstone. SPE Form. Eval. 2(3): 345–356.

Wu, T., and R.R. Berg. 2003. Relationship of reservoir properties for shaly sandstones based on effective porosity. Petrophysics 44(5): 328–341.

Zhang, J., J. Rojas, and D. Clark. 2008. Stressed-shale drilling strategy: Water-activity design improves drilling performance. Paper SPE 102498. SPE Drill. Complet. 23(4): 385–393.

Zhuang, J., J.F. McCarthy, E. Perfect, L.M. Mayer, and J.D. Jastrow. 2008. Soil water hysteresis in water-stable microaggregates as affected by organic Matter. Soil Sci. Soc. Am. J. 72(1): 212–220.

# Appendices

## Appendix 1 – Tables

Table 1: Estimated Brooks and Corey (1964) parameters for wetting. $\Psi_w$, $\theta_r$, and $\lambda$ values are estimated parameters with approximate standard errors from segmented regression analysis of capillary pressure-saturation data. $\phi$ values were fixed for the regression analysis. The top row for each rock type is estimated parameters from the minimum value of porosity, the middle row is the mean porosity for that rock type, and the bottom row is the maximum measured porosity. The shaded row for each rock type is the best fit and contains the parameters used for comparing $\Psi_w$, $\theta_r$, and $\lambda$ values between rock types.

| Shale Type (# of data pairs) | Water Entry ($\Psi_w$) (MPa) | Residual Water Content ($\theta_r$) (fraction) | Pore Size Distribution Index ($\lambda$) | Porosity ($\phi$) (fraction) | $R^2$ |
|---|---|---|---|---|---|
| Mancos (36) | 87.84 ± 37.26 | 0 | 1.27 ± 1.98 | 0.032 | 0.46 |
| | 29.04 ± 8.81 | 0 | 0.76 ± 0.24 | 0.063 | 0.84 |
| | 3.36 ± 0.22 | 0 | 0.40 ± 0.02 | 0.104 | 0.95 |
| Eagle Ford (36) | 28.38 ± 10.26 | 0.007 ± 0.006 | 3.34 ± 3.86 | 0.068 | 0.62 |
| | 2.61 ± 0.15 | 0.010 ± 0.002 | 1.54 ± 0.23 | 0.128 | 0.90 |
| | 2.56 ± 0.15 | 0.010 ± 0.002 | 1.54 ± 0.23 | 0.132 | 0.90 |
| Barnett (40) | 37.37 ± 25.98 | 0.019 ± 0.038 | 1.47 ± 2.52 | 0.109 | 0.85 |
| | 4.24 ± 0.36 | 0 | 0.39 ± 0.02 | 0.136 | 0.95 |
| | 2.27 ± 0.17 | 0 | 0.37 ± 0.02 | 0.169 | 0.95 |
| Chattanooga- Black (21) | 75.61 ± 11.27 | 0.008 ± 0.012 | 7.54 ± 27.3 | 0.020 | 0.36 |
| | 42.49 ± 12.19 | 0 | 1.06 ± 0.60 | 0.039 | 0.60 |
| | 1.35 ± 0.52 | 0 | 0.36 ± 0.06 | 0.067 | 0.66 |
| Chattanooga- Grey (21) | NA | NA | NA | 0.020 | NA |
| | | | | 0.025 | |
| | | | | 0.030 | |
| Marcellus- PA (19) | 38.94 ± 2.46 | 0.013 ± 0.005 | 4.13 ± 2.26 | 0.055 | 0.47 |
| | 0.88 ± 0.54 | 0 | 0.27 ± 0.06 | 0.081 | 0.56 |
| | 0.23 ± 0.20 | 0 | 0.27 ± 0.06 | 0.117 | 0.56 |
| Marcellus- WV (17) | 2.60 ± 0.88 | 0 | 0.26 ± 0.04 | 0.071 | 0.72 |
| | 1.12 ± 0.50 | 0 | 0.26 ± 0.04 | 0.092 | 0.72 |
| | 0.28 ± 0.18 | 0 | 0.26 ± 0.04 | 0.125 | 0.72 |

Table 2: Estimated Brooks and Corey (1964) parameters for drying. $\Psi_a$, $\theta_r$, and $\lambda$ values are estimated parameters with approximate standard errors from segmented regression analysis of capillary pressure-saturation data. $\phi$ values were fixed for the regression analysis. The top row for each rock type is estimated parameters from the minimum value of porosity, the middle row is the mean porosity for that rock type, and the bottom row is the maximum measured porosity. The shaded row for each rock type is the best fit and contains the parameters used for comparing $\Psi_a$, $\theta_r$, and $\lambda$ values between rock types.

| **Shale Type (# of data pairs)** | **Air Entry ($\Psi_a$) (MPa)** | **Residual Water Content ($\theta_r$) (fraction)** | **Pore Size Distribution Index ($\lambda$)** | **Porosity ($\phi$) (fraction)** | **$R^2$** |
|---|---|---|---|---|---|
| Mancos (63) | 118.1 ± 63.05 | 0.016 ± 0.033 | 4.00 ± 27.1 | 0.032 | 0.27 |
| | 22.38 ± 6.01 | 0 | 0.47 ± 0.10 | 0.063 | 0.85 |
| | 3.46 ± 0.22 | 0 | 0.34 ± 0.01 | 0.104 | 0.97 |
| Eagle Ford (78) | 4.11 ± 0.47 | 0.008 ± 0.003 | 1.20 ± 0.32 | 0.068 | 0.93 |
| | 2.34 ± 0.05 | 0.008 ± 0.001 | 1.19 ± 0.06 | 0.128 | 0.98 |
| | 2.28 ± 0.05 | 0.008 ± 0.001 | 1.19 ± 0.06 | 0.132 | 0.98 |
| Barnett (70) | 14.54 ± 2.30 | 0 | 0.47 ± 0.05 | 0.109 | 0.91 |
| | 5.02 ± 0.36 | 0 | 0.36 ± 0.01 | 0.136 | 0.96 |
| | 2.32 ± 0.10 | 0 | 0.34 ± 0.01 | 0.169 | 0.97 |
| Chattanooga- Black (54) | NA | NA | NA | 0.020 | NA |
| | 0.56 ± 0.22 | 0 | 0.19 ± 0.02 | 0.039 | 0.69 |
| | 2.26 ± 0.36 | 0.001 | 0.96 ± 0.28 | 0.067 | 0.66 |
| Chattanooga- Grey (61) | NA | NA | NA | 0.020 | NA |
| | | | | 0.025 | |
| | | | | 0.030 | |
| Marcellus- PA (69) | 21.23 ± 5.01 | 0 | 0.55 ± 0.10 | 0.055 | 0.46 |
| | 2.08 ± 0.45 | 0 | 0.30 ± 0.03 | 0.081 | 0.64 |
| | 0.60 ± 0.19 | 0 | 0.30 ± 0.03 | 0.117 | 0.64 |
| Marcellus- WV (44) | 1.16 ± 0.12 | 0 | 0.28 ± 0.01 | 0.071 | 0.95 |
| | 0.54 ± 0.07 | 0 | 0.28 ± 0.01 | 0.092 | 0.95 |
| | 0.16 ± 0.03 | 0 | 0.28 ± 0.01 | 0.125 | 0.95 |

Table 3: Summary of shale properties (average values ± standard deviations). Both bulk density and matrix density correlated with TOC at $p<0.05$ (Figures 8 and 9 respectively).

| Shale Type (# of samples) | Average Mass Loss (%) | Average Bulk Density ($g/cm^3$) | Average Matrix Density ($g/cm^3$) | Porosity (%) | | TOC (wt%) | |
|---|---|---|---|---|---|---|---|
| | | | | This Study (Min. & Max.) | Published Values | This Study*** | Published Values |
| Mancos** (4) | 1.15 ± 0.12 | 2.51 ± 0.08 | 2.68 ± 0.01 | 6.3 ± 3.3 (3.2, 10.4) | 6-8[b] | 1.32 | 0.4-3.1[b] |
| Eagle Ford* (3) | 0.43 ± 0.13 | 2.15 ± 0.01 | 2.46 ± 0.01 | 12.8 ± 0.7 (6.8, 13.2) | 3-12[c] | 5.09 | 0.7-5.4[c] |
| Barnett** (3) | 0.28 ± 0.03 | 1.96 ± 0.10 | 2.26 ± 0.02 | 13.6 ± 5.2 (10.9, 16.9) | 3-6[a] | 13.51 | 11-13[a] |
| Chattanooga-Black** (5) | 0.43 ± 0.12 | 2.40 ± 0.03 | 2.47 ± 0.004 | 3.9 ± 1.3 (2.0, 6.7) | 1.6[e] | 8.41 | 0.5-20 (average =4)[f] |
| Chattanooga-Grey** (5) | 0.66 ± 0.41 | 2.68 ± 0.05 | 2.75 ± 0.03 | 2.5 ± 2.7 (2.0, 3.0) | 1.6[e] | 0.44 | 0.5-20 (average =0.8)[f] |
| Marcellus-PA** (6) | 0.63 ± 0.17 | 2.34 ± 0.09 | 2.55 ± 0.07 | 8.1 ± 5.9 (5.5, 11.7) | 6-10[a] | 8.79 | 2-10[a] |
| Marcellus-WV** (5) | 0.62 ± 0.16 | 2.33 ± 0.19 | 2.56 ± 0.05 | 9.2 ± 5.7 (7.1, 12.5) | 6-10[a] | 6.36 | 2-10[a] |

Note: The number of samples refers to the number of samples used for the density measurements. Percent dissolution is the percent difference between the oven dry mass before sample wetting and drying, and the oven dry mass after sample wetting and drying. *= Bulk density calculated from caliper measurement of bulk volume. **=Bulk density calculated from 3D scanner measurement of bulk volume. ***=measured by Ellington and Associates Inc. a=Bruner and Smosna (2011). b=Morsy et al. (2014). c=Dong et al. (2013). d=Churcher (1991). e=Mountain States Research and Development and PRC Toups Corporation (1978). f=Roen (1984).

Table 4: Comparison of mean values for bulk density.

| Bulk Density Comparison | | | | |
|---|---|---|---|---|
| **Tukey Grouping** | | **Mean (g/cm$^3$)** | **N** | **Rock Type** |
| | A | 2.68 | 5 | Chattanooga Shale-Grey |
| | | | | |
| | B | 2.51 | 4 | Mancos Shale |
| | B | | | |
| C | B | 2.40 | 5 | Chattanooga Shale-Black |
| C | | | | |
| C | | 2.34 | 6 | Marcellus Shale-PA |
| C | | | | |
| C | | 2.33 | 5 | Marcellus Shale-WV |
| | | | | |
| | D | 2.15 | 3 | Eagle Ford Shale |
| | | | | |
| | E | 1.96 | 3 | Barnett Shale |

Note: This comparison is the result of a Tukey's Studentized Range Test. Tukey groupings with the same letter are not significantly different at $p<0.05$. ANOVA significant at $p<0.05$.

Table 5: Comparison of mean values for matrix density.

| Matrix Density Comparison | | | | |
|---|---|---|---|---|
| **Tukey Grouping** | | **Mean (g/cm$^3$)** | **N** | **Rock Type** |
| | A | 2.75 | 5 | Chattanooga Shale-Grey |
| | A | | | |
| | A | 2.68 | 4 | Mancos Shale |
| | | | | |
| | B | 2.56 | 5 | Marcellus Shale-WV |
| | B | | | |
| C | B | 2.55 | 6 | Marcellus Shale-PA |
| C | B | | | |
| C | B | 2.47 | 5 | Chattanooga Shale-Black |
| C | | | | |
| C | | 2.46 | 3 | Eagle Ford Shale |
| | | | | |
| | D | 2.26 | 3 | Barnett Shale |

Note: This comparison is the result of a Tukey's Studentized Range Test. Tukey groupings with the same letter are not significantly different at $p<0.05$. ANOVA significant at $p<0.05$.

Table 6: Comparison of mean values for porosity.

| Porosity Comparison | | | | | |
|---|---|---|---|---|---|
| **Tukey Grouping** | | | **Mean (fraction)** | **N** | **Rock Type** |
| | A | | 0.14 | 3 | Barnett Shale |
| | A | | | | |
| B | A | | 0.13 | 3 | Eagle Ford Shale |
| B | A | | | | |
| B | A | C | 0.09 | 5 | Marcellus Shale-WV |
| B | | C | | | |
| B | D | C | 0.08 | 6 | Marcellus Shale-PA |
| | D | C | | | |
| E | D | C | 0.06 | 4 | Mancos Shale |
| E | D | | | | |
| E | D | | 0.04 | 5 | Chattanooga Shale-Black |
| E | | | | | |
| E | | | 0.02 | 5 | Chattanooga Shale-Grey |

Note: This comparison is the result of a Tukey's Studentized Range Test. Tukey groupings with the same letter are not significantly different at $p<0.05$. ANOVA significant at $p<0.05$.

## Appendix 2 – Figures

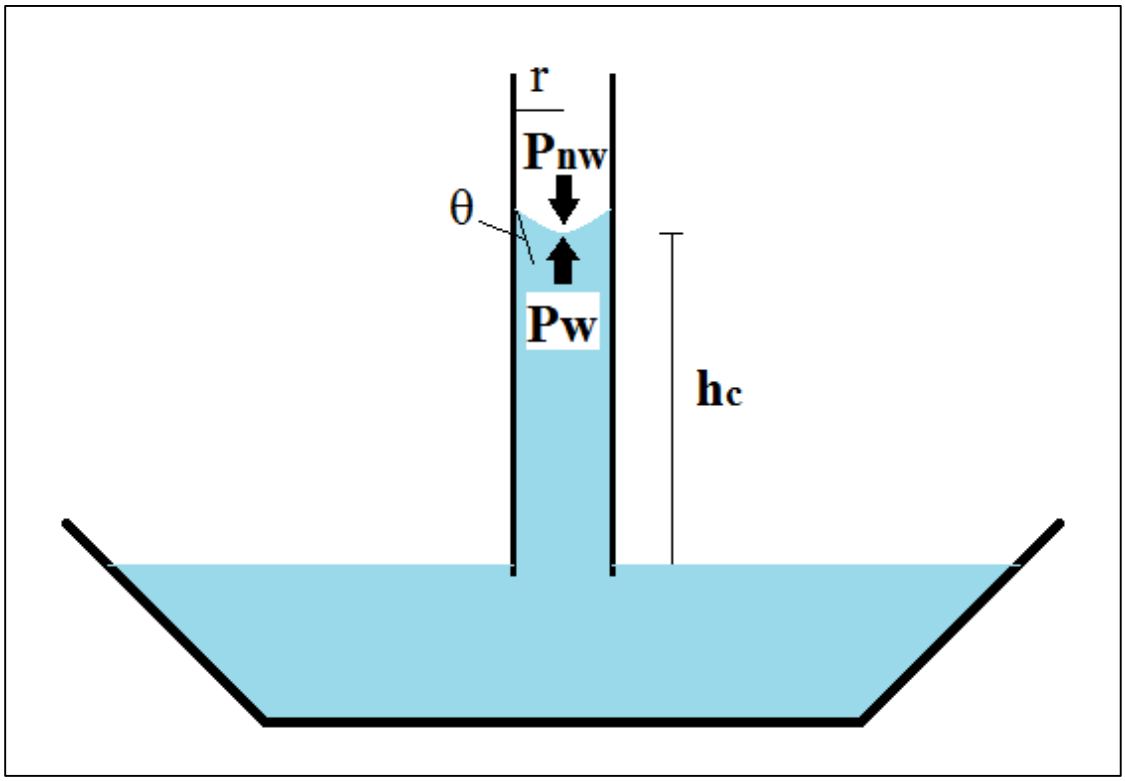


Figure 1: Capillary rise schematic. The wetting phase (blue) rises to height ($h_{c)}$ based on adhesive forces, the magnitude of which is determined by the interfacial tension between the solid and wetting phase, as well as the contact angle (θ). Capillary rise continues until the net adhesive forces drawing the liquid up the tube and the interfacial tension holding the liquid together in the center of the tube, are offset by gravity and the pressure of the non-wetting phase ($P_{nw}$). The meniscus is formed due to gravity and $P_{nw}$ and the height of the meniscus is equivalent to the radius (r) of the capillary tube. Capillary pressure ($P_c$) is the difference in pressure that exists across this meniscus ($P_c = P_{nw} – P_w$). Figure adapted from (Vavra et al., 1992; Fetter, 2001)

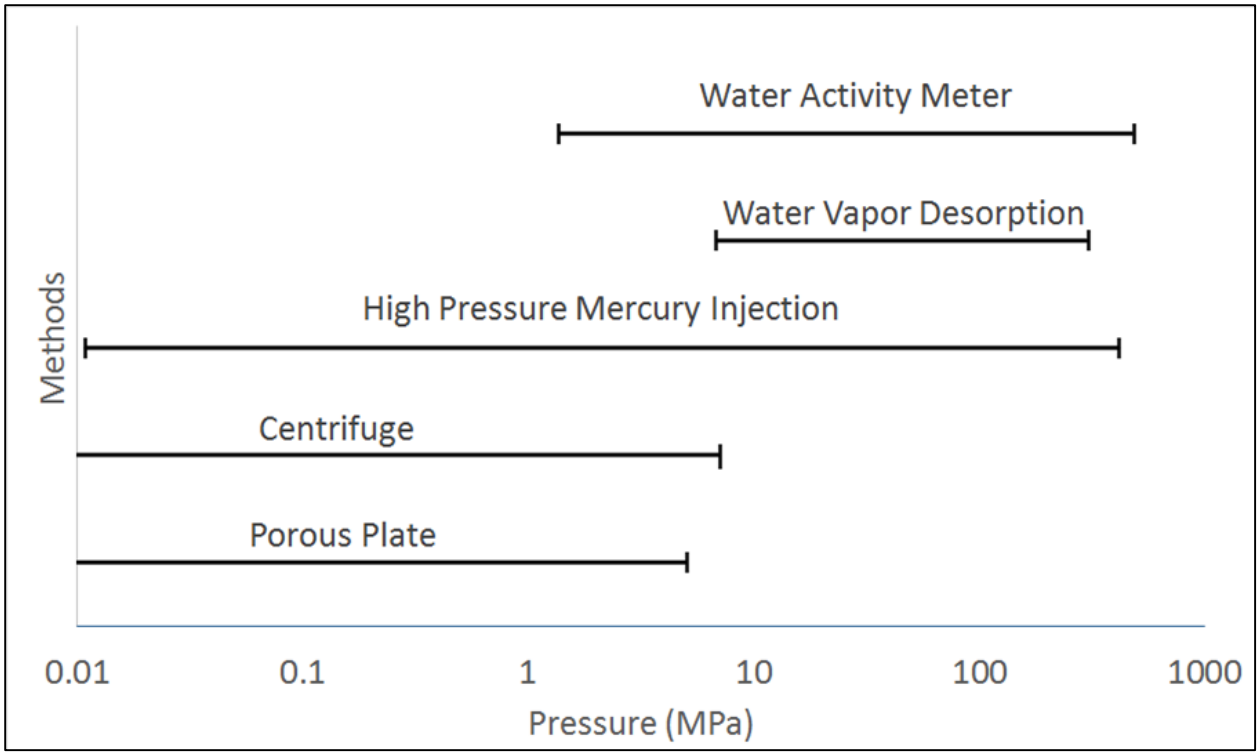


Figure 2: Accuracy ranges of various methods of measuring capillary pressure. Pressure ranges of all methods except water activity meter are from Newsham, (2004). Water activity meter accuracy range is from the manufacturer's specifications of the water activity meter used in this study (Novasina LabMaster-aw).

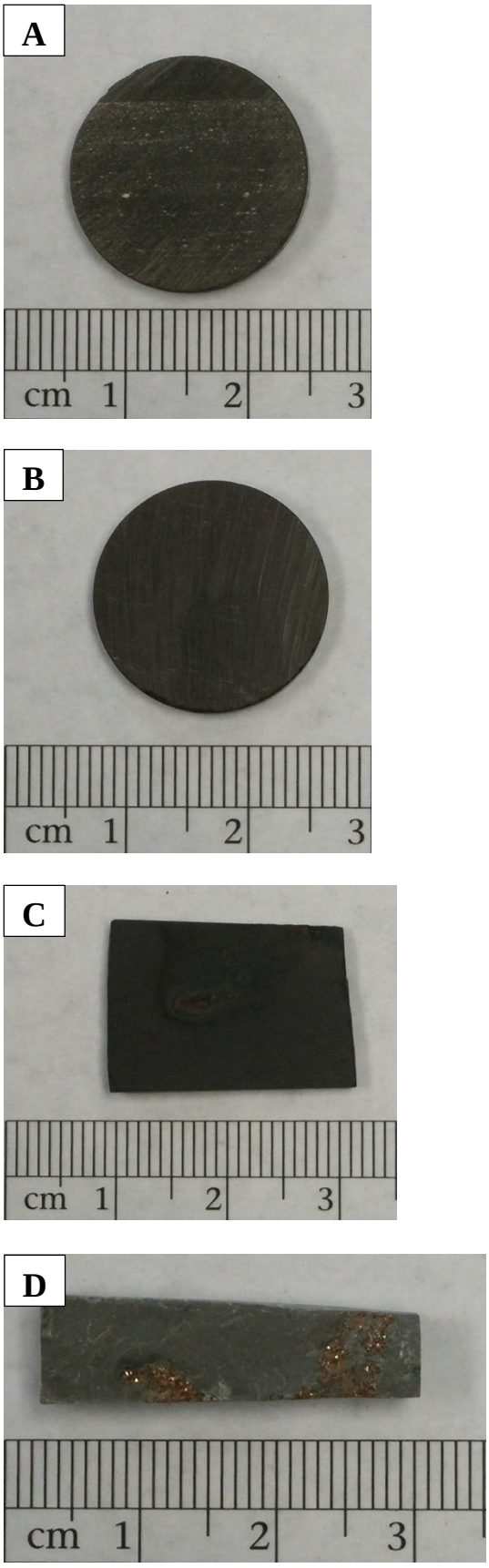


Figure 3: Representative subsamples of all shale types: (A) Eagle Ford, (B) Barnett, (C) Chattanooga- Black, (D) Chattanooga – Grey, (E) Mancos, (F) Marcellus- Pennsylvania, and (G) Marcellus- West Virginia. Note interbedding in (A) and (E), as well as pyrite grains on (D).

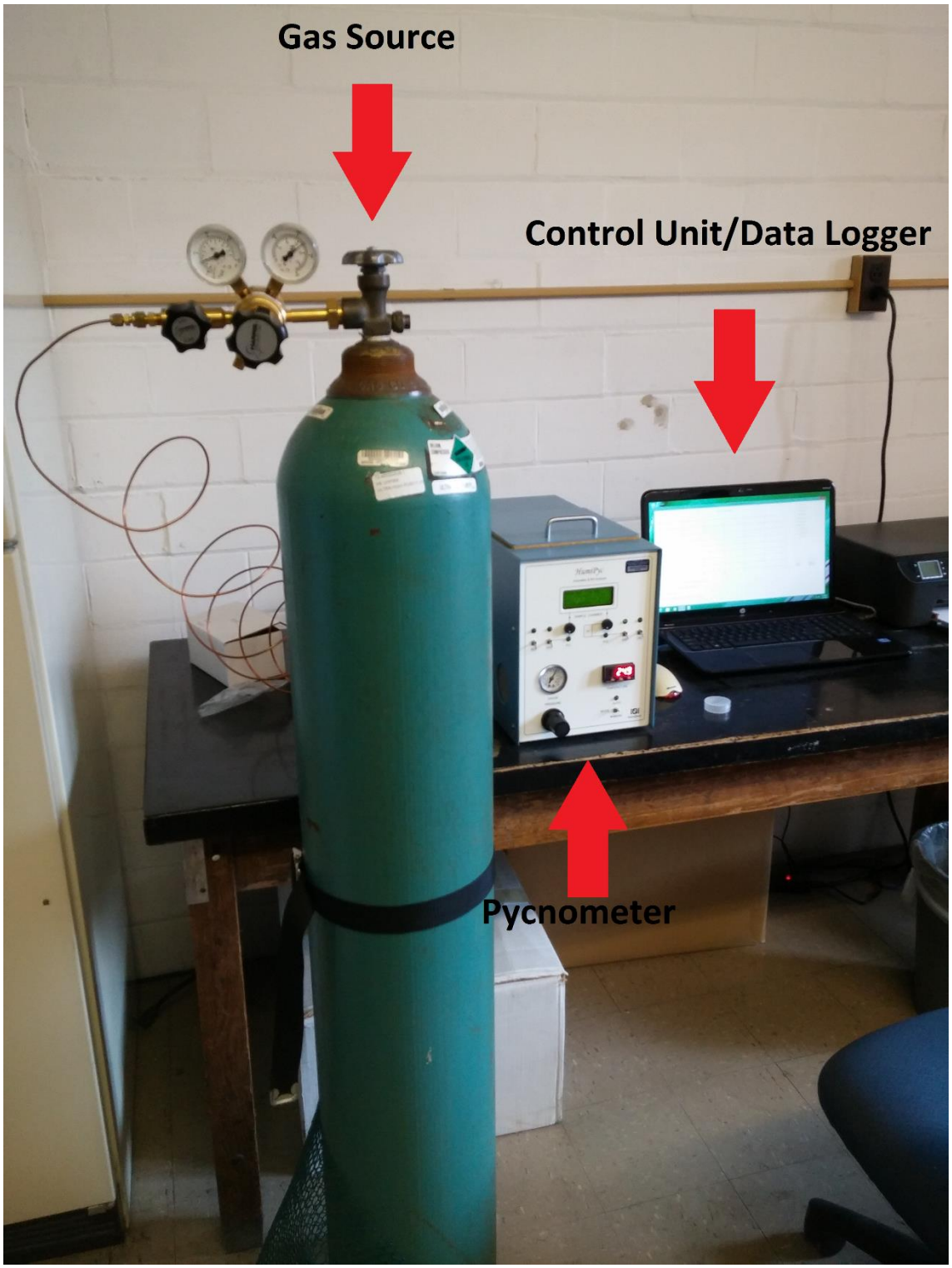


Figure 4: InstruQuest Inc. HumiPyc Gas Pycnometer

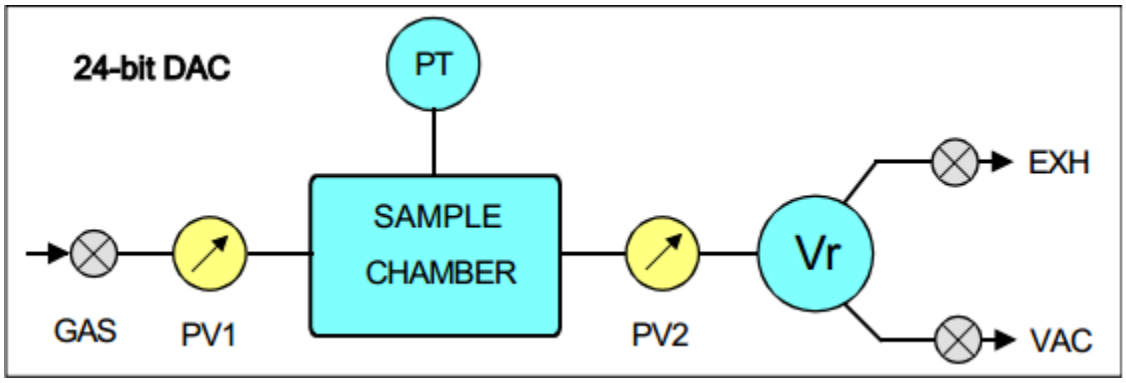


Figure 5: Schematic of Pycnometer (InstruQuest Inc., 2014). Operation is as follows: (1) Sample is placed in "Sample Chamber," (2) "PV1" (Pressure valve 1) is opened, allowing gas (helium) to flow into the "Sample Chamber," (3) "PV1" is closed when "PT" (Pressure Transducer) measures a predetermined gas pressure in the "Sample Chamber," (4)"PV2" (Pressure valve 2) is opened allowing gas from "Sample Chamber" to flow into "Vr" (Reference chamber of known volume), (5) "PT" measures the gas pressure of the connected "Sample Chamber" and "Vr," (6) helium is released through "EXH" (exhaust), (7) volume of free space in the "Sample Chamber" is calculated using ideal gas law, (8) process is repeated using an empty "Sample Chamber," (9) the matrix volume of the sample is the difference between the volume of the "Sample Chamber" containing the sample and the volume of the empty "Sample Chamber."

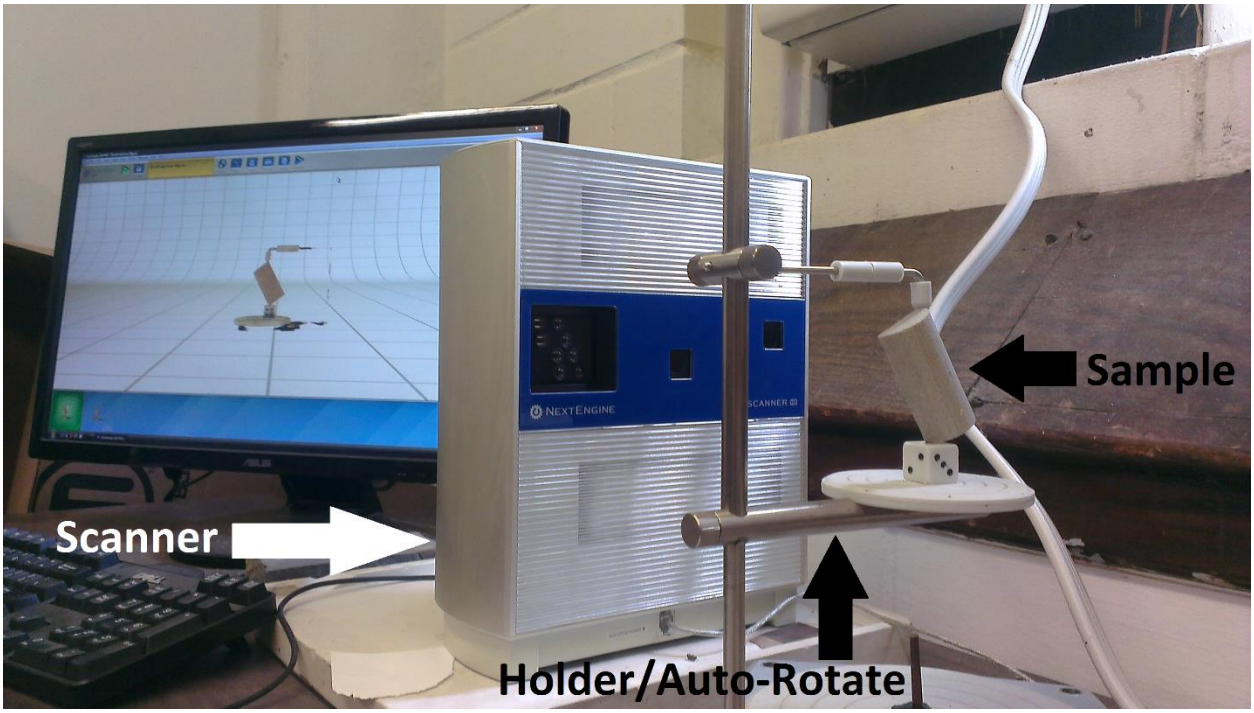

Figure 6: NextEngine Desktop 3D Scanner.

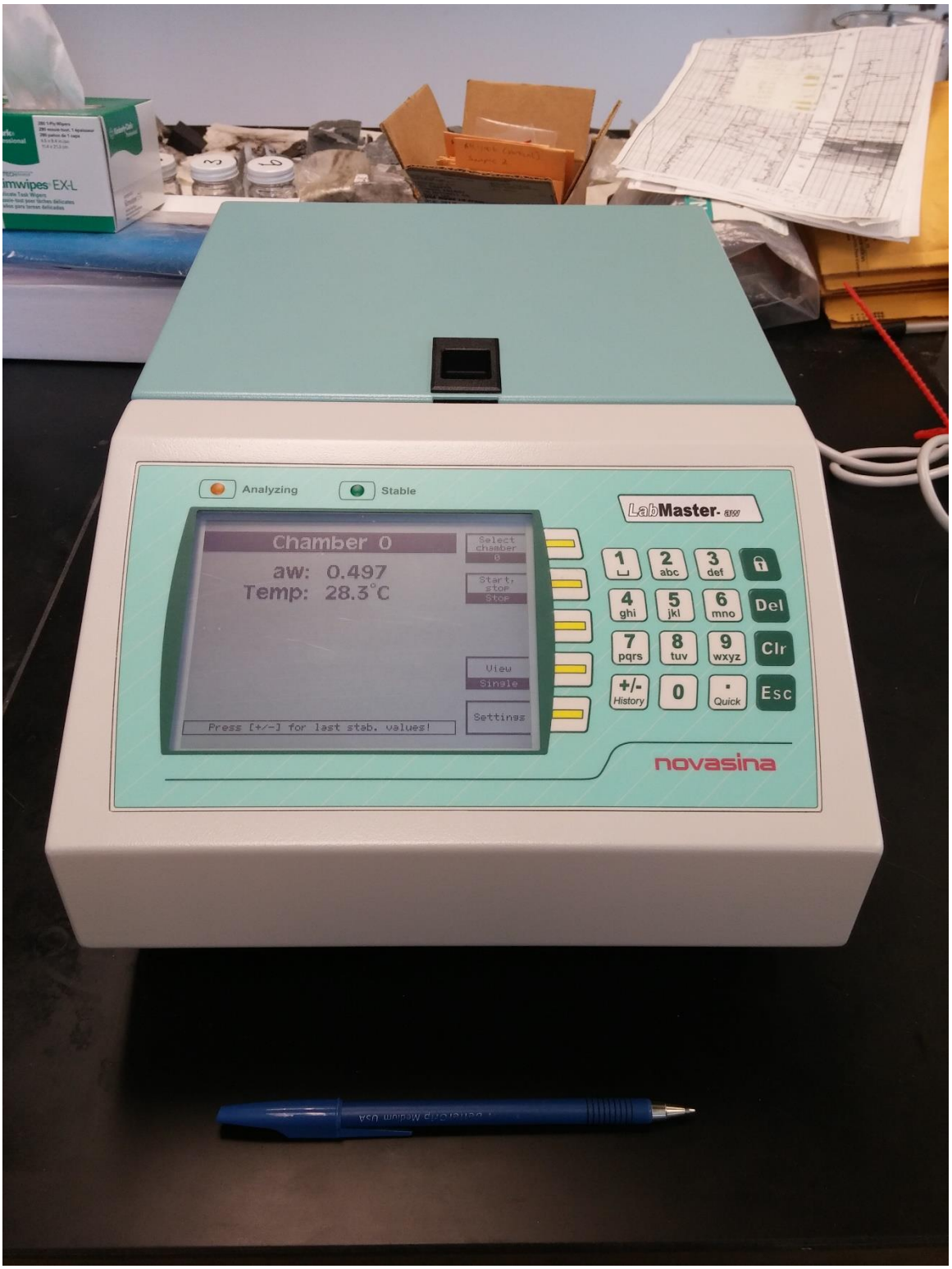


Figure 7: Novasina LabMaster-aw water activity meter (closed)


Figure 8: Water activity meter sensor and chambers (pen for scale)

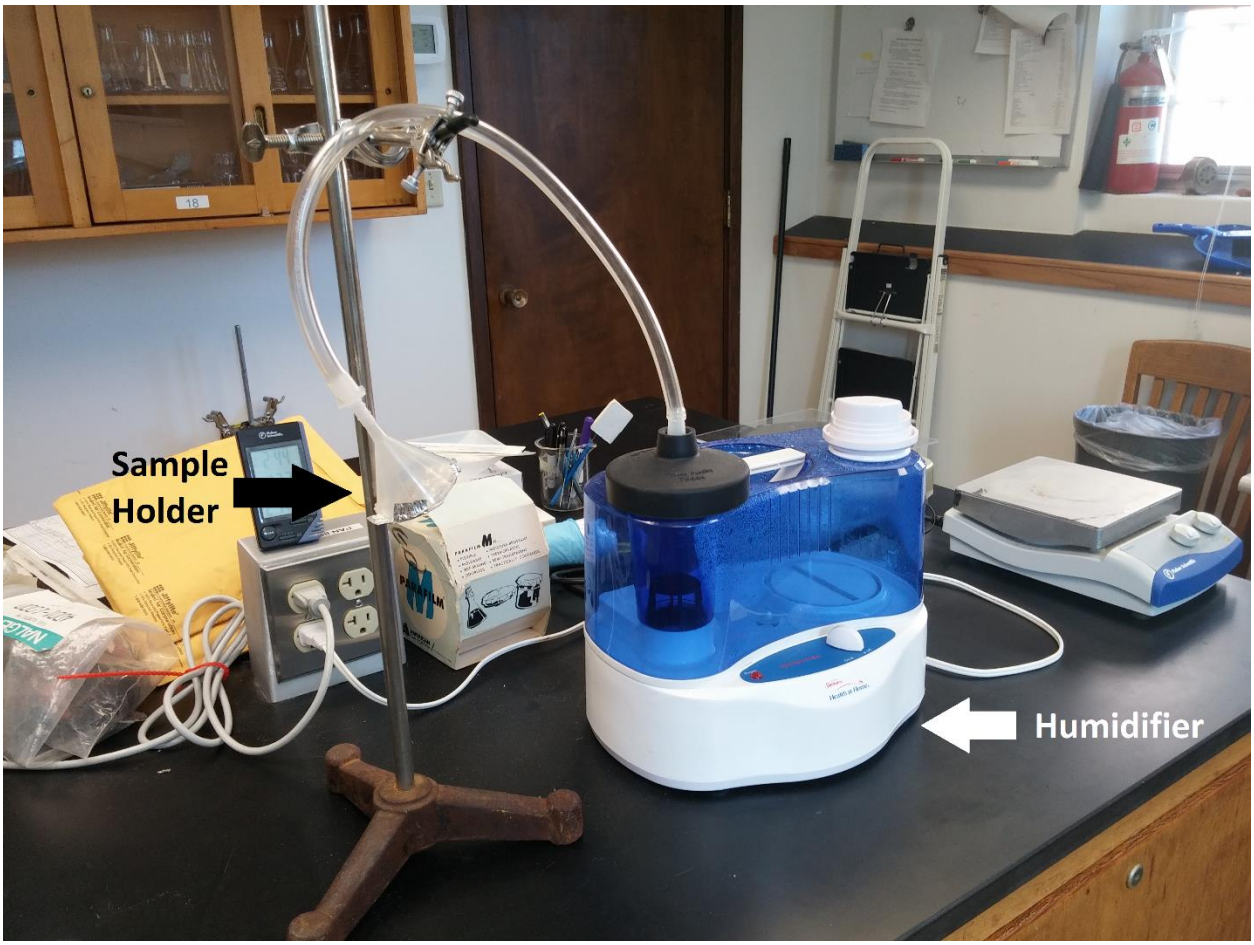

Figure 9: Ultrasonic humidifier used to wet samples

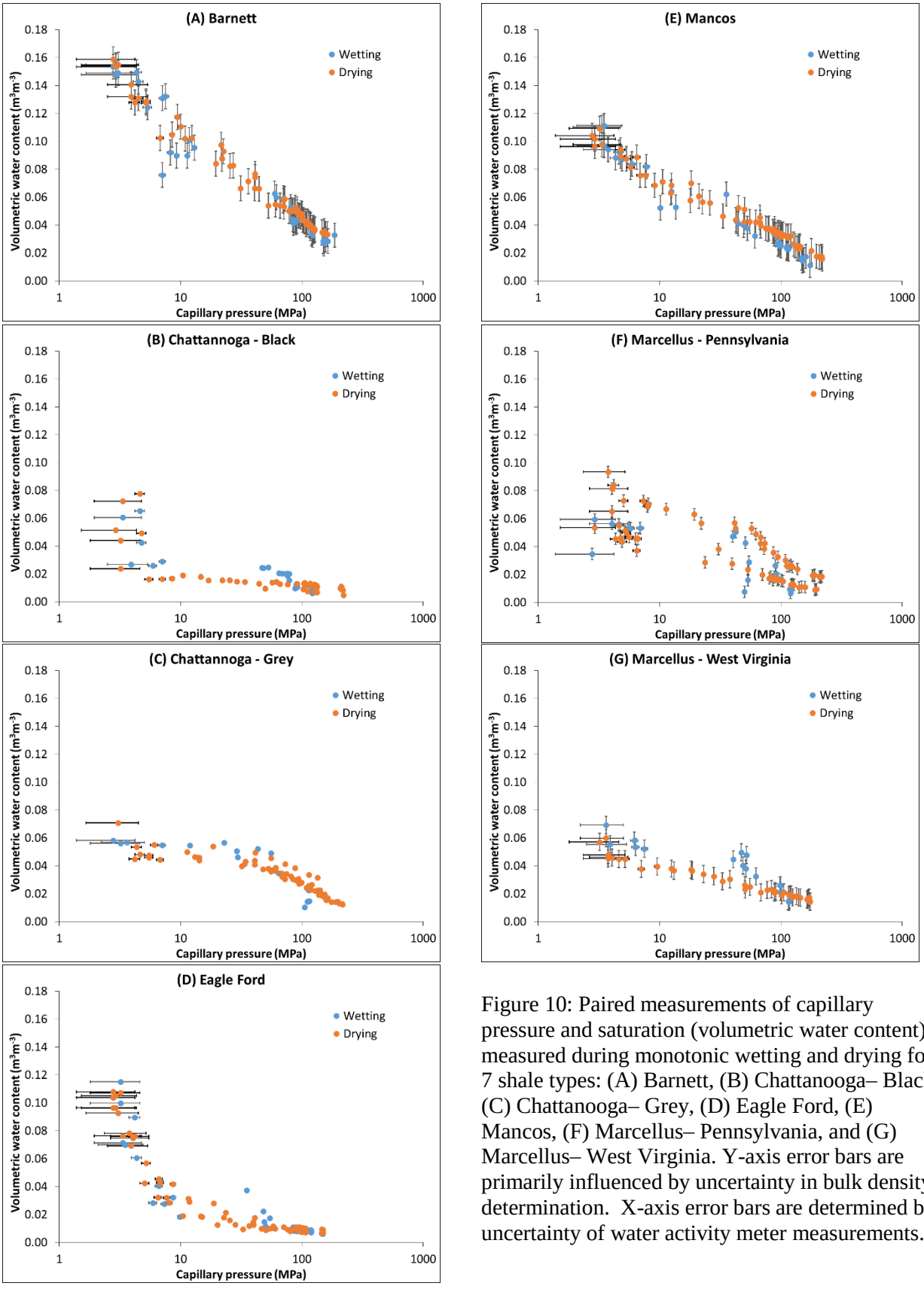


Figure 10: Paired measurements of capillary pressure and saturation (volumetric water content) measured during monotonic wetting and drying for 7 shale types: (A) Barnett, (B) Chattanooga– Black, (C) Chattanooga– Grey, (D) Eagle Ford, (E) Mancos, (F) Marcellus– Pennsylvania, and (G) Marcellus– West Virginia. Y-axis error bars are primarily influenced by uncertainty in bulk density determination. X-axis error bars are determined by uncertainty of water activity meter measurements.

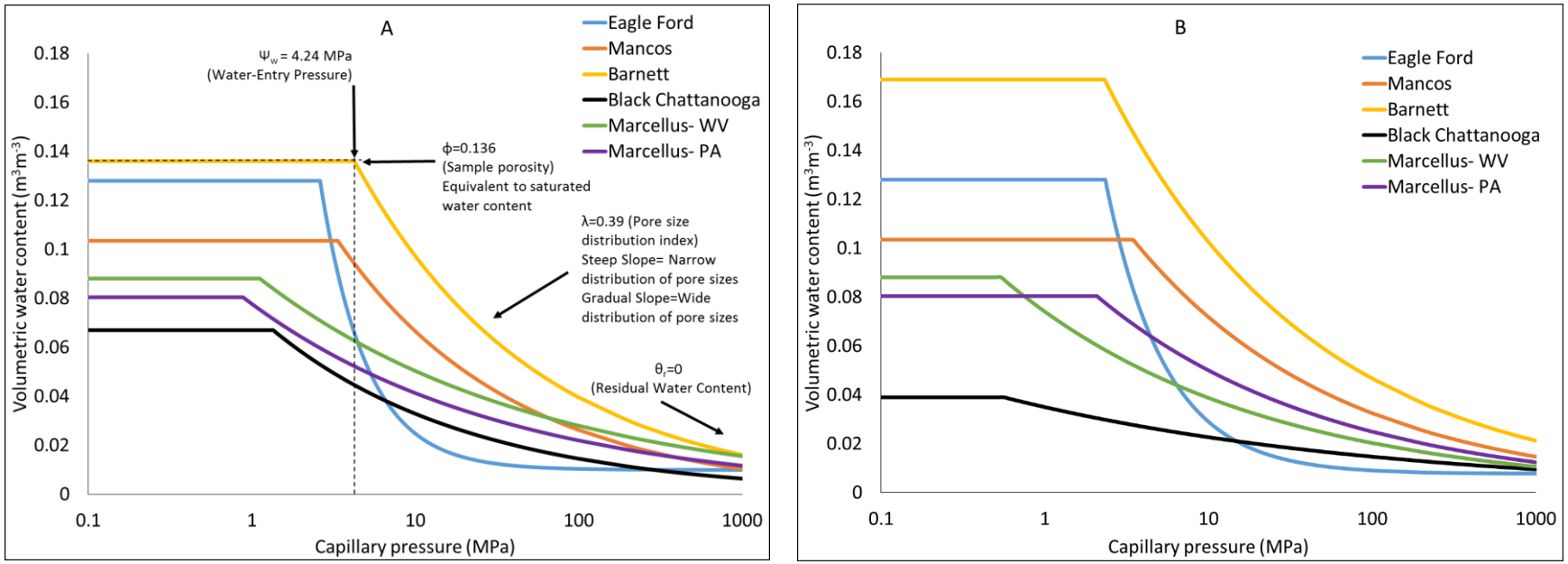


Figure 11: Predicted Brooks and Corey (1964) functions for wetting (A) and drying (B) for all shale types. These curves represent the best fit (highest $R^2$ value) for a given rock type; for parameters see Table 1 and Table 2. The wetting curve for Barnett Shale has been annotated with its Brooks and Corey (1964) parameters.

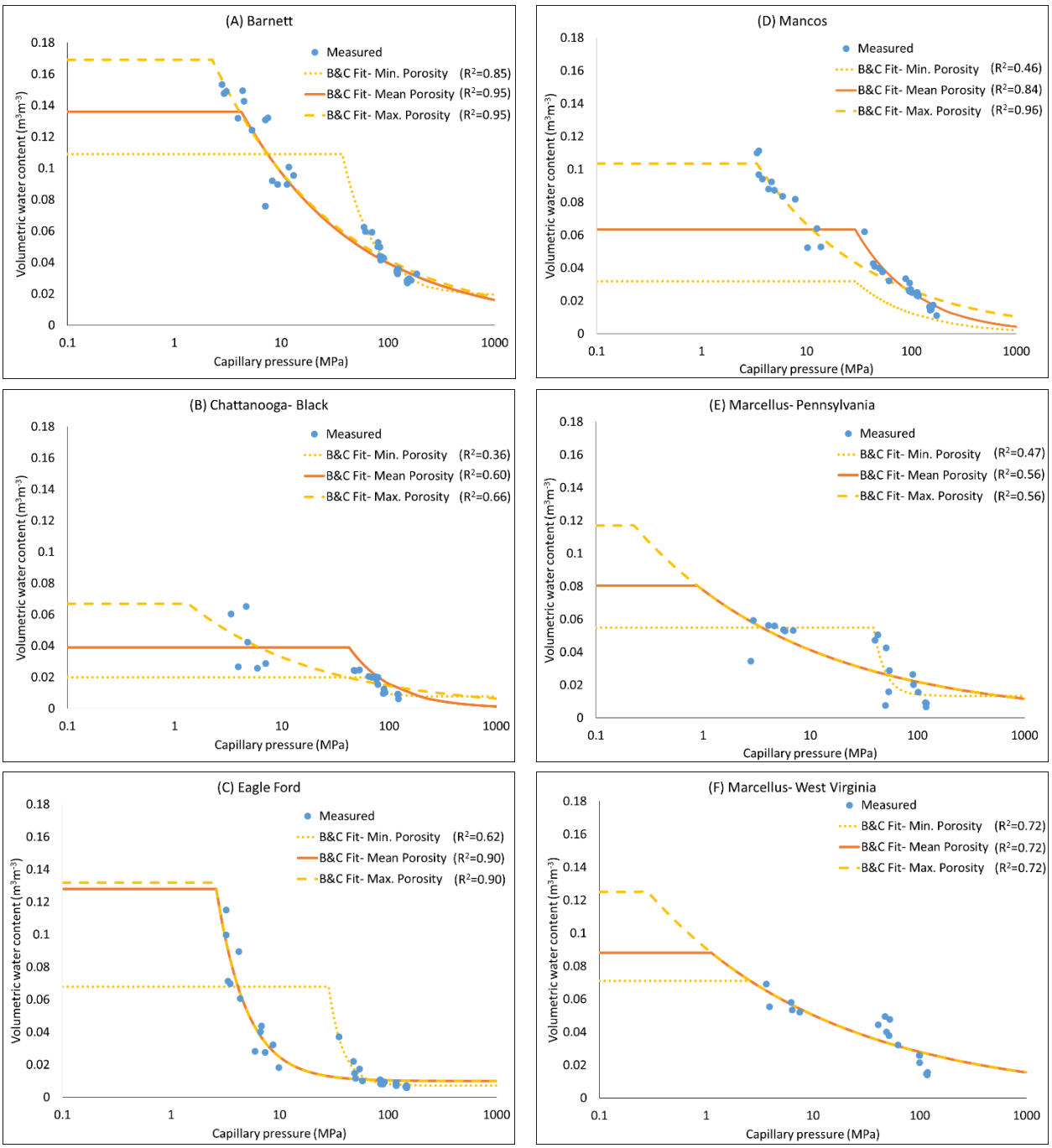


Figure 12: Brooks and Corey (1964) fits for wetting data using minimum value of porosity (dotted line), mean value of porosity (solid line), and maximum value of porosity (dashed line) for 7 shale types: (A) Barnett, (B) Chattanooga- Black, (C) Eagle Ford, (D) Mancos, (E) Marcellus- Pennsylvania, and (F) Marcellus- West Virginia. All parameters can be found in Table 1. The Brooks and Corey (1964) model did not successfully converge for the Chattanooga- Grey.

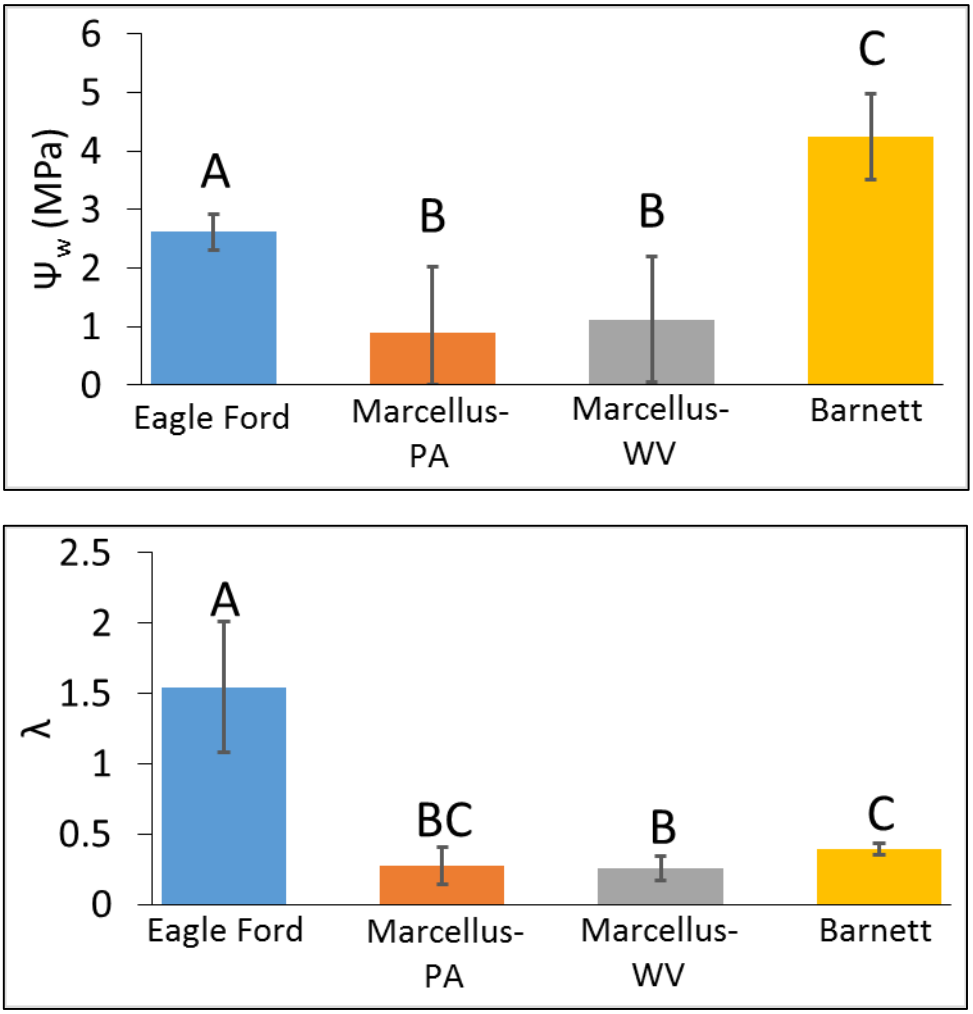


Figure 13: Comparison of Brooks and Corey (1964) parameters obtained from wetting data. Columns with the same letter are not significantly different from one another at 95% confidence level. Only shale types whose best Brooks and Corey fit (determined by $R^2$) were obtained using the mean value of porosity were compared.

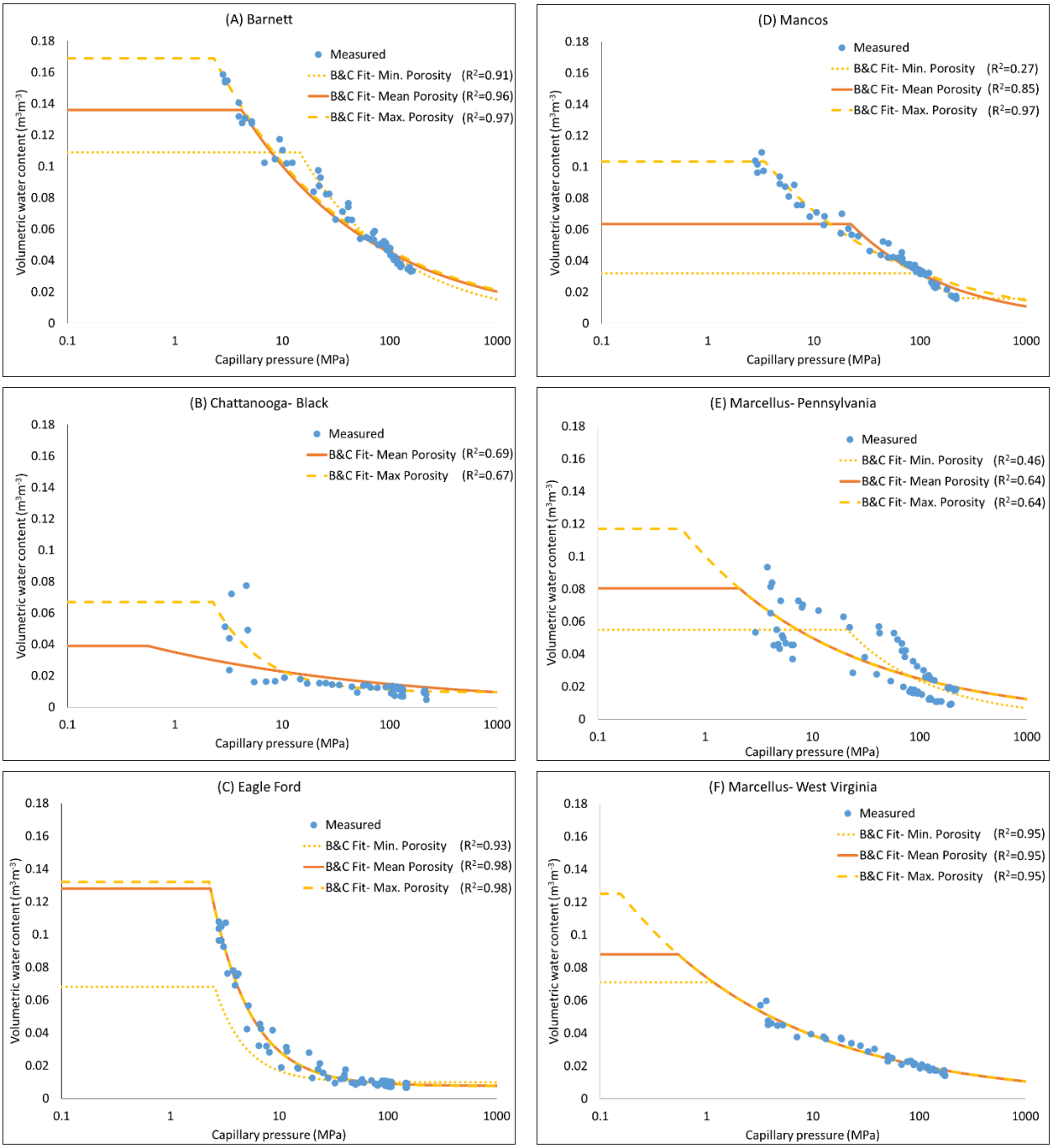


Figure 14: Brooks and Corey (1964) fits for drying data using minimum value of porosity (dotted line), mean value of porosity (solid line), and maximum value of porosity (dashed line) for 7 shale types: (A) Barnett, (B) Chattanooga- Black, (C) Eagle Ford, (D) Mancos, (E) Marcellus- Pennsylvania, and (F) Marcellus- West Virginia. All parameters can be found in Table 2. The Brooks and Corey (1964) model did not successfully converge for the Chattanooga- Grey or for the minimum porosity value of the Chattanooga- Black.

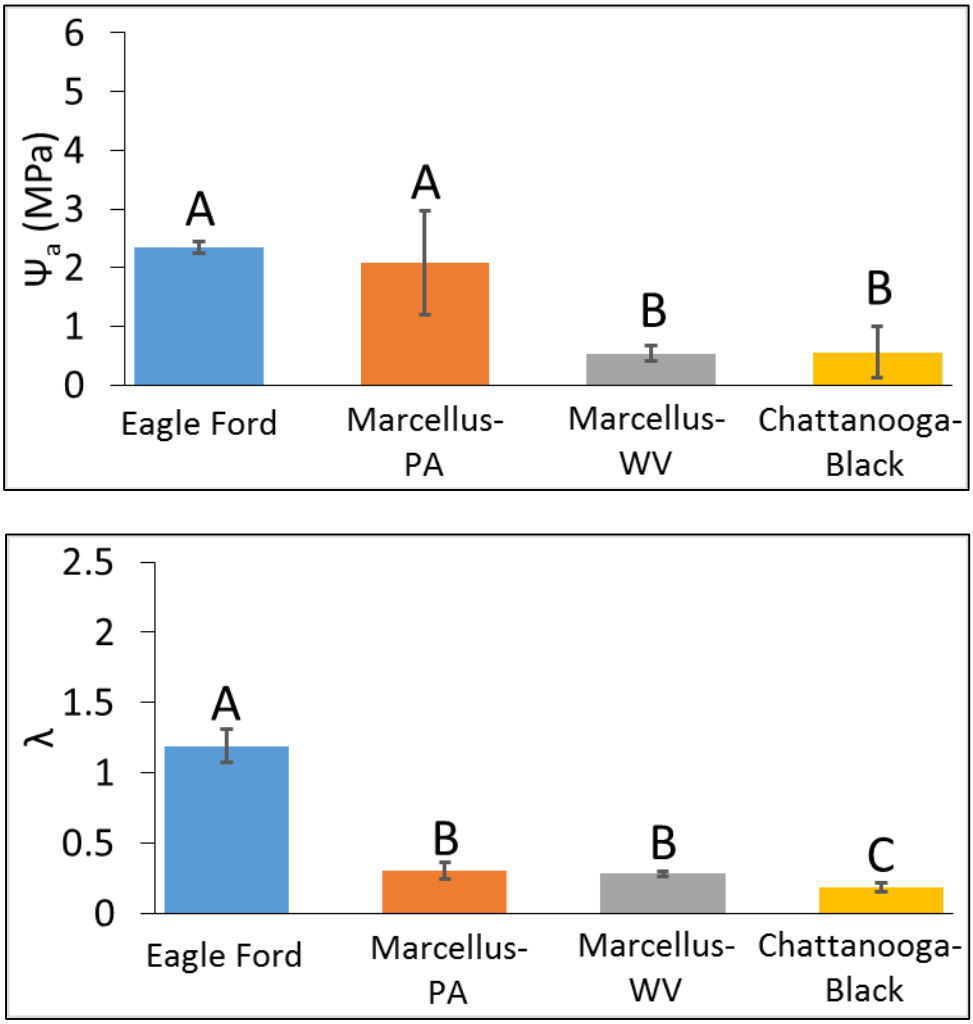


Figure 15 Comparison of Brooks and Corey (1964) parameters obtained from drying data. Columns with the same letter are not significantly different from one another at 95% confidence level. Only shale types whose best Brooks and Corey fit (determined by $R^2$) were obtained using the mean value of porosity were compared.

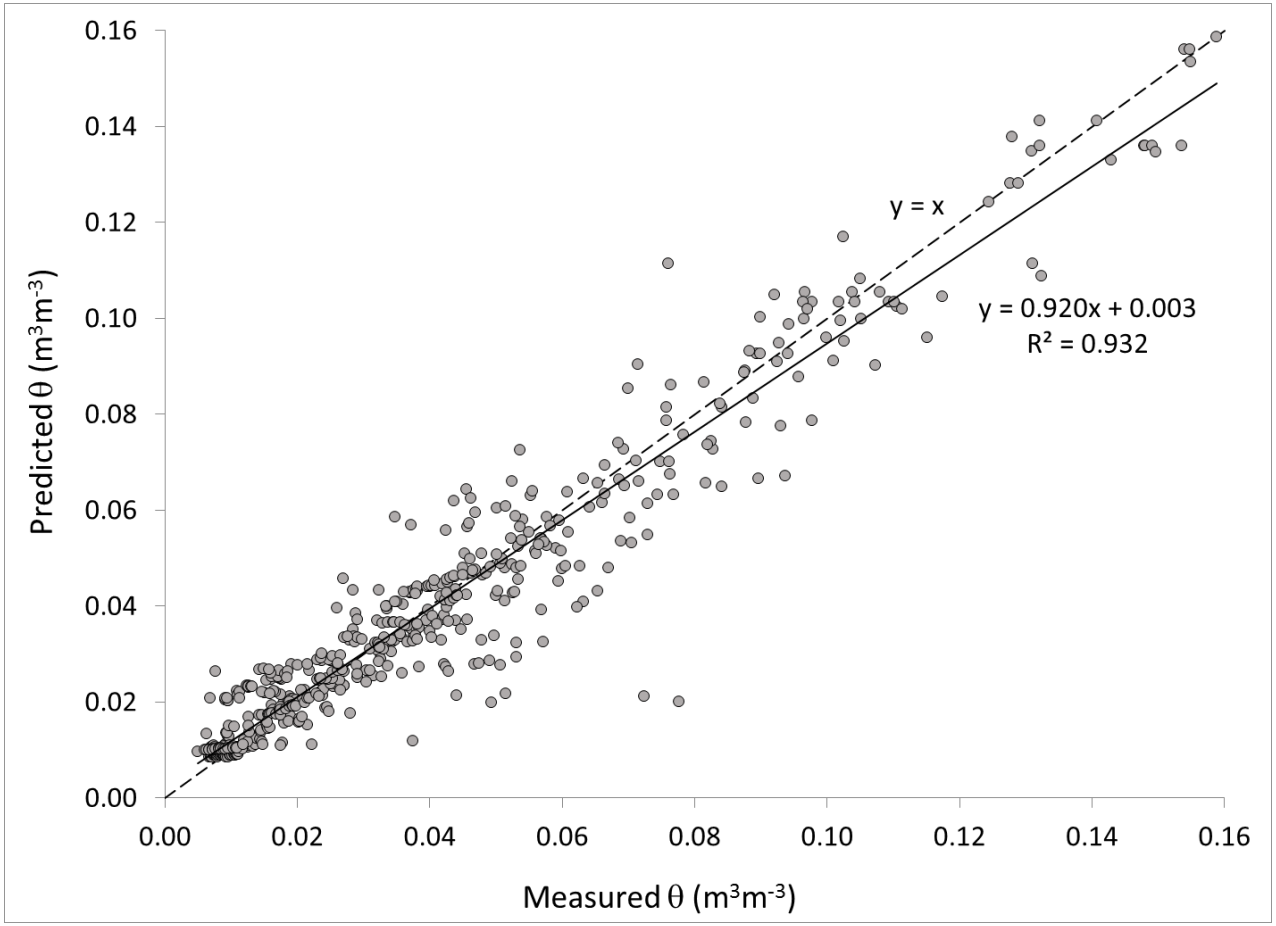


Figure 16. Observed versus predicted volumetric water contents (θ) from the Brooks and Corey (1964) model fitted to the wetting and drying capillary pressure saturation data for all of the shale types, except Chattanooga – Grey (these models did not converge successfully). The observed values were measured, while the predicted values were obtained using Eq. [5] in conjunction with the parameters associated with the highest $R^2$ values listed in Tables 1 and 2. The solid line is a best fit linear regression model, while the dashed line represents the ideal 1:1 relationship

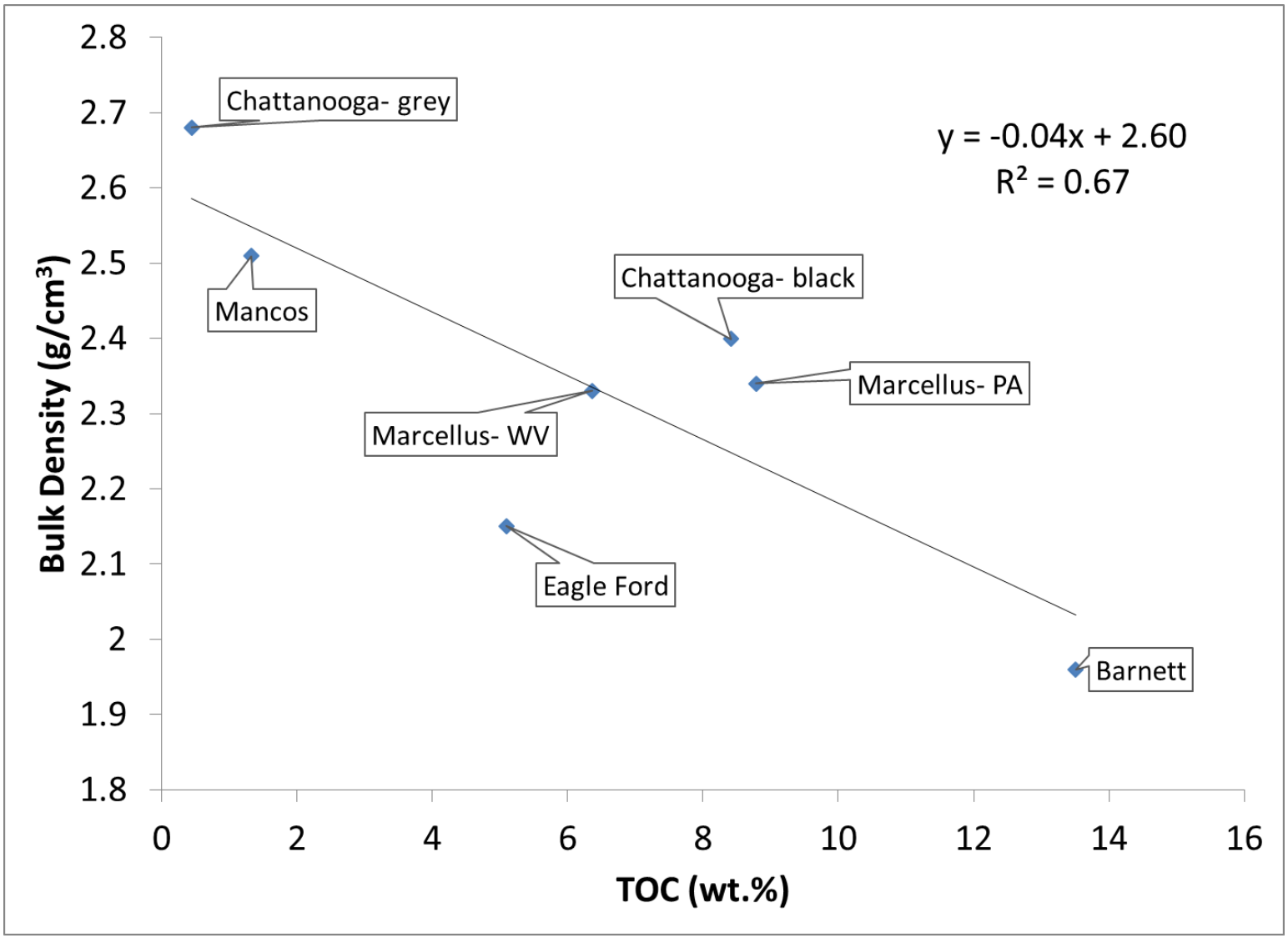


Figure 17: Correlation between TOC and bulk density (Regression significant at $p<0.05$)

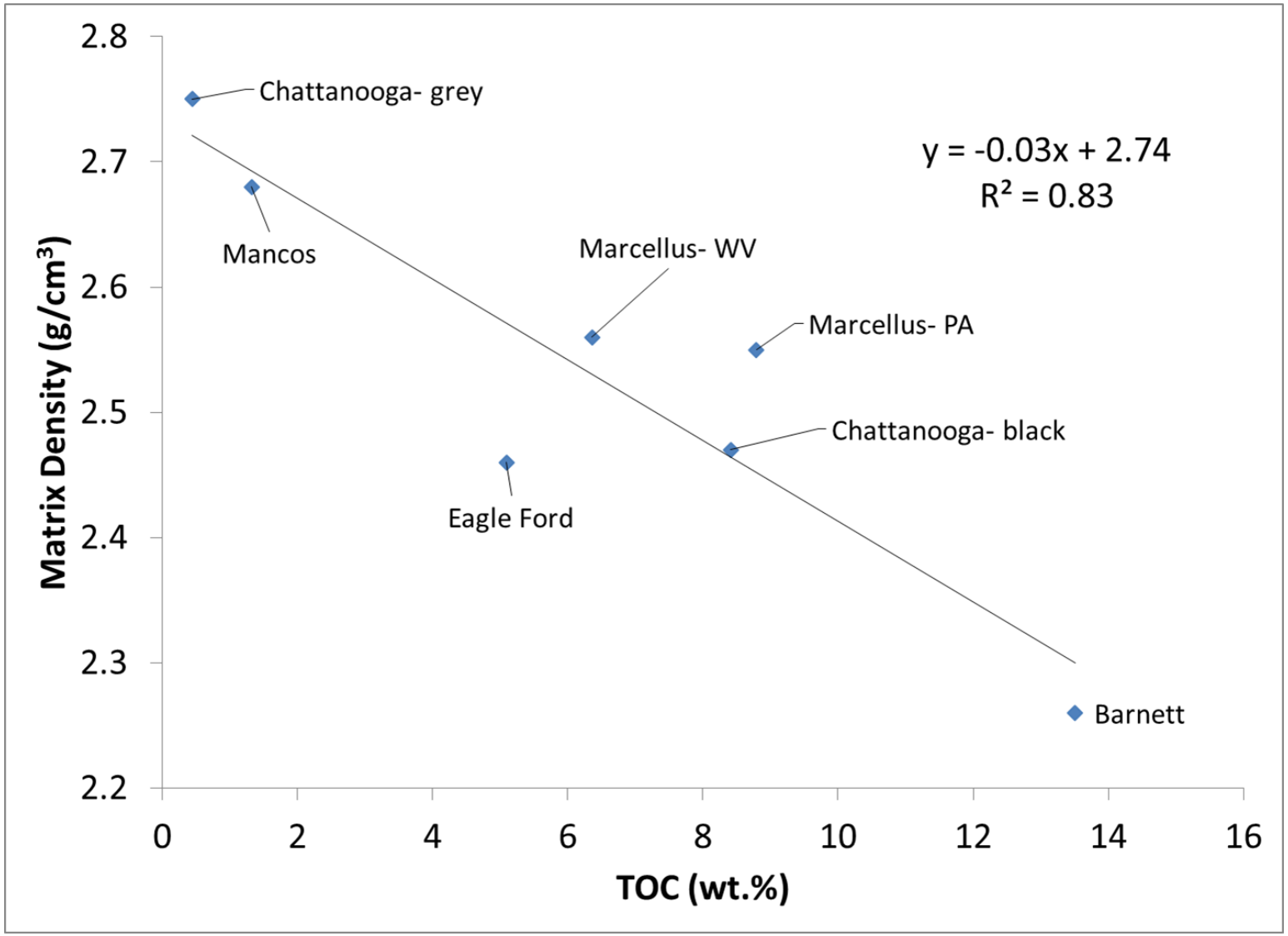


Figure 18: Correlation between TOC and matrix density (Regression significant at $p<0.05$)

## Appendix 3 - Data

*3.1 Mancos Shale*

| Subsample | Initial Oven Dry Mass (g) | Final Oven Dry Mass (g) |
|---|---|---|
| 1 | 2.2595 | 2.2365 |
| 2 | 2.0790 | 2.0583 |
| 3 | 1.6860 | 1.6657 |
| 4 | 1.7230 | 1.7029 |
| 5 | 2.2957 | 2.2672 |
| 6 | 1.5436 | 1.5238 |

| **Wetting** | | | | **Drying** | | | |
|---|---|---|---|---|---|---|---|
| Subsample | $a_w$ | $\Psi$ (MPa) | $\theta_v$ ($m^3m^{-3}$) | Subsample | $a_w$ | $\Psi$ (MPa) | $\theta_v$ ($m^3m^{-3}$) |
| 1 | 0.341 | 148.16 | 0.0164 | 1 | 0.274 | 178.29 | 0.0217 |
| 1 | 0.432 | 115.59 | 0.0230 | 1 | 0.386 | 131.09 | 0.0252 |
| 1 | 0.498 | 96.01 | 0.0260 | 1 | 0.471 | 103.68 | 0.0334 |
| 1 | 0.724 | 44.48 | 0.0410 | 1 | 0.501 | 95.18 | 0.0347 |
| 1 | 0.929 | 10.14 | 0.0524 | 1 | 0.566 | 78.38 | 0.0371 |
| 1 | 0.965 | 4.91 | 0.0874 | 1 | 0.637 | 62.11 | 0.0421 |
| 1 | 0.983 | 2.36 | 0.1056 | 1 | 0.785 | 33.34 | 0.0465 |
| 2 | 0.335 | 150.61 | 0.0145 | 1 | 0.914 | 12.38 | 0.0631 |
| 2 | 0.437 | 114.00 | 0.0245 | 1 | 0.951 | 6.92 | 0.0757 |
| 2 | 0.490 | 98.24 | 0.0270 | 1 | 0.966 | 4.76 | 0.0894 |
| 2 | 0.681 | 52.91 | 0.0377 | 1 | 0.979 | 2.92 | 0.1017 |
| 2 | 0.913 | 12.53 | 0.0640 | 1 | 0.983 | 2.36 | 0.1324 |
| 2 | 0.973 | 3.77 | 0.0942 | 2 | 0.240 | 196.53 | 0.0177 |
| 2 | 0.983 | 2.36 | 0.1055 | 2 | 0.373 | 135.81 | 0.0234 |
| 3 | 0.336 | 150.19 | 0.0166 | 2 | 0.450 | 109.96 | 0.0323 |
| 3 | 0.440 | 113.06 | 0.0252 | 2 | 0.489 | 98.52 | 0.0330 |
| 3 | 0.500 | 95.45 | 0.0310 | 2 | 0.536 | 85.88 | 0.0354 |
| 3 | 0.773 | 35.46 | 0.0622 | 2 | 0.610 | 68.07 | 0.0394 |
| 3 | 0.945 | 7.79 | 0.0819 | 2 | 0.734 | 42.59 | 0.0438 |
| 3 | 0.969 | 4.34 | 0.0882 | 2 | 0.878 | 17.92 | 0.0576 |
| 3 | 0.982 | 2.50 | 0.1606 | 2 | 0.936 | 9.11 | 0.0684 |
| 4 | 0.326 | 154.36 | 0.0149 | 2 | 0.959 | 5.77 | 0.0813 |
| 4 | 0.442 | 112.43 | 0.0244 | 2 | 0.979 | 2.92 | 0.0964 |
| 4 | 0.528 | 87.95 | 0.0336 | 2 | 0.983 | 2.36 | 0.1317 |
| 4 | 0.732 | 42.96 | 0.0428 | 3 | 0.221 | 207.89 | 0.0169 |

| Wetting | | | | Drying | | | |
|---|---|---|---|---|---|---|---|
| Subsample | $a_w$ | Ψ (MPa) | $\theta_v$ ($m^3m^{-3}$) | Subsample | $a_w$ | Ψ (MPa) | $\theta_v$ ($m^3m^{-3}$) |
| 4 | 0.906 | 13.59 | 0.0529 | 3 | 0.364 | 139.17 | 0.0229 |
| 4 | 0.976 | 3.35 | 0.1100 | 3 | 0.438 | 113.69 | 0.0309 |
| 4 | 0.981 | 2.64 | 0.1293 | 3 | 0.482 | 100.50 | 0.0316 |
| 5 | 0.283 | 173.84 | 0.0112 | 3 | 0.515 | 91.38 | 0.0330 |
| 5 | 0.443 | 112.12 | 0.0234 | 3 | 0.580 | 75.02 | 0.0378 |
| 5 | 0.504 | 94.36 | 0.0267 | 3 | 0.697 | 49.71 | 0.0423 |
| 5 | 0.699 | 49.32 | 0.0399 | 3 | 0.849 | 22.54 | 0.0567 |
| 5 | 0.958 | 5.91 | 0.0838 | 3 | 0.926 | 10.59 | 0.0711 |
| 5 | 0.975 | 3.49 | 0.0969 | 3 | 0.966 | 4.76 | 0.0940 |
| 5 | 0.983 | 2.36 | 0.1528 | 3 | 0.981 | 2.64 | 0.1155 |
| 6 | 0.312 | 160.40 | 0.0175 | 3 | 0.982 | 2.50 | 0.1930 |
| 6 | 0.444 | 111.81 | 0.0235 | 4 | 0.209 | 215.58 | 0.0173 |
| 6 | 0.484 | 99.93 | 0.0252 | 4 | 0.359 | 141.08 | 0.0246 |
| 6 | 0.642 | 61.03 | 0.0322 | 4 | 0.436 | 114.32 | 0.0320 |
| 6 | 0.967 | 4.62 | 0.0924 | 4 | 0.479 | 101.36 | 0.0333 |
| 6 | 0.975 | 3.49 | 0.1113 | 4 | 0.502 | 94.91 | 0.0342 |
| 6 | 0.984 | 2.22 | 0.2164 | 4 | 0.560 | 79.85 | 0.0378 |
| | | | | 4 | 0.669 | 55.36 | 0.0425 |
| | | | | 4 | 0.828 | 25.99 | 0.0559 |
| | | | | 4 | 0.913 | 12.53 | 0.0685 |
| | | | | 4 | 0.962 | 5.34 | 0.0876 |
| | | | | 4 | 0.980 | 2.78 | 0.1041 |
| | | | | 4 | 0.981 | 2.64 | 0.1603 |
| | | | | 5 | 0.206 | 217.57 | 0.0175 |
| | | | | 5 | 0.354 | 143.01 | 0.0250 |
| | | | | 5 | 0.416 | 120.78 | 0.0324 |
| | | | | 5 | 0.487 | 99.08 | 0.0343 |
| | | | | 5 | 0.525 | 88.74 | 0.0375 |
| | | | | 5 | 0.614 | 67.17 | 0.0456 |
| | | | | 5 | 0.695 | 50.11 | 0.0512 |
| | | | | 5 | 0.876 | 18.23 | 0.0702 |
| | | | | 5 | 0.954 | 6.49 | 0.0887 |
| | | | | 5 | 0.977 | 3.20 | 0.1093 |
| | | | | 5 | 0.982 | 2.50 | 0.1284 |
| | | | | 5 | 0.983 | 2.36 | 0.1861 |
| | | | | 6 | 0.204 | 218.91 | 0.0159 |
| | | | | 6 | 0.354 | 143.01 | 0.0236 |
| | | | | 6 | 0.397 | 127.22 | 0.0264 |

| Drying | | | |
|---|---|---|---|
| Subsample | $a_w$ | $\Psi$ (MPa) | $\theta_v$ ($m^3m^{-3}$) |
| 6 | 0.484 | 99.93 | 0.0321 |
| 6 | 0.523 | 89.26 | 0.0356 |
| 6 | 0.613 | 67.40 | 0.0418 |
| 6 | 0.723 | 44.67 | 0.0525 |
| 6 | 0.858 | 21.09 | 0.0608 |
| 6 | 0.946 | 7.64 | 0.0757 |
| 6 | 0.976 | 3.35 | 0.0977 |
| 6 | 0.981 | 2.64 | 0.1325 |
| 6 | 0.984 | 2.22 | 0.2516 |

*3.2 Eagle Ford Shale*

| Subsample | Initial Oven Dry Mass (g) | Final Oven Dry Mass (g) |
|---|---|---|
| 1 | 2.7424 | 2.7346 |
| 2 | 1.3209 | 1.3137 |
| 3 | 1.1300 | 1.1238 |
| 4 | 1.7857 | 1.7789 |
| 5 | 2.3985 | 2.3916 |
| 6 | 1.0915 | 1.0855 |

| **Wetting** | | | | **Drying** | | | |
|---|---|---|---|---|---|---|---|
| Subsample | $a_w$ | $\Psi$ (MPa) | $\theta_v$ ($m^3m^{-3}$) | Subsample | $a_w$ | $\Psi$ (MPa) | $\theta_v$ ($m^3m^{-3}$) |
| 1 | 0.340 | 148.57 | 0.0060 | 1 | 0.982 | 2.50 | 0.1249 |
| 1 | 0.421 | 119.14 | 0.0072 | 1 | 0.980 | 2.78 | 0.1079 |
| 1 | 0.541 | 84.60 | 0.0084 | 1 | 0.978 | 3.06 | 0.0927 |
| 1 | 0.657 | 57.85 | 0.0102 | 1 | 0.972 | 3.91 | 0.0692 |
| 1 | 0.948 | 7.35 | 0.0276 | 1 | 0.963 | 5.19 | 0.0567 |
| 1 | 0.958 | 5.91 | 0.0284 | 1 | 0.939 | 8.67 | 0.0417 |
| 1 | 0.982 | 2.50 | 0.1185 | 1 | 0.873 | 18.70 | 0.0280 |
| 2 | 0.342 | 147.76 | 0.0067 | 1 | 0.744 | 40.72 | 0.0176 |
| 2 | 0.421 | 119.14 | 0.0081 | 1 | 0.599 | 70.58 | 0.0111 |
| 2 | 0.542 | 84.35 | 0.0107 | 1 | 0.503 | 94.63 | 0.0110 |
| 2 | 0.674 | 54.33 | 0.0174 | 1 | 0.497 | 96.28 | 0.0107 |
| 2 | 0.939 | 8.67 | 0.0323 | 1 | 0.492 | 97.68 | 0.0103 |
| 2 | 0.977 | 3.20 | 0.1151 | 1 | 0.459 | 107.24 | 0.0102 |
| 2 | 0.983 | 2.36 | 0.1168 | 1 | 0.347 | 145.76 | 0.0095 |
| 3 | 0.344 | 146.95 | 0.0072 | 2 | 0.983 | 2.36 | 0.1245 |
| 3 | 0.422 | 118.81 | 0.0087 | 2 | 0.979 | 2.92 | 0.1051 |
| 3 | 0.542 | 84.35 | 0.0108 | 2 | 0.976 | 3.35 | 0.0764 |
| 3 | 0.706 | 47.94 | 0.0222 | 2 | 0.964 | 5.05 | 0.0424 |
| 3 | 0.952 | 6.77 | 0.0438 | 2 | 0.943 | 8.08 | 0.0284 |
| 3 | 0.977 | 3.20 | 0.0998 | 2 | 0.897 | 14.97 | 0.0183 |
| 3 | 0.982 | 2.50 | 0.1104 | 2 | 0.815 | 28.17 | 0.0127 |
| 4 | 0.344 | 146.95 | 0.0072 | 2 | 0.714 | 46.39 | 0.0098 |
| 4 | 0.426 | 117.51 | 0.0090 | 2 | 0.575 | 76.21 | 0.0091 |
| 4 | 0.536 | 85.88 | 0.0103 | 2 | 0.497 | 96.28 | 0.0088 |
| 4 | 0.701 | 48.92 | 0.0148 | 2 | 0.494 | 97.12 | 0.0086 |
| 4 | 0.953 | 6.63 | 0.0403 | 2 | 0.484 | 99.93 | 0.0083 |

| Wetting | | | | Drying | | | |
|---|---|---|---|---|---|---|---|
| Subsample | $a_w$ | Ψ (MPa) | $\theta_v$ ($m^3m^{-3}$) | Subsample | $a_w$ | Ψ (MPa) | $\theta_v$ ($m^3m^{-3}$) |
| 4 | 0.976 | 3.35 | 0.0714 | 2 | 0.459 | 107.24 | 0.0080 |
| 4 | 0.981 | 2.64 | 0.1118 | 2 | 0.347 | 145.76 | 0.0070 |
| 5 | 0.344 | 146.95 | 0.0062 | 3 | 0.982 | 2.50 | 0.1228 |
| 5 | 0.426 | 117.51 | 0.0075 | 3 | 0.980 | 2.78 | 0.1038 |
| 5 | 0.521 | 89.79 | 0.0080 | 3 | 0.971 | 4.05 | 0.0748 |
| 5 | 0.695 | 50.11 | 0.0117 | 3 | 0.954 | 6.49 | 0.0322 |
| 5 | 0.931 | 9.85 | 0.0184 | 3 | 0.927 | 10.44 | 0.0191 |
| 5 | 0.975 | 3.49 | 0.0699 | 3 | 0.864 | 20.13 | 0.0126 |
| 5 | 0.981 | 2.64 | 0.1099 | 3 | 0.789 | 32.64 | 0.0095 |
| 6 | 0.348 | 145.36 | 0.0067 | 3 | 0.694 | 50.30 | 0.0088 |
| 6 | 0.425 | 117.84 | 0.0084 | 3 | 0.559 | 80.09 | 0.0080 |
| 6 | 0.512 | 92.19 | 0.0094 | 3 | 0.497 | 96.28 | 0.0078 |
| 6 | 0.775 | 35.10 | 0.0373 | 3 | 0.488 | 98.80 | 0.0076 |
| 6 | 0.969 | 4.34 | 0.0607 | 3 | 0.476 | 102.23 | 0.0074 |
| 6 | 0.970 | 4.19 | 0.0895 | 3 | 0.460 | 106.94 | 0.0072 |
| 6 | 0.986 | 1.94 | 0.1051 | 3 | 0.344 | 146.95 | 0.0067 |
| | | | | 4 | 0.981 | 2.64 | 0.1204 |
| | | | | 4 | 0.980 | 2.78 | 0.0965 |
| | | | | 4 | 0.970 | 4.19 | 0.0762 |
| | | | | 4 | 0.952 | 6.77 | 0.0427 |
| | | | | 4 | 0.918 | 11.78 | 0.0290 |
| | | | | 4 | 0.848 | 22.71 | 0.0180 |
| | | | | 4 | 0.766 | 36.71 | 0.0119 |
| | | | | 4 | 0.676 | 53.92 | 0.0099 |
| | | | | 4 | 0.542 | 84.35 | 0.0094 |
| | | | | 4 | 0.500 | 95.45 | 0.0090 |
| | | | | 4 | 0.484 | 99.93 | 0.0089 |
| | | | | 4 | 0.470 | 103.98 | 0.0088 |
| | | | | 4 | 0.459 | 107.24 | 0.0083 |
| | | | | 4 | 0.340 | 148.57 | 0.0078 |
| | | | | 5 | 0.981 | 2.64 | 0.1164 |
| | | | | 5 | 0.979 | 2.92 | 0.0964 |
| | | | | 5 | 0.973 | 3.77 | 0.0782 |
| | | | | 5 | 0.953 | 6.63 | 0.0455 |
| | | | | 5 | 0.919 | 11.63 | 0.0315 |
| | | | | 5 | 0.843 | 23.52 | 0.0214 |
| | | | | 5 | 0.750 | 39.62 | 0.0145 |
| | | | | 5 | 0.657 | 57.85 | 0.0117 |

| Drying | | | |
|---|---|---|---|
| Subsample | $a_w$ | $\Psi$ (MPa) | $\theta_v$ ($m^3m^{-3}$) |
| 5 | 0.525 | 88.74 | 0.0109 |
| 5 | 0.503 | 94.63 | 0.0108 |
| 5 | 0.480 | 101.08 | 0.0105 |
| 5 | 0.464 | 105.75 | 0.0099 |
| 5 | 0.463 | 106.04 | 0.0098 |
| 5 | 0.340 | 148.57 | 0.0092 |
| 6 | 0.986 | 1.94 | 0.1175 |
| 6 | 0.977 | 3.20 | 0.1072 |
| 6 | 0.971 | 4.05 | 0.0760 |
| 6 | 0.946 | 7.64 | 0.0320 |
| 6 | 0.899 | 14.66 | 0.0188 |
| 6 | 0.832 | 25.33 | 0.0158 |
| 6 | 0.749 | 39.80 | 0.0124 |
| 6 | 0.647 | 59.96 | 0.0099 |
| 6 | 0.511 | 92.46 | 0.0085 |
| 6 | 0.504 | 94.36 | 0.0081 |
| 6 | 0.481 | 100.79 | 0.0079 |
| 6 | 0.467 | 104.86 | 0.0077 |
| 6 | 0.461 | 106.64 | 0.0075 |
| 6 | 0.340 | 148.57 | 0.0069 |

*3.3 Barnett Shale*

| Subsample | Initial Oven Dry Mass (g) | Final Oven Dry Mass (g) |
|---|---|---|
| 1 | 1.0736 | 1.0706 |
| 2 | 1.6784 | 1.6737 |
| 3 | 0.8790 | 0.8761 |
| 4 | 0.9863 | 0.9838 |
| 5 | 1.6053 | 1.6009 |
| 6 | 0.9994 | 0.9968 |

| **Wetting** | | | | **Drying** | | | |
|---|---|---|---|---|---|---|---|
| Subsample | $a_w$ | $\Psi$ (MPa) | $\theta_v$ ($m^3m^{-3}$) | Subsample | $a_w$ | $\Psi$ (MPa) | $\theta_v$ ($m^3m^{-3}$) |
| 1 | 0.259 | 186.04 | 0.0329 | 1 | 0.978 | 3.06 | 0.1549 |
| 1 | 0.403 | 125.16 | 0.0362 | 1 | 0.970 | 4.19 | 0.1279 |
| 1 | 0.518 | 90.58 | 0.0431 | 1 | 0.952 | 6.77 | 0.1024 |
| 1 | 0.541 | 84.60 | 0.0440 | 1 | 0.868 | 19.50 | 0.0840 |
| 1 | 0.950 | 7.06 | 0.0759 | 1 | 0.797 | 31.25 | 0.0663 |
| 1 | 0.972 | 3.91 | 0.1321 | 1 | 0.681 | 52.91 | 0.0539 |
| 1 | 0.978 | 3.06 | 0.1490 | 1 | 0.567 | 78.14 | 0.0501 |
| 2 | 0.305 | 163.53 | 0.0286 | 1 | 0.506 | 93.81 | 0.0468 |
| 2 | 0.410 | 122.78 | 0.0328 | 1 | 0.474 | 102.81 | 0.0437 |
| 2 | 0.524 | 89.00 | 0.0422 | 1 | 0.432 | 115.59 | 0.0408 |
| 2 | 0.530 | 87.43 | 0.0436 | 1 | 0.410 | 122.78 | 0.0379 |
| 2 | 0.935 | 9.26 | 0.0898 | 1 | 0.345 | 146.55 | 0.0350 |
| 2 | 0.942 | 8.23 | 0.0920 | 2 | 0.979 | 2.92 | 0.1538 |
| 2 | 0.979 | 2.92 | 0.1479 | 2 | 0.968 | 4.48 | 0.1309 |
| 3 | 0.320 | 156.91 | 0.0297 | 2 | 0.940 | 8.52 | 0.1049 |
| 3 | 0.413 | 121.78 | 0.0355 | 2 | 0.853 | 21.90 | 0.0876 |
| 3 | 0.544 | 83.84 | 0.0499 | 2 | 0.769 | 36.17 | 0.0714 |
| 3 | 0.556 | 80.84 | 0.0528 | 2 | 0.645 | 60.39 | 0.0549 |
| 3 | 0.921 | 11.33 | 0.0899 | 2 | 0.550 | 82.33 | 0.0508 |
| 3 | 0.950 | 7.06 | 0.1309 | 2 | 0.499 | 95.73 | 0.0465 |
| 3 | 0.979 | 2.92 | 0.1478 | 2 | 0.468 | 104.56 | 0.0430 |
| 4 | 0.331 | 152.26 | 0.0291 | 2 | 0.431 | 115.91 | 0.0402 |
| 4 | 0.415 | 121.11 | 0.0346 | 2 | 0.408 | 123.46 | 0.0375 |
| 4 | 0.543 | 84.09 | 0.0441 | 2 | 0.345 | 146.55 | 0.0347 |
| 4 | 0.599 | 70.58 | 0.0593 | 3 | 0.979 | 2.92 | 0.1547 |
| 4 | 0.918 | 11.78 | 0.1009 | 3 | 0.963 | 5.19 | 0.1276 |

| Wetting | | | | Drying | | | |
|---|---|---|---|---|---|---|---|
| Subsample | $a_w$ | Ψ (MPa) | $\theta_v$ ($m^3m^{-3}$) | Subsample | $a_w$ | Ψ (MPa) | $\theta_v$ ($m^3m^{-3}$) |
| 4 | 0.969 | 4.34 | 0.1495 | 3 | 0.924 | 10.89 | 0.1020 |
| 4 | 0.980 | 2.78 | 0.1535 | 3 | 0.831 | 25.49 | 0.0824 |
| 5 | 0.333 | 151.43 | 0.0270 | 3 | 0.744 | 40.72 | 0.0663 |
| 5 | 0.417 | 120.45 | 0.0337 | 3 | 0.619 | 66.05 | 0.0539 |
| 5 | 0.540 | 84.86 | 0.0416 | 3 | 0.532 | 86.91 | 0.0505 |
| 5 | 0.640 | 61.46 | 0.0599 | 3 | 0.491 | 97.96 | 0.0461 |
| 5 | 0.910 | 12.99 | 0.0956 | 3 | 0.461 | 106.64 | 0.0425 |
| 5 | 0.962 | 5.34 | 0.1244 | 3 | 0.429 | 116.55 | 0.0399 |
| 5 | 0.981 | 2.64 | 0.1532 | 3 | 0.404 | 124.81 | 0.0381 |
| 6 | 0.337 | 149.79 | 0.0285 | 3 | 0.330 | 152.68 | 0.0358 |
| 6 | 0.417 | 120.45 | 0.0343 | 4 | 0.980 | 2.78 | 0.1588 |
| 6 | 0.559 | 80.09 | 0.0502 | 4 | 0.963 | 5.19 | 0.1289 |
| 6 | 0.649 | 59.54 | 0.0626 | 4 | 0.914 | 12.38 | 0.1025 |
| 6 | 0.947 | 7.50 | 0.1323 | 4 | 0.821 | 27.16 | 0.0827 |
| 6 | 0.968 | 4.48 | 0.1429 | 4 | 0.725 | 44.29 | 0.0660 |
| 6 | 0.985 | 2.08 | 0.1458 | 4 | 0.597 | 71.04 | 0.0533 |
| | | | | 4 | 0.516 | 91.12 | 0.0492 |
| | | | | 4 | 0.479 | 101.36 | 0.0436 |
| | | | | 4 | 0.455 | 108.44 | 0.0406 |
| | | | | 4 | 0.427 | 117.19 | 0.0381 |
| | | | | 4 | 0.400 | 126.18 | 0.0361 |
| | | | | 4 | 0.321 | 156.48 | 0.0333 |
| | | | | 5 | 0.981 | 2.64 | 0.1590 |
| | | | | 5 | 0.972 | 3.91 | 0.1321 |
| | | | | 5 | 0.930 | 9.99 | 0.1105 |
| | | | | 5 | 0.849 | 22.54 | 0.0930 |
| | | | | 5 | 0.742 | 41.09 | 0.0743 |
| | | | | 5 | 0.601 | 70.12 | 0.0576 |
| | | | | 5 | 0.527 | 88.21 | 0.0524 |
| | | | | 5 | 0.488 | 98.80 | 0.0484 |
| | | | | 5 | 0.449 | 110.27 | 0.0426 |
| | | | | 5 | 0.427 | 117.19 | 0.0396 |
| | | | | 5 | 0.398 | 126.87 | 0.0368 |
| | | | | 5 | 0.320 | 156.91 | 0.0335 |
| | | | | 6 | 0.985 | 2.08 | 0.1513 |
| | | | | 6 | 0.972 | 3.91 | 0.1407 |
| | | | | 6 | 0.934 | 9.40 | 0.1174 |
| | | | | 6 | 0.855 | 21.57 | 0.0976 |

| Drying | | | |
|---|---|---|---|
| Subsample | $a_w$ | $\Psi$ (MPa) | $\theta_v$ ($m^3m^{-3}$) |
| 6 | 0.742 | 41.09 | 0.0767 |
| 6 | 0.593 | 71.96 | 0.0589 |
| 6 | 0.515 | 91.38 | 0.0513 |
| 6 | 0.482 | 100.50 | 0.0479 |
| 6 | 0.441 | 112.75 | 0.0419 |
| 6 | 0.425 | 117.84 | 0.0399 |
| 6 | 0.395 | 127.92 | 0.0370 |
| 6 | 0.308 | 162.18 | 0.0335 |

*3.4 Chattanooga Shale- Black*

| Subsample | Initial Oven Dry Mass (g) | Final Oven Dry Mass (g) |
|---|---|---|
| 1 | 0.7322 | 0.7287 |
| 2 | 0.6201 | 0.6170 |
| 3 | 1.1945 | 1.1912 |
| 4 | N/A | 2.6099 |
| 5 | N/A | 3.9895 |
| 6 | N/A | 3.0315 |

| **Wetting** | | | | **Drying** | | | |
|---|---|---|---|---|---|---|---|
| Subsample | $a_w$ | Ψ (MPa) | $\theta_v$ ($m^3m^{-3}$) | Subsample | $a_w$ | Ψ (MPa) | $\theta_v$ ($m^3m^{-3}$) |
| 1 | 0.412 | 122.11 | 0.0062 | 1 | 0.976 | 3.35 | 0.0723 |
| 1 | 0.514 | 91.65 | 0.0105 | 1 | 0.961 | 5.48 | 0.0161 |
| 1 | 0.58 | 75.02 | 0.0203 | 1 | 0.852 | 22.06 | 0.0154 |
| 1 | 0.625 | 64.73 | 0.0206 | 1 | 0.662 | 56.80 | 0.0138 |
| 1 | 0.705 | 48.14 | 0.0242 | 1 | 0.47 | 103.98 | 0.0131 |
| 1 | 0.972 | 3.91 | 0.0268 | 1 | 0.434 | 114.95 | 0.0125 |
| 1 | 0.976 | 3.35 | 0.0605 | 1 | 0.4 | 126.18 | 0.0118 |
| 2 | 0.416 | 120.78 | 0.0093 | 1 | 0.384 | 131.81 | 0.0112 |
| 2 | 0.528 | 87.95 | 0.0097 | 1 | 0.214 | 212.32 | 0.0105 |
| 2 | 0.565 | 78.62 | 0.0154 | 2 | 0.967 | 4.62 | 0.0776 |
| 2 | 0.566 | 78.38 | 0.0201 | 2 | 0.95 | 7.06 | 0.0163 |
| 2 | 0.681 | 52.91 | 0.0247 | 2 | 0.832 | 25.33 | 0.0155 |
| 2 | 0.950 | 7.06 | 0.0290 | 2 | 0.639 | 61.67 | 0.0144 |
| 2 | 0.967 | 4.62 | 0.0652 | 2 | 0.465 | 105.45 | 0.0136 |
| 3 | 0.417 | 120.45 | 0.0092 | 2 | 0.428 | 116.87 | 0.0132 |
| 3 | 0.521 | 89.79 | 0.0126 | 2 | 0.396 | 127.57 | 0.0124 |
| 3 | 0.576 | 75.97 | 0.0186 | 2 | 0.382 | 132.53 | 0.0116 |
| 3 | 0.606 | 68.98 | 0.0202 | 2 | 0.217 | 210.40 | 0.0109 |
| 3 | 0.711 | 46.97 | 0.0245 | 3 | 0.966 | 4.76 | 0.0492 |
| 3 | 0.958 | 5.91 | 0.0259 | 3 | 0.940 | 8.52 | 0.0167 |
| 3 | 0.966 | 4.76 | 0.0425 | 3 | 0.810 | 29.02 | 0.0145 |
| | | | | 3 | 0.619 | 66.05 | 0.0127 |
| | | | | 3 | 0.462 | 106.34 | 0.0123 |
| | | | | 3 | 0.423 | 118.49 | 0.0121 |
| | | | | 3 | 0.392 | 128.97 | 0.0113 |
| | | | | 3 | 0.381 | 132.89 | 0.0109 |

| Drying | | | |
|---|---|---|---|
| Subsample | $a_w$ | Ψ (MPa) | $\theta_v$ ($m^3m^{-3}$) |
| 3 | 0.222 | 207.27 | 0.0096 |
| 4 | 0.977 | 3.20 | 0.0440 |
| 4 | 0.927 | 10.44 | 0.0189 |
| 4 | 0.782 | 33.86 | 0.0144 |
| 4 | 0.574 | 76.45 | 0.0125 |
| 4 | 0.454 | 108.75 | 0.0119 |
| 4 | 0.415 | 121.11 | 0.0116 |
| 4 | 0.386 | 131.09 | 0.0109 |
| 4 | 0.381 | 132.89 | 0.0107 |
| 4 | 0.215 | 211.68 | 0.0091 |
| 5 | 0.979 | 2.92 | 0.0514 |
| 5 | 0.899 | 14.66 | 0.0179 |
| 5 | 0.725 | 44.29 | 0.0131 |
| 5 | 0.515 | 91.38 | 0.0128 |
| 5 | 0.449 | 110.27 | 0.0116 |
| 5 | 0.403 | 125.16 | 0.0114 |
| 5 | 0.381 | 132.89 | 0.0107 |
| 5 | 0.381 | 132.89 | 0.0109 |
| 5 | 0.206 | 217.57 | 0.0084 |
| 6 | 0.977 | 3.20 | 0.0238 |
| 6 | 0.884 | 16.98 | 0.0153 |
| 6 | 0.697 | 49.71 | 0.0095 |
| 6 | 0.475 | 102.52 | 0.0091 |
| 6 | 0.445 | 111.50 | 0.0073 |
| 6 | 0.398 | 126.87 | 0.0072 |
| 6 | 0.382 | 132.53 | 0.0074 |
| 6 | 0.381 | 132.89 | 0.0069 |
| 6 | 0.203 | 219.59 | 0.0049 |

*3.5 Chattanooga Shale- Grey*

| Subsample | Initial Oven Dry Mass (g) | Final Oven Dry Mass (g) |
|---|---|---|
| 1 | 2.0951 | 2.0864 |
| 2 | 3.4638 | 3.4490 |
| 3 | 2.8716 | 2.8393 |
| 4 | N/A | 7.8678 |
| 5 | N/A | 7.6868 |
| 6 | N/A | 7.1558 |

| **Wetting** | | | | **Drying** | | | |
|---|---|---|---|---|---|---|---|
| Subsample | $a_w$ | Ψ (MPa) | $\theta_v$ ($m^3m^{-3}$) | Subsample | $a_w$ | Ψ (MPa) | $\theta_v$ ($m^3m^{-3}$) |
| 1 | 0.438 | 113.69 | 0.0255 | 1 | 0.988 | 1.66 | 0.0822 |
| 1 | 0.466 | 105.15 | 0.0103 | 1 | 0.970 | 4.19 | 0.0450 |
| 1 | 0.668 | 55.56 | 0.0491 | 1 | 0.952 | 6.77 | 0.0443 |
| 1 | 0.731 | 43.15 | 0.0522 | 1 | 0.793 | 31.94 | 0.0397 |
| 1 | 0.847 | 22.87 | 0.0566 | 1 | 0.707 | 47.75 | 0.0377 |
| 1 | 0.974 | 3.63 | 0.0568 | 1 | 0.608 | 68.52 | 0.0323 |
| 1 | 0.988 | 1.66 | 0.0708 | 1 | 0.525 | 88.74 | 0.0297 |
| 2 | 0.439 | 113.37 | 0.0224 | 1 | 0.453 | 109.05 | 0.0243 |
| 2 | 0.447 | 110.89 | 0.0144 | 1 | 0.368 | 137.67 | 0.0191 |
| 2 | 0.659 | 57.43 | 0.0370 | 1 | 0.349 | 144.97 | 0.0187 |
| 2 | 0.810 | 29.02 | 0.0507 | 1 | 0.281 | 174.81 | 0.0141 |
| 2 | 0.917 | 11.93 | 0.0545 | 2 | 0.984 | 2.22 | 0.0782 |
| 2 | 0.977 | 3.20 | 0.0562 | 2 | 0.961 | 5.48 | 0.0474 |
| 2 | 0.984 | 2.22 | 0.0665 | 2 | 0.902 | 14.20 | 0.0441 |
| 3 | 0.434 | 114.95 | 0.0226 | 2 | 0.743 | 40.91 | 0.0437 |
| 3 | 0.435 | 114.63 | 0.0147 | 2 | 0.644 | 60.60 | 0.0386 |
| 3 | 0.626 | 64.51 | 0.0346 | 2 | 0.583 | 74.31 | 0.0343 |
| 3 | 0.807 | 29.53 | 0.0462 | 2 | 0.507 | 93.54 | 0.0307 |
| 3 | 0.950 | 7.06 | 0.0548 | 2 | 0.439 | 113.37 | 0.0255 |
| 3 | 0.980 | 2.78 | 0.0583 | 2 | 0.359 | 141.08 | 0.0225 |
| 3 | 0.982 | 2.50 | 0.0682 | 2 | 0.328 | 153.51 | 0.0197 |
| | | | | 2 | 0.251 | 190.36 | 0.0141 |
| | | | | 3 | 0.982 | 2.50 | 0.0994 |
| | | | | 3 | 0.961 | 5.48 | 0.0460 |
| | | | | 3 | 0.902 | 14.20 | 0.0459 |
| | | | | 3 | 0.743 | 40.91 | 0.0409 |

| Drying | | | |
|---|---|---|---|
| Subsample | $a_w$ | $\Psi$ (MPa) | $\theta_v$ ($m^3m^{-3}$) |
| 3 | 0.644 | 60.60 | 0.0365 |
| 3 | 0.554 | 81.33 | 0.0324 |
| 3 | 0.487 | 99.08 | 0.0280 |
| 3 | 0.423 | 118.49 | 0.0229 |
| 3 | 0.351 | 144.18 | 0.0199 |
| 3 | 0.305 | 163.53 | 0.0170 |
| 3 | 0.237 | 198.26 | 0.0143 |
| 4 | 0.985 | 2.08 | 0.0878 |
| 4 | 0.957 | 6.05 | 0.0550 |
| 4 | 0.874 | 18.55 | 0.0539 |
| 4 | 0.741 | 41.28 | 0.0494 |
| 4 | 0.668 | 55.56 | 0.0456 |
| 4 | 0.590 | 72.66 | 0.0414 |
| 4 | 0.528 | 87.95 | 0.0383 |
| 4 | 0.436 | 114.32 | 0.0336 |
| 4 | 0.377 | 134.34 | 0.0315 |
| 4 | 0.330 | 152.68 | 0.0176 |
| 4 | 0.228 | 203.60 | 0.0130 |
| 5 | 0.982 | 2.50 | 0.0724 |
| 5 | 0.969 | 4.34 | 0.0534 |
| 5 | 0.921 | 11.33 | 0.0498 |
| 5 | 0.780 | 34.22 | 0.0430 |
| 5 | 0.681 | 52.91 | 0.0381 |
| 5 | 0.611 | 67.85 | 0.0347 |
| 5 | 0.543 | 84.09 | 0.0305 |
| 5 | 0.417 | 120.45 | 0.0265 |
| 5 | 0.373 | 135.81 | 0.0226 |
| 5 | 0.338 | 149.38 | 0.0188 |
| 5 | 0.210 | 214.92 | 0.0127 |
| 6 | 0.978 | 3.06 | 0.0708 |
| 6 | 0.967 | 4.62 | 0.0481 |
| 6 | 0.909 | 13.14 | 0.0464 |
| 6 | 0.783 | 33.69 | 0.0413 |
| 6 | 0.667 | 55.77 | 0.0360 |
| 6 | 0.591 | 72.43 | 0.0306 |
| 6 | 0.503 | 94.63 | 0.0273 |
| 6 | 0.393 | 128.62 | 0.0221 |
| 6 | 0.363 | 139.55 | 0.0193 |

| Drying | | | |
|---|---|---|---|
| Subsample | $a_w$ | $\Psi$ (MPa) | $\theta_v$ ($m^3m^{-3}$) |
| 6 | 0.317 | 158.21 | 0.0155 |
| 6 | 0.209 | 215.58 | 0.0123 |

*3.6 Marcellus Shale- Pennsylvania*

| Subsample | Initial Oven Dry Mass (g) | Final Oven Dry Mass (g) |
|---|---|---|
| 1 | 0.9507 | 0.9430 |
| 2 | 2.5528 | 2.5405 |
| 3 | 1.5304 | 1.5211 |
| 4 | N/A | 6.6986 |
| 5 | N/A | 5.3721 |
| 6 | N/A | 6.6016 |

| **Wetting** | | | | **Drying** | | | |
|---|---|---|---|---|---|---|---|
| Subsample | $a_w$ | Ψ (MPa) | $\theta_v$ ($m^3m^{-3}$) | Subsample | $a_w$ | Ψ (MPa) | $\theta_v$ ($m^3m^{-3}$) |
| 1 | 0.423 | 118.49 | 0.0093 | 1 | 0.979 | 2.92 | 0.0536 |
| 1 | 0.479 | 101.36 | 0.0157 | 1 | 0.965 | 4.34 | 0.0455 |
| 1 | 0.678 | 54.54 | 0.0290 | 1 | 0.954 | 4.91 | 0.0435 |
| 1 | 0.673 | 53.52 | 0.0160 | 1 | 0.969 | 6.49 | 0.0371 |
| 1 | 0.951 | 6.92 | 0.0533 | 1 | 0.842 | 23.68 | 0.0288 |
| 1 | 0.980 | 2.92 | 0.0595 | 1 | 0.678 | 53.52 | 0.0236 |
| 1 | 0.979 | 2.78 | 0.0347 | 1 | 0.559 | 80.09 | 0.0172 |
| 2 | 0.418 | 120.12 | 0.0068 | 1 | 0.535 | 86.14 | 0.0162 |
| 2 | 0.520 | 90.05 | 0.0265 | 1 | 0.414 | 121.45 | 0.0123 |
| 2 | 0.748 | 42.40 | 0.0505 | 1 | 0.414 | 121.45 | 0.0125 |
| 2 | 0.735 | 39.99 | 0.0473 | 1 | 0.359 | 141.08 | 0.0108 |
| 2 | 0.960 | 5.62 | 0.0536 | 1 | 0.250 | 190.91 | 0.0091 |
| 2 | 0.982 | 4.05 | 0.0564 | 2 | 0.971 | 4.05 | 0.0653 |
| 2 | 0.971 | 2.50 | 0.0540 | 2 | 0.963 | 5.19 | 0.0515 |
| 3 | 0.416 | 120.78 | 0.0090 | 2 | 0.962 | 5.34 | 0.0500 |
| 3 | 0.515 | 91.38 | 0.0205 | 2 | 0.960 | 5.62 | 0.0469 |
| 3 | 0.691 | 50.90 | 0.0428 | 2 | 0.801 | 30.56 | 0.0383 |
| 3 | 0.695 | 50.11 | 0.0076 | 2 | 0.600 | 70.35 | 0.0200 |
| 3 | 0.967 | 5.77 | 0.0530 | 2 | 0.526 | 88.47 | 0.0181 |
| 3 | 0.981 | 4.62 | 0.0560 | 2 | 0.500 | 95.45 | 0.0170 |
| 3 | 0.959 | 2.64 | 0.0409 | 2 | 0.407 | 123.80 | 0.0129 |
| | | | | 2 | 0.401 | 125.84 | 0.0125 |
| | | | | 2 | 0.342 | 147.76 | 0.0112 |
| | | | | 2 | 0.245 | 193.69 | 0.0094 |
| | | | | 3 | 0.967 | 4.62 | 0.0551 |
| | | | | 3 | 0.966 | 4.76 | 0.0461 |

| Drying | | | |
|---|---|---|---|
| Subsample | $a_w$ | Ψ (MPa) | $\theta_v$ ($m^3m^{-3}$) |
| 3 | 0.955 | 6.34 | 0.0458 |
| 3 | 0.953 | 6.63 | 0.0457 |
| 3 | 0.750 | 39.62 | 0.0278 |
| 3 | 0.549 | 82.58 | 0.0185 |
| 3 | 0.505 | 94.08 | 0.0160 |
| 3 | 0.469 | 104.27 | 0.0153 |
| 3 | 0.406 | 124.13 | 0.0131 |
| 3 | 0.395 | 127.92 | 0.0125 |
| 3 | 0.317 | 158.21 | 0.0110 |
| 3 | 0.240 | 196.53 | 0.0095 |
| 4 | 0.982 | 2.50 | 0.0896 |
| 4 | 0.970 | 4.19 | 0.0840 |
| 4 | 0.948 | 7.35 | 0.0728 |
| 4 | 0.943 | 8.08 | 0.0705 |
| 4 | 0.869 | 19.34 | 0.0631 |
| 4 | 0.659 | 57.43 | 0.0531 |
| 4 | 0.637 | 62.11 | 0.0490 |
| 4 | 0.533 | 86.65 | 0.0358 |
| 4 | 0.504 | 94.36 | 0.0326 |
| 4 | 0.454 | 108.75 | 0.0303 |
| 4 | 0.266 | 182.37 | 0.0194 |
| 4 | 0.221 | 207.89 | 0.0185 |
| 5 | 0.982 | 2.50 | 0.0771 |
| 5 | 0.964 | 5.05 | 0.0729 |
| 5 | 0.944 | 7.94 | 0.0688 |
| 5 | 0.852 | 22.06 | 0.0567 |
| 5 | 0.736 | 42.21 | 0.0530 |
| 5 | 0.611 | 67.85 | 0.0421 |
| 5 | 0.590 | 72.66 | 0.0384 |
| 5 | 0.428 | 112.43 | 0.0261 |
| 5 | 0.442 | 116.87 | 0.0259 |
| 5 | 0.405 | 124.47 | 0.0253 |
| 5 | 0.257 | 187.11 | 0.0191 |
| 6 | 0.214 | 212.32 | 0.0178 |
| 6 | 0.982 | 2.50 | 0.1059 |
| 6 | 0.973 | 3.77 | 0.0936 |
| 6 | 0.971 | 4.05 | 0.0816 |
| 6 | 0.921 | 11.33 | 0.0669 |

| Drying | | | |
|---|---|---|---|
| Subsample | $a_w$ | Ψ (MPa) | $\theta_v$ ($m^3m^{-3}$) |
| 6 | 0.740 | 41.47 | 0.0570 |
| 6 | 0.610 | 68.07 | 0.0467 |
| 6 | 0.585 | 73.83 | 0.0424 |
| 6 | 0.417 | 120.45 | 0.0270 |
| 6 | 0.417 | 120.45 | 0.0270 |
| 6 | 0.37 | 136.92 | 0.0239 |
| 6 | 0.253 | 189.27 | 0.0198 |
| 6 | 0.207 | 216.90 | 0.0186 |

*3.7 Marcellus Shale- West Virginia*

| Subsample | Initial Oven Dry Mass (g) | Final Oven Dry Mass (g) |
|---|---|---|
| 1 | 1.5187 | 1.5117 |
| 2 | 1.0348 | 1.0283 |
| 3 | 1.4781 | 1.4667 |
| 4 | N/A | 4.5653 |
| 5 | N/A | 4.1725 |
| 6 | N/A | 3.8446 |

| **Wetting** | | | | **Drying** | | | |
|---|---|---|---|---|---|---|---|
| Subsample | $a_w$ | $\Psi$ (MPa) | $\theta_v$ ($m^3m^{-3}$) | Subsample | $a_w$ | $\Psi$ (MPa) | $\theta_v$ ($m^3m^{-3}$) |
| 1 | 0.433 | 115.27 | 0.0148 | 1 | 0.983 | 2.36 | 0.0603 |
| 1 | 0.486 | 99.37 | 0.0260 | 1 | 0.973 | 3.77 | 0.0478 |
| 1 | 0.636 | 62.32 | 0.0324 | 1 | 0.933 | 9.55 | 0.0396 |
| 1 | 0.688 | 51.50 | 0.0381 | 1 | 0.816 | 28.00 | 0.0326 |
| 1 | 0.947 | 7.50 | 0.0523 | 1 | 0.609 | 68.30 | 0.0210 |
| 1 | 0.981 | 2.64 | 0.0575 | 1 | 0.480 | 101.08 | 0.0187 |
| 1 | 0.983 | 2.36 | 0.0648 | 1 | 0.404 | 124.81 | 0.0174 |
| 2 | 0.429 | 116.55 | 0.0141 | 1 | 0.284 | 173.35 | 0.0141 |
| 2 | 0.490 | 98.24 | 0.0260 | 2 | 0.974 | 3.63 | 0.0598 |
| 2 | 0.685 | 52.10 | 0.0478 | 2 | 0.971 | 4.05 | 0.0460 |
| 2 | 0.702 | 48.73 | 0.0402 | 2 | 0.909 | 13.14 | 0.0366 |
| 2 | 0.981 | 6.20 | 0.0581 | 2 | 0.787 | 32.99 | 0.0289 |
| 2 | 0.956 | 3.63 | 0.0693 | 2 | 0.571 | 77.17 | 0.0228 |
| 2 | 0.974 | 2.64 | 0.0628 | 2 | 0.464 | 105.75 | 0.0210 |
| 3 | 0.426 | 117.51 | 0.0157 | 2 | 0.378 | 133.97 | 0.0183 |
| 3 | 0.485 | 99.65 | 0.0215 | 2 | 0.289 | 170.95 | 0.0174 |
| 3 | 0.710 | 47.17 | 0.0496 | 3 | 0.982 | 2.50 | 0.0592 |
| 3 | 0.745 | 40.54 | 0.0446 | 3 | 0.963 | 5.19 | 0.0449 |
| 3 | 0.955 | 6.34 | 0.0535 | 3 | 0.876 | 18.23 | 0.0373 |
| 3 | 0.972 | 3.91 | 0.0554 | 3 | 0.759 | 37.97 | 0.0304 |
| 3 | 0.982 | 2.50 | 0.0578 | 3 | 0.545 | 83.59 | 0.0233 |
| | | | | 3 | 0.430 | 116.22 | 0.0191 |
| | | | | 3 | 0.362 | 139.93 | 0.0174 |
| | | | | 3 | 0.292 | 169.52 | 0.0168 |
| | | | | 4 | 0.977 | 3.20 | 0.0571 |
| | | | | 4 | 0.973 | 3.77 | 0.0453 |

| Drying | | | |
|---|---|---|---|
| Subsample | $a_w$ | Ψ (MPa) | $\theta_v$ ($m^3m^{-3}$) |
| 4 | 0.913 | 12.53 | 0.0381 |
| 4 | 0.692 | 50.70 | 0.0231 |
| 4 | 0.526 | 88.47 | 0.0207 |
| 4 | 0.421 | 119.14 | 0.0188 |
| 4 | 0.350 | 144.57 | 0.0173 |
| 4 | 0.299 | 166.26 | 0.0157 |
| 5 | 0.983 | 2.36 | 0.0546 |
| 5 | 0.967 | 4.62 | 0.0449 |
| 5 | 0.874 | 18.55 | 0.0365 |
| 5 | 0.668 | 55.56 | 0.0250 |
| 5 | 0.518 | 90.58 | 0.0215 |
| 5 | 0.413 | 121.78 | 0.0193 |
| 5 | 0.300 | 163.98 | 0.0160 |
| 5 | 0.304 | 165.80 | 0.0159 |
| 6 | 0.982 | 2.50 | 0.0445 |
| 6 | 0.950 | 7.06 | 0.0377 |
| 6 | 0.846 | 23.03 | 0.0341 |
| 6 | 0.693 | 50.50 | 0.0263 |
| 6 | 0.525 | 88.74 | 0.0218 |
| 6 | 0.420 | 119.47 | 0.0197 |
| 6 | 0.300 | 165.80 | 0.0155 |
| 6 | 0.282 | 174.32 | 0.0146 |

# Vita

Brendan Donnelly was born in New Orleans, Louisiana to Susan and Sonny Donnelly. The oldest of three sons, he attended St. Paul's School in Covington, Louisiana and graduated in 2006. From there, he enrolled in the Department of Geology and Geophysics at the Louisiana State University in Baton Rouge, LA where he met his now wife, Kathleen. In December of 2009, he graduated with a B.S. in Geology. In 2011 he moved to Knoxville, TN with Kathleen who had been accepted into a doctorate program at the University of Tennessee. Brendan held a variety of positions at a local car dealership until the summer of 2013 when he entered the graduate program in the Department of Earth and Planetary Sciences at the University of Tennessee. Brendan graduated with a Master of Science Degree in Geology in August 2015 and vows to never work for minimum wage again.